8-6-2018

Polyethylene Oxide Hydration in Solutions, Nanoconfinement and Nanostructures

Udaya Dahal
University of Connecticut - Storrs, udaya.dahal@uconn.edu

Polyethylene Oxide Hydration in Solutions, Nanoconfinement and Nanostructures

Udaya Raj Dahal, PhD

University of Connecticut, 2018

Abstract

Amphiphilic water-soluble polymers are actively used in designing novel nanomaterials and have been the subject of extensive experimental and simulation studies. Polyethylene oxide (PEO) is a water soluble, biocompatible, non-toxic synthetic polymer capable of preventing protein adsorption which is widely used in industry and biomedicine for protein crystallization, control of particle aggregation and drug delivery. Most of the applications of PEO and PEO-based nanoparticles are utilized in an aqueous environment as PEO is highly soluble in water due to its ability to form hydrogen bonds with water and therefore understanding the role of water on the conformation and dynamics of PEO and PEO-based nanomaterials is essential in improving and designing new nanomaterials for a variety of applications.

Using all-atom molecular dynamics simulations, we studied PEO in bulk solutions, under nanoconfinement in carbon nanotubes and in nanostructures (PEO brushes grafted to a planar surface and nanoparticles). In the bulk solution, we find that PEO forms a globule like structure in hexane, coil-like structure in water or benzene and an extended rod-like or helical structure is isobutyric acid. The conformation and mobility of PEO in water and in isobutyric acid is dictated by the hydrogen bonding with PEO. As part of our confinement studies, we found that PEO is spontaneously encapsulated from aqueous solution into carbon nanotubes and forms rod-like, helical and wrapped chain conformation depending on the size of the carbon nanotube. The stable

helix inside the carbon-nanotube is a consequence of the stable water arrangement around PEO. As part of our studies of PEO brushes we investigated PEO grafted to gold nanoparticles and planar gold surfaces at varying grafting densities. We found that PEO hydration in the brush depends on grafting density and for gold nanoparticles also varies with the radial distance and nanoparticle radius of curvature. Our simulation results agree well with the classical scaling theories and we were able to explain the curvature dependent hydration based on bulk-solution PEO behavior.

Polyethylene Oxide Hydration in Solutions, Nanoconfinement and Nanostructures

Udaya Raj Dahal

M.S, University of Connecticut, 2014

A Dissertation

Submitted in Partial Fulfillment of the

Requirements for the Degree of

Doctor of Philosophy

At the

University of Connecticut

2018

APPROVAL PAGE

Doctor of Philosophy Dissertation

Polyethylene Oxide Hydration in Solutions, Nanoconfinement and Nanostructures

Presented by

Udaya Raj Dahal

Major Advisor _____

Elena E. Dormidontova

Associate Advisor _____

Gayanath W. Fernando

Associate Advisor _____

Jose A. Gascon

Acknowledgement

I would like to express my sincere gratitude to my advisor Prof. Elena Dormidontova for the continuous support and encouragement during my Ph.D. research. Her help and guidance made it possible for me to achieve this goal.

I would also like to thank my fellow labmates Dr. Zilu Wang, Hari Sharma and Michael Richter for the stimulating discussions and for their help and support during the time we worked together. Also, I would like to thank all of my Nepalese friends at UCONN who were always there on my side and shared my joys and sorrows together.

I would like to thank all my family members specially my mother Sharada Dahal and my father Late Bishnu Prasad Dahal who sacrificed a lot to make me a better person today than I was yesterday. Without their love, support and guidance, I would not be here where I am standing today. I would also like to thank my brother Surya Raj Dahal for his constant support and guidance from my kindergarten days till this day where I am finishing my Ph.D. I am happy that I am able to fulfill his dream of successfully completing my Ph.D. degree.

Last but not the least, I would like to thank my wife, Sabita Gelal for all her support, encouragement and immense love which helped to get through the difficult times in the most positive way.

Table of Contents

List of Tables

List of Figures

Chapter 1.

Introduction

A macromolecule's properties are defined by its conformation and dynamics in the environment it is exposed to. The study of different conformational states in various natural and synthetic macromolecules is an active research area[1,2] and it is a well-established notion that water plays significant role in the biochemical functioning of these macromolecules. There have been a number of significant studies concerning hydration in naturally occurring biopolymers but much less effort has been focused on synthetic polymers. Amphiphilic water-soluble polymers have gained significant interest in recent years because of their broad application in industry and biomedicine. [3] One of the most actively used synthetic polymers of this class is polyethylene oxide (PEO). PEO $[\boldsymbol{CH3-(O-CH2-CH2)_N-O-CH3}]$, a very simple amphiphilic polymer which can be used for protein crystallization, surface modification, colloidal stabilization, lubrication, anti-fouling surfaces, etc.,[4–9] The use of PEO in designing new nanomaterials is widespread because of its solubility in water and non-toxicity (PEO is known to be non-immunogenic when injected in living organisms). One of the important applications of PEO is its ability to inhibit protein adsorption on surfaces. When PEO is grafted to surfaces it retains a thick hydration shell which is believed to produce net repulsive forces on proteins which prevents their adsorption. The brush thickness/height should be sufficiently large to overcome the electrostatic and Vander Waals interaction between the surface and the protein and the grafting density must be high enough to prevent enough void space for smaller particles to penetrate through.[8,10] As most of the industrial applications (e.g. detergents, paints, emulsions etc.) or biomedical applications (drug and gene delivery etc.) of macromolecules involves an aqueous environment, understanding the conformational and dynamical behavior of PEO polymers in water is essential. Most

hydrocarbons show an upper critical solution temperature (UCST) below which there will be two phases but many water-soluble polymers show a lower critical solution temperature (LCST) below which the polymer is miscible. PEO is unique in the sense that it shows both UCST and LCST making a closed loop miscibility gap in the temperature-concentration phase diagram as can be seen in figure 1.1. But the temperature-induced immiscibility does not occur until fairly high temperature (depending on molecular weight and concentration) resulting in very high solubility of PEO in water over a wide range of temperatures as well as concentrations.

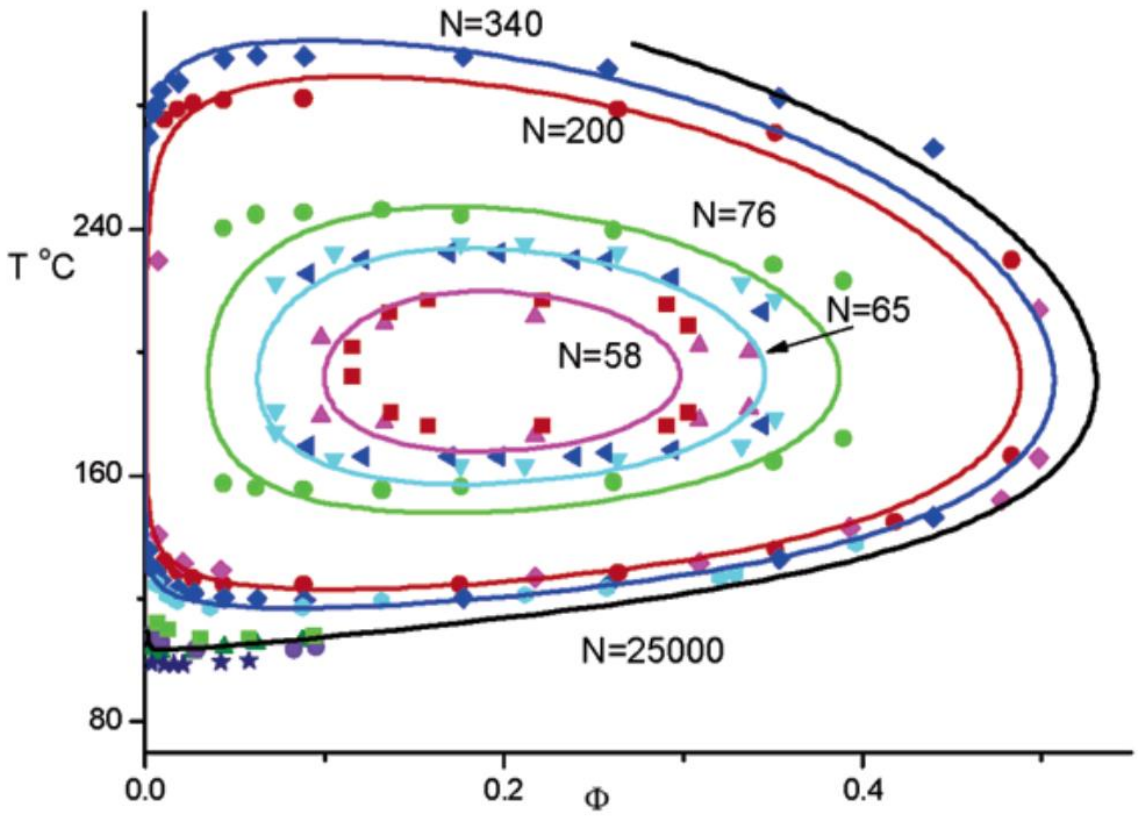

Figure 1.1: Phase diagram for aqueous solutions of PEO reprinted from analytical paper from Dormidontova.[16] Figure shows the temperature vs concentration of PEO chains of different lengths and we see the circular loops inside which there are two phases and outside PEO and water are miscible.

Several theories have been proposed to explain the solubility gap in PEO water at high temperatures.[4,11–16]. One of the theories is by Dormidontova[15], which uses a purely statistical analysis of hydrogen bonding between water-water and PEO-water obtained from minimizing free energy equation. This theory explains well the PEO-water phase diagram based on a hydrogen bonding perspective. Thus, the solubility of PEO in water comes from its ability to form hydrogen bonds with water due to the existence of the polar oxygen in the ether-like chemical structure. The interplay between hydrophobic ethylene unit and hydrophilic oxygen of PEO is responsible for its peculiar behavior and therefore makes it a candidate not only for a variety of applications but also for engendering a significant number of fundamental studies which can have wider implications. Many efforts have been made to understand the hydration shell around PEO both from experiments and computer simulations but a full understanding is still lacking. As it is not always easy to probe all the molecular details in experiments, computational tools are effective in gaining molecular level insights on the role of water in the conformation and dynamics of PEO chains. In our work we use molecular dynamics (MD) simulations to investigate the conformation, hydration and mobility of PEO chains in solutions, under confinement and in nanostructures.

In this thesis, we will present our work on PEO and PEO nanostructures carried out using computer simulations. Before we try to understand the behavior of PEO in different conditions, it is necessary to first understand solution behavior. In this regard, we studied PEO in organic solvents and in pure water (to help establish the appropriate force field parameters) and a binary mixture of isobutyric acid (IBA) and water. The result of simulation matches well with experimental observations. This result is published in PCCP[17] and is included in chapter 3 of the thesis. Here, we established the role of hydrogen bonding in the conformation and dynamics of PEO in pure solution and binary mixtures.

The study of biomacromolecules under confinement has been a subject of both theoretical and experimental studies for decades. Since, nanopores and nanochannels play important role in biological phenomena as well as in material design and application, the study of biopolymers under different confinement conditions has gained a great deal of interest in recent years. The pore formation in biological membranes and how a protein folds inside those translation channels is still a question which is not fully understood and water is considered to be an important component that plays significant role in driving different mechanism inside these membranes. There is also an ever-growing interest in manufacturing nanostructures like nanopores, nanochannels or nanotubes for biomedical to energy related applications. Hence, an overall understanding of biopolymers and their synthetic counterparts under nanoconfinement and the gained insight into the role of water at the molecular level in structural transition and encapsulation has potential implications in designing nanomaterials for biotechnological applications. It has been shown experimentally that inserting a carbon nanotube into cell membranes and bilayers,[18] can create an artificial ion channel to transport small ions, DNA, water etc. Thus, it will be insightful to understand the behavior of a polymer inside a nanotube which helps experimentalists to improve these novel nanomaterials and also understand several unanswered problems in biophysics. These motivations led us to study the behavior of PEO under nanoconfinement using an open single walled carbon nanotube(CNT). The result of the simulation showed that PEO present in aqueous solution in a random coil conformation, is spontaneously encapsulated inside the carbon nanotube and forms either a rod-like, helical or wrapped chain conformation, depending on the size of the carbon nanotube. For range of nanotubes sizes, we observed stable helical conformation of PEO resembling the crystalline state in some cases and found that the stable water arrangement around PEO is responsible for helical stability. This result is included in chapter 4 and was published in PRL.[19]

PEO when combined (covalently bonded) with other hydrophobic molecules like polypropylene oxide can form self-assembled structures in water. These structures (or micelle) has inner hydrophobic core and outer PEO corona and has range of application from detergents to drug delivery. Similar to these self-assembled structures, PEO can be grafted to solid surfaces like gold or silver to form brush-like structures with a solid core and PEO corona (outer layer). Polymer brushes can be used for colloidal stabilization, lubrication on surfaces, creating non-fouling surfaces etc. Since, PEO is known to prevent protein adsorption on surfaces, it is one of the most used polymers for drug delivery and creating non-fouling surfaces. Since water plays important role in determining the properties of PEO brushes, it is essential to understand hydration in polymer brushes. Thus, from single chain behavior, we further extended our research to planar PEO brushes. We studied the mobility as well as hydration of planar PEO brushes from very low to very high grafting density. Here, we included in our studies grafting densities which have not yet been attained experimentally and hence this research can be insightful for experimentalists in the future in designing new materials using high density grafted polymer brushes. The result of this research is included in chapter 5 and was published in Macromolecules.[20]

The use of silver and gold nanoparticles in nanomedicine is increasing exponentially due to their potential in both imaging and therapeutics.[21,22] Due to the particular quantum effects observed for smaller size metallic particles, different interesting features are observed which can be used in designing new materials for various applications. Since silver and gold nanoparticles can be used as drug carriers, it is desirable to have a longer circulation life-time for gold nanoparticles in blood and prevent renal clearance. This can be achieved by grafting PEO chains onto the gold nanoparticles. The preference for PEO water hydrogen bonding helps to retain a thick hydration shell inside spherical PEO brushes and helps to prevent the protein adsorption. Thus, we extended

our research on planar brushes to spherical PEO brushes. Here, we study spherical PEO brushes at seven different grafting densities starting from low to very high as in planar brushes. To understand the effect of curvature, we simultaneously studied PEO brushes grafted to gold nanoparticles of varying sizes i.e. radii 1,2 and 3nm. Thus, we studied 21 systems which covered a spectrum of grafting densities and curvature and we were able to understand the hydration and dynamics in spherical PEO brushes. The result of this simulation is included in chapter 6 and is submitted for publication.

In summary, hydrogen bonding between PEO and water is responsible for the high solubility of PEO and the competition between PEO-water hydrogen bonding and water-water hydrogen bonding in aqueous environment leads to quicker exchange of water contributing to higher flexibility of PEO chain. Since water loves to be in contact with PEO, PEO always retains the hydration shell around it and the thick hydration shell in a polymer brush is a consequence of hydrogen bonding between PEO and water. The stable hydration shell around PEO helps to prevent surfaces from the intrusion of foreign particle as well as increases the circulation half-life of particles. Thus, PEO hydration is one of the important properties that determines its behavior in many systems and understanding this behavior helps to enhance the design of new nanomaterials for biotechnology.

1.1 References

(1) Liese, S.; Gensler, M.; Krysiak, S.; Schwarzl, R.; Achazi, A.; Paulus, B.; Hugel, T.; Rabe, J. P.; Netz, R. R. Hydration Effects Turn a Highly Stretched Polymer from an Entropic into an Energetic Spring. *ACS Nano* **2017**, *11* (1), 702–712 DOI: 10.1021/acsnano.6b07071.

(2) Bellissent-Funel, M.-C.; Hassanali, A.; Havenith, M.; Henchman, R.; Pohl, P.; Sterpone, F.; van der Spoel, D.; Xu, Y.; Garcia, A. E. Water Determines the Structure and Dynamics

of Proteins. *Chem. Rev.* **2016**, acs.chemrev.5b00664 DOI: 10.1021/acs.chemrev.5b00664.

(3) Bedrov, D.; Smith, G. Molecular Dynamics Simulation Study of the Structure of Poly (Ethylene Oxide) Brushes on Nonpolar Surfaces in Aqueous Solution. *Langmuir* **2006**, *22* (14), 6189–6194 DOI: 10.1021/la060535r.

(4) Bekiranov, S.; Bruinsma, R.; Pincus, P. Solution Behavior of Polyethylene Oxide in Water as a Function of Temperature and Pressure. *Phys. Rev. E* **1997**, *55* (1), 577–585 DOI: 10.1103/PhysRevE.55.577.

(5) Pincus, P. Colloid Stabilization with Grafted Polyelectrolytes. *Macromolecules* **1991**, *24* (10), 2912–2919 DOI: 10.1021/ma00010a043.

(6) Vogiatzis, G. G.; Theodorou, D. N. Structure of Polymer Layers Grafted to Nanoparticles in Silica-Polystyrene Nanocomposites. *Macromolecules* **2013**, *46* (11), 4670–4683 DOI: 10.1021/ma400107q.

(7) Lee, J.; Lee, H.; Andrade, J. Blood Compatibility of Polyethylene Oxide Surfaces. *Prog. Polym. Sci.* **1995**, *20* (6), 1043–1079 DOI: 10.1016/0079-6700(95)00011-4.

(8) Harris, J. M.; Chess, R. B. Effect of Pegylation on Pharmaceuticals. *Nat. Rev. Drug Discov.* **2003**, *2* (3), 214–221 DOI: 10.1038/nrd1033.

(9) Liu, H.; Doane, T. L.; Cheng, Y.; Lu, F.; Srinivasan, S.; Zhu, J.-J.; Burda, C. Control of Surface Ligand Density on PEGylated Gold Nanoparticles for Optimized Cancer Cell Uptake. *Part. Part. Syst. Charact.* **2015**, *32* (2), 197–204 DOI: 10.1002/ppsc.201400067.

(10) Gon, S.; Kumar, K.-N.; Nüsslein, K.; Santore, M. M. How Bacteria Adhere to Brushy PEG Surfaces: Clinging to Flaws and Compressing the Brush. *Macromolecules* **2012**, *45* (20), 8373–8381 DOI: 10.1021/ma300981r.

(11) Kjellander, R.; Florin, E. Water Structure and Changes in Thermal Stability of the System Poly(Ethylene Oxide)–water. *J. Chem. Soc. Faraday Trans. 1 Phys. Chem. Condens. Phases* **1981**, *77* (9), 2053–2077 DOI: 10.1039/f19817702053.

(12) Karlstrom, G. A New Model for Upper and Lower Critical Solution Temperatures in Poly(Ethylene Oxide) Solutions. *J. Phys. Chem.* **1985**, *89* (2), 4962–4964 DOI: 10.1021/j100269a015.

(13) Goldstein, R. E. On the Theory of Lower Critical Solution Points in Hydrogen-Bonded Mixtures. *J. Chem. Phys.* **1984**, *80* (10), 5340–5341 DOI: 10.1063/1.446567.

(14) Matsuyama, A.; Tanaka, F. Theory of Solvation-Induced Reentrant Phase Separation in Polymer Solutions. *Phys. Rev. Lett.* **1990**, *65* (3), 341–344 DOI: 10.1103/PhysRevLett.65.341.

(15) Dormidontova, E. E. Role of Competitive PEO−Water and Water−Water Hydrogen Bonding in Aqueous Solution PEO Behavior. *Macromolecules* **2002**, *35* (3), 987–1001 DOI: 10.1021/ma010804e.

(16) Dormidontova, E. E. Influence of End Groups on Phase Behavior and Properties of PEO in Aqueous Solutions. *Macromolecules* **2004**, *37* (20), 7747–7761 DOI:

10.1021/ma035609.

(17) Dahal, U. R.; Dormidontova, E. E. The Dynamics of Solvation Dictates the Conformation of Polyethylene Oxide in Aqueous, Isobutyric Acid and Binary Solutions. *Phys. Chem. Chem. Phys.* **2017**, *19* (15), 9823–9832 DOI: 10.1039/C7CP00526A.

(18) Geng, J.; Kim, K.; Zhang, J.; Escalada, A.; Tunuguntla, R.; Comolli, L. R.; Allen, F. I.; Shnyrova, A. V; Cho, K. R.; Munoz, D.; Wang, Y. M.; Grigoropoulos, C. P.; Ajo-Franklin, C. M.; Frolov, V. A.; Noy, A. Stochastic Transport through Carbon Nanotubes in Lipid Bilayers and Live Cell Membranes. *Nature* **2014**, *514* (7524), 612–615 DOI: 10.1038/nature13817.

(19) Dahal, U. R.; Dormidontova, E. E. Spontaneous Insertion, Helix Formation, and Hydration of Polyethylene Oxide in Carbon Nanotubes. *Phys. Rev. Lett.* **2016**, *117* (2), 027801 DOI: 10.1103/PhysRevLett.117.027801.

(20) Dahal, U. R.; Wang, Z.; Dormidontova, E. E. Hydration and Mobility of Poly(Ethylene Oxide) Brushes. *Macromolecules* **2017**, *50* (17), 6722–6732 DOI: 10.1021/acs.macromol.7b01369.

(21) Boisselier, E.; Astruc, D. Gold Nanoparticles in Nanomedicine: Preparations, Imaging, Diagnostics, Therapies and Toxicity. *Chem. Soc. Rev.* **2009**, *38* (6), 1759 DOI: 10.1039/b806051g.

(22) Cabuzu, D.; Cirja, A.; Puiu, R.; Grumezescu, A. M. Biomedical Applications of Gold Nanoparticles. *Curr. Top. Med. Chem.* **2015**, *15* (16), 1605–1613 DOI: 10.2174/1568026615666150414144750.

Chapter 2.

Molecular Dynamics Simulation

2.1. Introduction

Molecular dynamics (MD) is one of the simulation methods which is used for computing equilibrium and transport properties of classical many-body systems.[1] MD simulation solves Newton's equation of motion for N interacting particles. For a given a potential energy function for N interacting particles, the force can be obtained by the negative derivative with respect to position. If $V(\vec{r_1}, \vec{r_2}, \vec{r_3}, \ldots\ldots, \vec{r_N})$ is the potential energy function for N particles, we can obtain force as,

$$\vec{F_i} = \nabla_i V \tag{2.11}$$

$$\frac{d^2\vec{r_i}}{dt^2} = \frac{\vec{F_i}}{m_i}; \tag{2.12}$$

where $i = 1..N$, $\vec{r_i}$ is the position vector and m_i is the mass of i^{th} particle. Solving equation 2.12 gives us the velocity and coordinates for individual particles at a given time t. This instantaneous coordinate, velocity and forces can be used to calculate various equilibrium and transport properties of a system. There are many software packages that are capable of carrying out MD simulations, eg. GROMACS, LAMMPS, AMBER, CHARMM etc. Since we use GROMACS (GROningen Machine for Computer Simulations) for MD simulations, the description of algorithms will be based on what is available/implemented in GROMACS.[2] In order to solve these equations of motions numerically, we have various choices of algorithms. Out of many existing algorithms, we use the leap-frog algorithm which is the default integrator in GROMACS. The leap-frog algorithm[1] can be summarized by equation 2.13 and 2.14, where it uses positions $\vec{r}$ at time t, velocities v at time $t - \frac{1}{2}\Delta t$ and updates $\vec{r}\ and\ \vec{v}$ iteratively using forces $\vec{F}(t)$ and

equations 2.13 and 2.14. This algorithm gets its name leap-frog as velocity($\vec{v}$) and position ($\vec{r}$) leap over each other as shown in figure 2.11

$$\vec{v}\left(t+\frac{1}{2}\Delta t\right)=\vec{v}\left(t-\frac{1}{2}\Delta t\right)+\frac{\Delta t}{m}\,\vec{F}(t) \tag{2.13}$$

$$\vec{r}(t+\Delta t)=\vec{r}(t)+\Delta t\; v\left(t+\frac{1}{2}\Delta t\right) \tag{2.14}$$

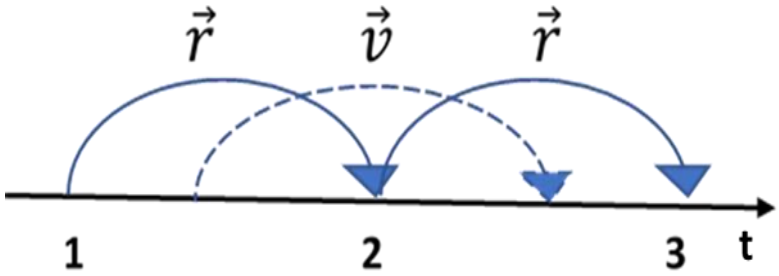

Figure 2.11: Pictorial representation of leap-frog algorithm showing alternate half-time calculation of positions and velocities.

2.2. Interaction Potentials and Force-Field

As mentioned in section 2.1, the potential energy function defines the complex energy landscape of molecular interactions which determines the overall properties of the system. The target of molecular dynamics simulation is to reach a global minimum state of this energy landscape and explore different states of the system in accordance with the ergodic hypothesis. In general, the molecular mechanics potential energy function consists of bonded and non-bonded interaction terms. The non-bonded interaction consists of Van der Waals interactions and electrostatic interaction. Van der Waals interaction in general is represented by either the Lennard-Jones potential(LJ) or Buckingham Potential. The LJ potential can be written as:

$$V_{LJ} = 4\epsilon \left(\frac{\sigma^{12}}{r_{ij}^{12}} - \frac{\sigma^{6}}{r_{ij}^{6}}\right) \text{ or } \left(\frac{C_{ij}^{12}}{r_{ij}^{12}} - \frac{C_{ij}^{6}}{r_{ij}^{6}}\right) \text{ where } C_{ij}^{6} = 4\epsilon\sigma^{6}, C_{ij}^{12} = 4\epsilon\sigma^{12} \quad (2.21)$$

Here, σ, ϵ represent Lennard-Jones parameters, r_{ij} represents interatomic distance between atoms i and j. If the LJ parameters are not defined between hetero atoms, then GROMACS uses three types of combination rule:

a) Geometrical Averages:

$$C_{ij}^{6} = \sqrt{C_{ii}^{6}\, C_{jj}^{6}} \text{ and } C_{ij}^{12} = \sqrt{C_{ii}^{12}\, C_{jj}^{12}} \quad (2.22)$$

$$\sigma_{ij} = \frac{1}{2}\left(\sigma_{ii} + \sigma_{jj}\right) \text{ and } \epsilon_{ij} = \sqrt{\left(\epsilon_{ii}\epsilon_{jj}\right)} \quad (2.23a)$$

b) Lorentz-Berthelot rules: or

$$\sigma_{ij} = \sqrt{\sigma_{ii}\sigma_{jj}} \text{ and } \epsilon_{ij} = \sqrt{\left(\epsilon_{ii}\epsilon_{jj}\right)} \quad (2.23b)$$

Bonded interactions in general consist of bond interaction, angle interaction and dihedral interaction but can have some extra parameters depending on the constraints in the system. The bond vibration energy is represented by harmonic potential:

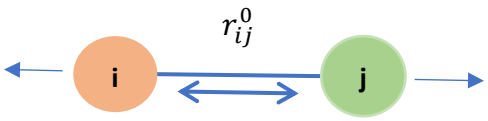

$$V_{bond} = \frac{1}{2} k_b \left(r_{ij} - r_{ij}^{0}\right)^2 \quad (2.24)$$

Here k_b and r_{ij}^{0} represent respectively the force constant and equilibrium bond distance for bonded atoms i and j. Similarly, the bond-angle vibration between atoms i-j-k is also represented by harmonic angle potential:

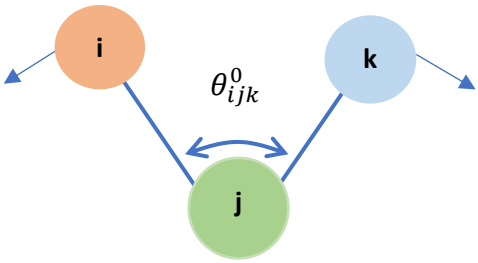

$$V_{angle} = k^{\theta}_{ijk}\left(\theta_{ijk} - \theta^0_{ijk}\right)^2 \quad (2.25)$$

Here, k^{θ}_{ijk} and θ^0_{ijk} represent force constant and equilibrium angle for angle between atoms i, j and k.

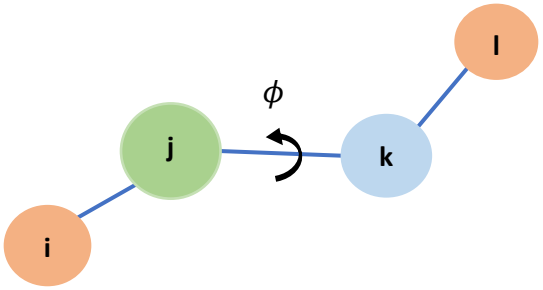

$$V_{dihedrals} = \sum_{n=0}^{5} C_n\left(Cos(\psi)\right)^n \quad (2.26)$$

$$\psi = \phi - 180°$$

For the dihedral interaction equation 2.26 is used and $C_0 \ldots . C_5$ are the dihedral parameters and ϕ is the dihedral angle. This is a proper dihedral using Ryckert-Bellemans potential. If necessary improper dihedrals are also implement. There are many different force fields existing in the literature. Some of the popular force fields include, OPLS, CHARMM, GROMOS, AMBER etc. Most of our simulations were done using an OPLS all atom force field.[3]

2.1. Temperature and Pressure Coupling

To mimic the experimental reality, the simulation is carried out either in a canonical(NVT) ensemble or an isobaric-isothermal(NPT) ensemble which requires a thermal and pressure bath to couple with the system. There are many thermostats as well as barostats but one should be careful in choosing them and should follow the correct protocol to avoid any artifact.

Berendsen Thermostat:

The Berendsen algorithm[4] is a weak coupling scheme in which a system couples to an external bath with a given temperature T_0. This thermostat slowly corrects the thermal deviation from temperature T_0 according to:

$$\frac{dT}{dt} = \frac{T_0 - T}{\tau} \tag{2.31}$$

where τ is coupling time constant and T is the temperature of the system. Solving this equation, we find that a temperature deviation from the target temperature decays exponentially with a time constant τ. This scheme helps to reach the target temperature quickly and facilitates faster equilibration with a short coupling constant. However, for reliable equilibrium runs in order to preserve conservative dynamics a larger coupling time is required. One of the drawbacks of using Berendsen thermostat is that is suppresses the fluctuation of kinetic energy which prevents from generating correct canonical ensemble.[1] This error in temperature fluctuation scales as 1/N and for larger system this error tends to be small but extreme care should be taken in calculating properties for eg. heat capacity which comes directly from the thermal fluctuations.

Velocity-rescaling Thermostat:

Velocity-rescaling thermostat is an extension of Berendsen thermostat designed to produce the correct canonical ensemble. In this method a random force is added in a way such that it enforces correct redistribution of kinetic energy.[5] However, the drawback of this system is that when system size is small or when the observable quantities depends on fluctuations rather than on averages, this method cannot be used.[5]

Nose-Hoover Thermostat:

As mentioned earlier, the weak-coupling algorithm doesn't produce the correct canonical ensemble. The Nose-Hoover thermostat[6,7] produces a canonical ensemble when the system is ergodic. In cases when the observables of interest require using temperature fluctuations as is the case for the heat capacity, it is not desirable to use Berendsen or velocity-rescale thermostat. The general idea is to use Berendsen thermostat which is extremely efficient for relaxing the system to target temperature. Once the target temperature is reached, it is better to use a thermostat that produces the correct canonical ensemble. Berendsen thermostat is efficient as it has exponential relaxation as compared to the Nose-Hoover thermostat which yields oscillatory relaxation and helps to reduce the time to reach the equilibrium temperature in short time. Thus, the general idea is to use Berendsen thermostat for the initial relaxation of the system and once the target temperature is reached, it is better to use a thermostat that produces the correct canonical ensemble.[1,5]

Pressure Coupling

Most of the equilibration simulation and even production simulation is run in the isobaric-isothermal ensemble (NPT) to mimic the real system. Therefore, we need to ensure that the pressure bath will couple to the system. Pressure coupling helps to equilibrate the system and maintain the real density of the system. In GROMACS, we can use either an isotropic pressure coupling or semi-isotropic pressure coupling algorithm. For systems with interfaces where pressure coupling requires only two dimensions, semi-isotropic pressure coupling is used otherwise isotropic pressure coupling is used. Pressure coupling follows the similar principle as temperature coupling. GROMACS supports two pressure coupling schemes:

Berendsen Barostat:

The Berendsen pressure coupling algorithm[4] rescales the coordinates as well as the simulation box vectors after every coupling steps with a matrix $\boldsymbol{\mu}$, which relaxes the system towards the barostat's reference pressure $\boldsymbol{P}_0$ using the following equation:

$$\frac{d\boldsymbol{P}}{dt} = \frac{\boldsymbol{P}_0 - \boldsymbol{P}}{\tau_p} \tag{2.31}$$

The scaling matrix $\boldsymbol{\mu}$, is given by

$$\boldsymbol{\mu} = \mathbf{1} - \frac{\beta\,\Delta t}{3\tau_p}\left(\boldsymbol{P}_0 - \boldsymbol{P}(t)\right) \tag{2.31}$$

where β is the isothermal compressibility,τ_p is the relaxation time constant and **P**(t) is the instantaneous pressure.

Parrinello-Rahman Barostat:

Similar to temperature fluctuations, if the pressure fluctuations (or volume fluctuations) are important to calculate a thermodynamic property, we need to couple the system that produces a true NPT ensemble. In this sense, weak coupling schemes like Berendsen fails to produce correct ensemble and hence we use Parrinello-Rahman barostat[8,9] which is similar to Nose-Hoover temperature coupling and produces true NPT ensemble.

2.2. References

(1) Frenkel, D.; Smit, B. *Understanding Molecular Simulation*; Elsevier, 2002; Vol. 50.

(2) Van Der Spoel, D.; Lindahl, E.; Hess, B.; Groenhof, G.; Mark, A. E.; Berendsen, H. J. C. *J. Comput. Chem.* **2005**, *26* (16), 1701–1718.

(3) Jorgensen, W. L.; Maxwell, D. S.; Tirado-Rives, J. *J. Am. Chem. Soc.* **1996**, *118* (15), 11225–11236.

(4) Berendsen, H. J. C.; Postma, J. P. M.; Van Gunsteren, W. F.; Dinola, A.; Haak, J. R. *J. Chem. Phys.* **1984**, *81* (8), 3684–3690.

(5) Bussi, G.; Donadio, D.; Parrinello, M. *J. Chem. Phys.* **2007**, *126* (1).

(6) Nosé, S. *Mol. Phys.* **1984**, *52* (2), 255–268.

(7) Hoover, W. G. *Phys. Rev. A* **1985**, *31* (3), 1695–1697.

(8) Parrinello, M.; Rahman, A. *J. Appl. Phys.* **1981**, *52* (12), 7182–7190.

(9) Nosé, S.; Klein, M. L. *Mol Phys* **1983**, *50* (5), 1055–1076.

Chapter 3.

Polyethylene Oxide in Solutions

3.1.Introduction

The role of amphiphilic water-soluble polymers in nanomaterial design and its application in polymer industry to biomedicine is widespread. One of the most commonly used polymers of this class is Polyethylene oxide (PEO). One of the main factors what determines the conformation of a polymer in solution is the volume interaction with solvent and therefore an unfavorable interaction (bad solvent) with solvent causes the polymer collapse whereas a favorable interaction (good solvent) with solvent leads to expanded conformation. The solubility of polymer in protic solvents(proton-donating) depends on the extend of hydrogen bonding. While the equilibrium static behavior of hydrogen bonding is studied in experiments and simulations,[1–11] not much has been studied on dynamics of hydrogen bonding and its role in dynamical behavior of polymers.[2,12–14] Even more interesting and less understood is the behavior of polymer is mixed solvents capable of forming hydrogen bonds with polymer and each other. One of the complex behavior of mixture of good solvents is the origin of cononsolvency due to competition of hydrogen bonds. In this chapter we discuss the details of all-atom simulations of the effect of dynamics of solvation of PEO in water, isobutyric acid and their mixture at different concentrations to understand its effect on PEO conformation and local chain dynamics.

While the PEO-water system has been extensively studied both in experiments and in computer simulations but in other solvents where solvent is capable of forming hydrogen bonds is not studied as extensively as in water. A polymer can behave differently in mixture of different good solvents compared to pure solution where behavior would be completely different. Experimental reports show that PEO forms helical structure in isobutyric acid[15–17] which is different from other good

solvents including water where PEO forms a coil-like structure in dilute or semi-dilute conditions. PEO is known for its 3_{10} helical conformation in crystalline state in presence of small amount of water[18–20] or under confinement of carbon nanotube[21] but not as a free chain in solutions. The helix formation in isobutyric acid hasn't been studied yet by computer simulations and still remains a subject to understand such behavior at molecular level. Here, we present the result of computer simulations of helix formation in isobutyric acid and the insightful result obtained from comparing behavior of PEO in aqueous and isobutyric acid solutions. This sort of comparison contributes to our understanding of polymer behavior in various solvents which are capable of forming hydrogen bonds with solute and/or each other. The behavior of polymer in mixed solvent may differ significantly from that in pure solvent and the conjecture drawn for mixed solvent from the knowledge of pure solvents would not suffice to explain the real properties of polymers. If the miscibility is greatly affected by the presence of polymer or solvent concentration, then the question becomes where polymer would prefer to reside in binary mixture, how the behavior would be different from one phase state to two phase state and what role hydrogen bonding plays in these circumstances.[22,23] This chapter outlines the general conformational behavior in pure water and organic solvents and the behavior of PEO in mixed isobutyric acid/water and help to increase our understanding of polymer behavior in mixture of solvent capable of forming hydrogen bonds.

3.2. Simulation Details

We performed atomistic molecular dynamics simulations of polyethylene oxide (PEO) in different solvents using the GPU version of GROMACS-4.6.5. We used the OPLS force-field[24] for isobutyric acid, benzene and hexane and the SPCE model for water. It has been discussed in literature that OPLS,[24] as well as the GROMOS model of PEO, has lower partial atom charges

than necessary to reproduce correctly the polymer behavior in general and hydration in particular, which has led to several modified models for PEO.[3,10,11,25] We followed this trend and slightly modified charges for PEO (-0.48e for oxygen and 0.06e for hydrogen) in agreement with the modified united atom model to reproduce correctly PEO conformation and other properties in different solvents, as discussed below. We studied CH_3-O-[CH_2-CH_2-O]$_n$-CH_3 chains of different lengths n=9,18,17 and 36 with most of the results described for n=36. To make PEO hydration homogeneous along the chain we used a -0.41e charge on the terminal oxygens. All bonds were constrained using the LINCS algorithm. We performed NVT simulations for the initial equilibration and NPT simulations for the production run with simulation times ranging from 20ns to 200ns (with the integration time step 2fs) depending on the system size. The system was equilibrated at T=298K and pressure 1 bar. The Berendsen barostat with the coupling constant of 1ps was used for pressure coupling. Temperature coupling was done using the Berendsen thermosat with coupling constant of 1ps, which has been extensively used in molecular dynamics simulations of PEO in aqueous solutions. Electrostatic interactions were calculated using PME (Particle-Mesh Ewald) summation. A long-range dispersion correction was applied for energy and pressure. To characterize the shape of the polymer we calculated the asphericity[26] of the chain:

$$Asphericity = \lambda_1 - \frac{1}{2}(\lambda_2 + \lambda_3) \tag{3.21}$$

where $\lambda' s$ are the principal components of the diagonalized tensor of gyration with eigenvalues in descending order $\lambda_1 \geq \lambda_2 \geq \lambda_3$. An asphericity equal to zero corresponds to a sphere and a larger asphericity reflects the deviation from a spherically symmetric shape. The trace of this diagonalized gyration tensor yields the radius of gyration as $R_g = \sqrt{\lambda_1 + \lambda_2 + \lambda_3}$. We studied the hydration of PEO by analyzing the water hydrogen bonded to polymer and the overall number of

hydrogen bonds. We used a geometrical criterion for h-bonds, (donor-acceptor distance) $r_{DA} \leq 3.5$Å and (hydrogen-donor-acceptor) $H-D-A$ angle $\leq 30°$. For calculation of the residence time of water and/or isobutyric acid hydrogen bonded to PEO, we extracted our data for the analysis every 1ps and every 10 ps, correspondingly. For visualization of chain conformation and hydration, Visual Molecular Dynamics (VMD)[27] has been used.

3.3. Result and Discussion

3.3.1. PEO in Hexane, Benzene and Water:

We first investigated the single chain PEO in pure solutions (benzene, hexane, water and isobutyric acid) and we find that PEO forms coil-like conformation in benzene and water where both water and benzene are good solvents. In isobutyric acid PEO shows nearly rod-like extended and helical-like conformation and globule like collapsed conformation in hexane in agreement to experimental observations.[15,28–32] Figure 3.31 shows the globule like conformation in hexane, coil-like in water or benzene and extended rod-like conformation in isobutyric acid. The chain dimension can be characterized by the average radius of gyration (R_g) and end to end distance (R_{end}). Table 3.31 shows the average radius of gyration and end-to-end distance for PEO in different solvents. From the table, we see that the collapse globule chain in hexane has an end-to-end distance $R_{end} = 1.6nm$, coil-like chain in water or benzene with $R_{end} \approx 3nm$ in benzene and expanded conformation in isobutyric acid shows $R_{end} \approx 6nm$. The obtained values for the radius of gyration agree well with experimental and computer simulations data.[15,17,28,32–34] Comparing the size distribution for the radius of gyration and end-to-end distance of PEO in water and in isobutyric acid shown in Figure 3.32, one can see that it follows typical Gaussian-like shape for

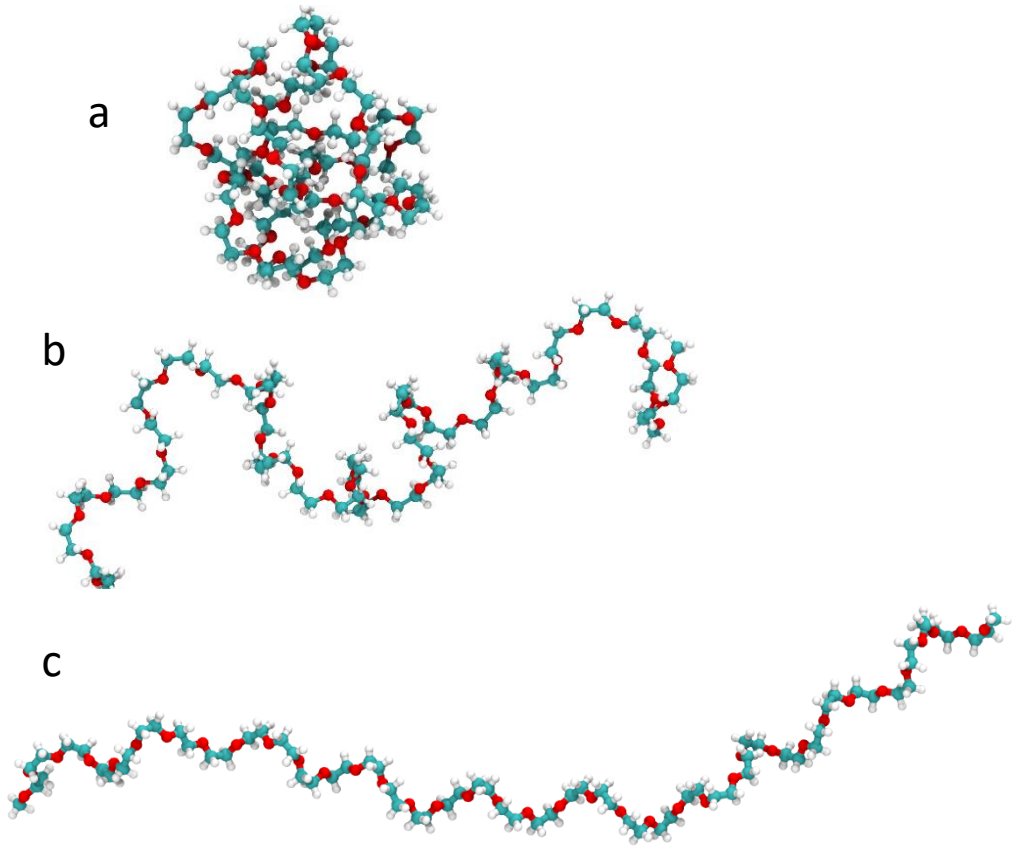

Figure:3.31: Snapshots for PEO (n=36) conformation in a) Hexane b) water and c) isobutyric acid respectively.

water and is noticeably narrower in isobutyric acid. The size distribution reflects the obvious difference in chain conformation seen in Figure 3.31. Aspect ratio$\left(\frac{R_{end}}{R_g}\right)$ is one of the shape descriptors which helps us to understand the shape of a polymer chain. A Gaussian coil has an $R_{end}/R_g = \sqrt{6} = 2.45$, while for a cylinder $R_{end}/R_g = \sqrt{12} = 3.46$. For PEO in water $R_{end}/R_g \sim 2.50 \pm 0.51$ (with a similar value in benzene) as shown in Table 3.31 which confirms that PEO behaves as a Gaussian-like chain, while in isobutyric acid $R_{end}/R_g \sim 2.87 \pm 0.22$ indicating that PEO conformation is closer to a rod-like shape, in agreement with experimental observations.[15,17,32] The asphericity, calculated using eq. 3.21, provides an even more sensitive measure of chain shape in different solvents. Indeed, as is seen from Table 1, in hexane the

asphericity for a PEO chain with 36 repeat units is about 0.2 (corresponding to a nearly perfect sphere), in water and benzene it is about 1.2-1.3, as expected for a Gaussian-like chain. In isobutyric acid the asphericity is about 3.5, consistent with the strongly non-spherical shape, as is seen in Figure 3.32b.

Table 3.31. The average end-to-end distance R_{end}, radius of gyration, R_g, aspect ratio R_{end}/R_g and asphericity (eq. 1) for PEO in different solvents.

SOLVENT	**R_{end} (nm)**	**R_g (nm)**	**R_{end}/R_g**	**Asphericity (nm^2)**
Hexane	1.61±0.6	0.75±0.08	2.15±0.78	0.21±0.13
Benzene	3.08±1.3	1.30±0.30	2.32±0.71	1.18±0.87
Water	3.42±1.0	1.35±0.19	2.50±0.51	1.31±0.62
Isobutyric Acid	5.95±0.46	2.07±0.08	2.87±0.22	3.50±0.70

One of the main factors for different PEO conformation in different solvents is the volume interaction of PEO with solvent but when the solvent is capable of forming hydrogen bond, the overall conformation will be the result of both volume interaction and hydrogen bonding. Theoretical studies always seem to consider volume interaction argument in defining various conformational behavior but not much has been discussed pertaining to the role of hydrogen bonding other than in defining phase separation or coil-globular transition. Even though both water and isobutyric are protic solvents, we yet see the significant difference in the PEO chain conformations as can be seen in figure 3.32. This indeed requires deeper investigation to fully understand the role of hydrogen bonds.

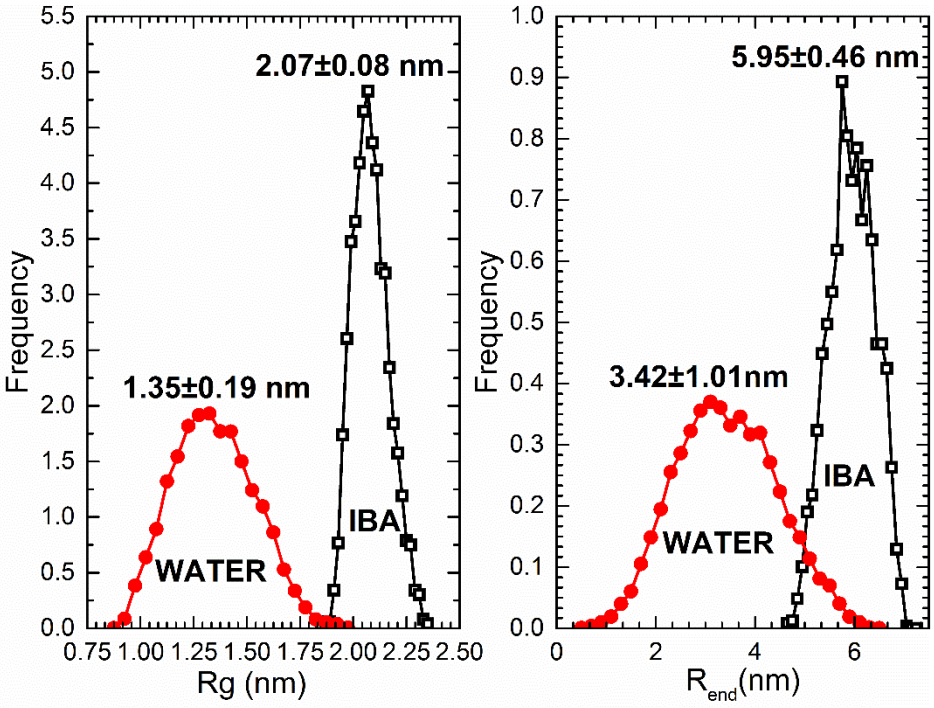

Figure 3.32: Radius of gyration R_g (a) and end-to-end distance R_{end} (b) distributions for PEO (n=36) in water (solid symbols, red) and in isobutyric acid (IBA, open symbols, black).

Hydrogen bonding and in general hydration of PEO in water is actively discussed for decades. Depending on the experimental technique used or the definition applied to computer simulations, the hydration number i.e. the number of water per repeat unit of PEO varies from 1 to 6.[1,4,5,7,8,12,35,36] We used the geometrical criteria for calculation of hydrogen bonds as explained in simulation details section 3.2. If not using geometrical criteria, one can use energy criteria for hydrogen bonding which also leads to very similar results as obtained by geometrical criteria.[37] Figure 3.33a., shows the water molecules hydrogen bonded to PEO(n=36). On average, there are 0.83 ± 0.06 hydrogen bonded water molecules and 1.2 ± 0.07 hydrogen bonds per repeat unit of PEO, as shown in Table 3.32. The PEO water hydrogen bond analysis shows two categories of hydrogen bonded water: water forming a single hydrogen bond to PEO oxygen ("singly-bonded water") and water having two hydrogen bonds with two oxygens of PEO ("doubly bound water").

The singly-bonded water has only one site bonded to PEO whereas doubly bonded water has both hydrogens bonded to PEO.

Doubly-bound water normally connects the i and i+2 oxygens of PEO, as is seen in Figure 3.33a, thereby stabilizing the bent TGT conformation of PEO chain segments, in agreement with reports on the enhancement of TGT conformers in water (compared to dimethoxymethane).[38–40] Doubly-bound water connecting i and i+2 oxygens of PEO has been previously reported in quantum

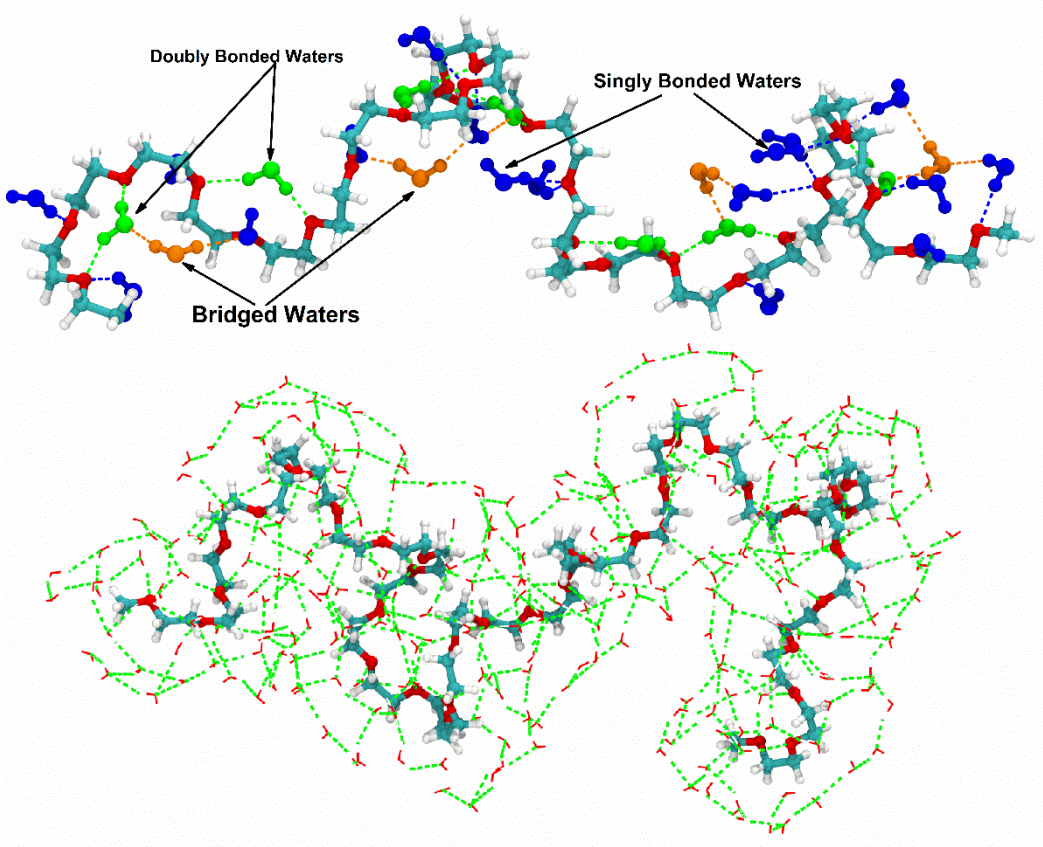

Figure 3.33: a) PEO water hydrogen bonds showing singly bonded waters (blue), doubly bonded waters (green) and bridged water molecules (orange). The dashed line represents hydrogen bonds for respective water molecules. b) Solvation layer of water (red lines) around PEO at a uniform distance from PEO. Dashed lines (green) represent hydrogen bonding between water-water as well as PEO water.

mechanical calculations as one of the most favorable water arrangements near PEO and has been suggested experimentally by results of IR spectroscopy. [41]

Comparing the number of single and doubly bonded waters to PEO, we found that singly bonded waters are 1.4 times more abundant than doubly bound waters, as is seen from Table 3.32, but the contribution to the overall number of hydrogen bonds is 1.42 times larger for doubly bonded waters. Furthermore, doubly bound waters play a major role in PEO conformation stabilization and local chain dynamics as will be discussed below. Besides doubly bonded water, some additional stabilization of the polymer conformation can come from water bridging the first hydration shell, i.e. forming two hydrogen bonds (doubly bonded) with water directly bound to PEO, as shown in Figure 3.33a. While the number of such "bridge waters" is more than 6 times smaller than number of waters directly hydrogen bonded to PEO (Table 3.32), the dynamics of these "bridge waters" can be noticeably affected by the behavior of the water in the first hydration shell. Thus, it is likely that the rotational dynamics of water directly hydrogen bonded to PEO as well as the "bridge waters" can be slower than that in bulk water, which leads to the overall value of 0.97 "slower rotating waters" per repeat unit of PEO, in agreement with NMR relaxation measurements and differential scanning calorimetry showing which suggest one bound water molecule per repeat unit of PEO.[42–45]

In addition to water molecules hydrogen bonded to PEO, there are also water molecules in direct contact with PEO but forming no hydrogen bonds. Using the same distance criterion as for hydrogen bonding, i.e. accounting all water molecules within 3.5Å from any atom of the polymer, we arrived at ~5.82 water molecules per repeat unit of PEO, which matches the experimentally determined hydration number of 5.5 based on dielectric relaxation and ultrasonic

measurements.[7,46,47] These waters, which include hydrogen bonded waters, can be viewed as the PEO hydration shell, as shown in Figure 3.33b. Several experimental reports[1,9,36,48] arrived at a hydration number of ~ 2.4 water molecules per repeat unit of PEO using acoustic, DSC and IR measurements. If we account for water molecules hydrogen bonded to PEO plus water molecules hydrogen bonded to them, then such a hydration shell would consist of 2.49 ± 0.2 water molecules per repeat unit. Also, if we consider all water separated by 3.5Å from PEO, then we arrive at 1.5 water per repeat unit of PEO. These hydration numbers are consistent with the experimentally obtained values that range from 1.6 to 3.7.[1,48,49]

Table 3.32: The average number of hydrogen bonds, singly and doubly bonded water, bridged water, total water and hydrogen bonded isobutyric acid molecules per repeat unit of PEO.

Solvent	***h-bond number***	***Doubly Bonded water***	***Singly Bonded solvent***	***Total directly h-bonded water***
First Shell Water	1.213±0.073	0.347±0.056	0.489±0.097	0.836±0.060
Bridged Water	0.201±0.092	0.071±0.040	-	
Isobutyric acid	0.847±0.050	-	0.847±0.050	

Besides the hydration number, which represents the equilibrium number of water molecules hydrogen bonded or otherwise interacting with PEO in aqueous media, the dynamics of the water near the PEO can be equally important in understanding properties of PEO. As the lifetime of a hydrogen bond is rather small,[13,50] it is more informative to calculate the residence time of water hydrogen bonded to any oxygen of PEO. To this end we marked all water molecules hydrogen bonded to PEO at time t=0 and calculated the following correlation function:

$$C(t) = \left\langle \frac{N_w(t)}{N_w(0)} \right\rangle \qquad (3.32)$$

where $N_W(0)$ is total number of water molecules hydrogen bonded to PEO at time $t = 0$ and $N_w(t)$ is the number of water molecules among those originally marked which remain hydrogen bonded to (not necessary to the same oxygen of) PEO at time t. The ensemble average of the residence time autocorrelation function for singly bonded, doubly bonded and total water molecules hydrogen bonded to PEO are shown in figure 3.34 as functions of time. The residence time for the total water molecules hydrogen bonded to PEO include all water molecules regardless whether they are singly or doubly bound to PEO.

As is seen from figure 3.34 the correlation function C(t) for singly bound water decreases most rapidly, while C(t) for the total water and doubly-bound water decays more slowly. In all cases the C(t) dependences can be fitted by a triple exponential decay function

$$C(t) = A_1 e^{-\frac{t}{\tau_1}} + A_2 e^{-\frac{t}{\tau_2}} + A_3 e^{-\frac{t}{\tau_3}} \qquad (3.33)$$

where $A_1, A_2, A_3 = 1 - A_1 - A_2, \tau_1, \tau_2$ and τ_3 are fitting parameters, which are listed in Table 3. As is seen from Table 3, about 30% of singly bonded water is short-lived with τ_1=12ps (which is of the order of the hydrogen bond lifetime[13]), while the majority (~50%) of singly bound water has a residence life time of $\tau_2 \sim 70ps$ and ~20% of long-lived singly bound water with $\tau_3 \sim 330ps$. The latter likely corresponds to the water bridge sequence shown in figure 3.33a. Among doubly bound waters the majority has a residence life time of $\sim 120ps$ and about 20% of doubly bound water is long-lived with $\tau_2 = 440p$s. As expected, doubly bound water has a significantly longer lifetime compared to singly bound water: on average the residence time of doubly bound water nearly twice longer than that for singly bound water, which confirms its stabilizing role in e.g.

helix formation under confinement.[21] The analysis of all water hydrogen bonded to PEO (regardless singly or doubly bound) shows that there is about 18% of short-lived water with $\tau_1 = 13ps$, similar to singly bound water, the majority of hydrogen bonded water has a residence lifetime of $\sim 100ps$, which is only slightly shorter than the lifetime of doubly bound water and there is also about 18% of long-lived water with $\tau_3 = 420ps$, also consistent with doubly bound water.

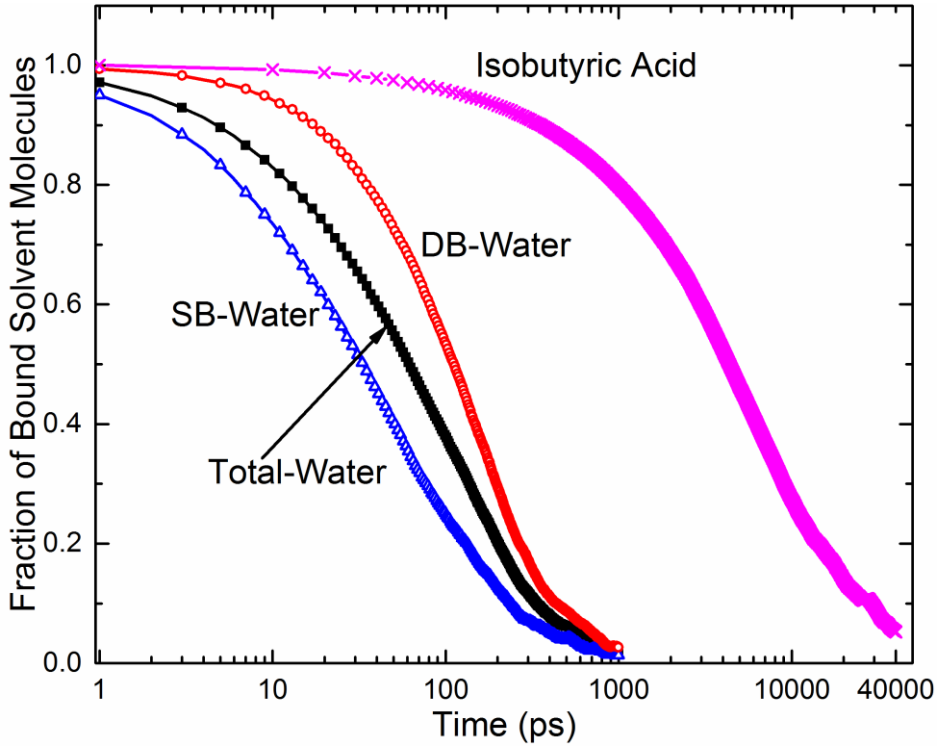

Figure 3.34: Residence time autocorrelation function eq. 3.32 of singly bonded (open triangles), doubly bonded (open circles) and total water hydrogen bonded to PEO (solid squares) and residence time autocorrelation function for isobutyric acid hydrogen bonded to PEO (crosses).

Table 3.33: Fitting parameters for eq. 3.33 for the hydrogen bonded solvent residence time correlation functions C(t).

Type	A_1	τ_1(ps)	A_2	τ_2(ps)	A_3	τ_3(ps)
Singly Bound Water	0.32	12.0±0.3	0.49	69.8±0.9	0.18	332.9±3.2
Doubly Bound Water	0.80	124.0±0.9	0.20	443.6±6.5	-	-
Total Bound Water	0.18	12.9±0.4	0.64	101.5±0.7	0.18	422.1±3.6
Bound Isobutyric Acid	0.06	278.8±12.0	0.61	4522.3±14.7	0.33	22687.0±75.7

Compared to aqueous solution, PEO in isobutyric acid has a more expanded conformation, as discussed above and as is seen in figure 3.31. Furthermore, in agreement with experimental data[15,17] PEO has more helical conformation, at least locally, as is shown in figure 3.35. The helical conformation is rather similar to that for PEO in the crystal state.[19,20,51,52] Indeed the period of the helix in isobutyric acid, 19.3Å is only slightly smaller and somewhat wider (3.9Å in diameter) than that in crystal state (19.48Å period with 3.3-3.5Å in diameter)[51]. The helix rise (i.e. the pitch per repeat unit) of 2.4Å is smaller than in crystal state (2.78Å), but rather similar to the helix formed by PEO inside narrow carbon nanotubes (2.5Å helix rise)[21] which in all cases corresponds to the so-called 3_{10} helix in Bragg's nomenclature. Similar to what we have found in the case of PEO inside narrow carbon nanotubes, helix stabilization is due to the formation of stable hydrogen bonds, as shown in figure 3.35. In the case of isobutyric acid there are on average 0.85 ± 0.05 hydrogen bonds per repeat unit of PEO, i.e. practically each oxygen forms one hydrogen bond with an isobutyric acid molecule. These hydrogen bonds are quite stable. Indeed, the residence time autocorrelation function eq. 3.32 for isobutyric acid exhibits a very slow decay, as is seen in

figure 3.34 and can be fitted by a triple-exponential decay function with the fitting parameters shown in Table 3.33. As is seen, the majority (~60%) of isobutyric acid molecules has a residence lifetime of ~4500ps which is 45 times larger than that for water (100ps) with 30% of isobutyric acid having even longer residence lifetime of ~23000 ps. This can be attributed to larger size of the isobutyric acid molecule, which diffuses much slower than water, but can also be due to a different energy of the hydrogen bond. Despite the stable hydrogen bonding, the helical conformation PEO in isobutyric acid is not universal – helical sections alternated with folded and deformed sections of the chain, as is seen in figure 3.35. The main reason is the entropic gain corresponding to less regular conformations.

The observed difference in hydrogen bond stability between PEO-water and PEO-isobutyric acid (Figure 3.34) manifests itself not only in conformational differences (Figure 3.31), but also in chain flexibility. High flexibility of PEO in water is believed to be one of the reasons for PEO exceptional capability to inhibit protein adsorption, as the high segmental mobility of the polymer

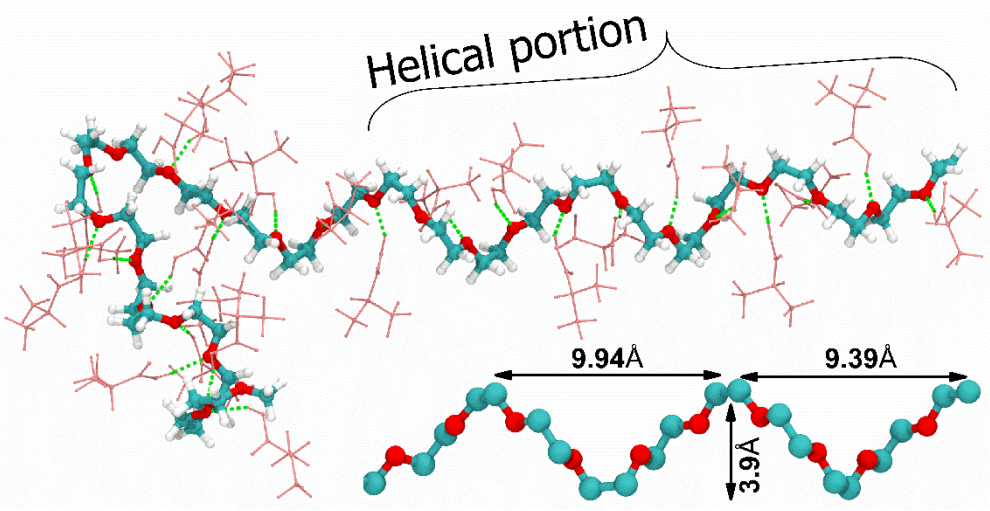

Figure 3.35: Simulation snapshot of PEO conformation for a portion of the chain and hydrogen bonding (green dashed lines) between PEO and isobutyric acid (shown in pink). The lower picture shows a helical portion of the PEO chain (hydrogens are omitted for clarity).

precludes stable protein attachment.[53] As a measure of the rotational segmental polymer dynamics, we calculated the orientation autocorrelation function for end-monomer O-C-C-O vector, shown in figure 3.36:

$$P(t) =< 0.5(3Cos^2\theta - 1)> \qquad (3.34)$$

where $Cos\theta = \boldsymbol{u_i}(0) \cdot \boldsymbol{u_i}(t)$ and $\boldsymbol{u}_i = \boldsymbol{r}_{O_i} - \boldsymbol{r}_{O_{i+1}} / \left|\boldsymbol{r}_{O_i} - \boldsymbol{r}_{O_{i+1}}\right|$ is the unit vector along the last (O-C-C-O) monomer. In practice, we have averaged the contribution from both ends. The autocorrelation functions for PEO in water and in isobutyric acid are compared in figure 3.36. As is seen, the autocorrelation function sharply decays for PEO in water indicating high flexibility. The correlation function can be successfully fitted by a double exponential ($P(t) = A_0 + A_1 e^{-\frac{t}{\tau_1}} + A_2 e^{-\frac{t}{\tau_2}}$), with fitting parameters listed in Table 4. As is seen, the

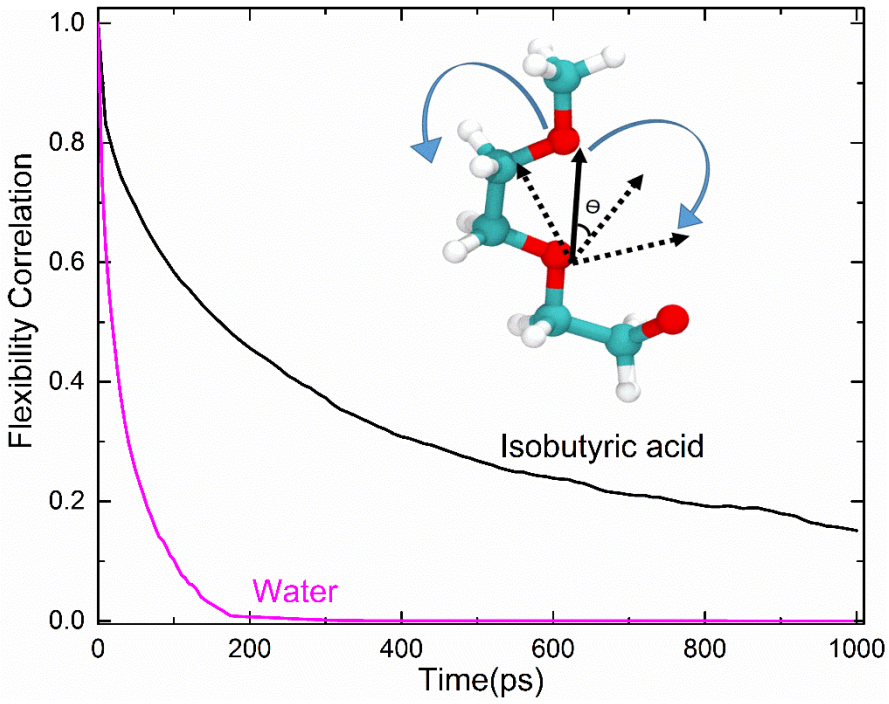

Figure 3.36: Tail orientation autocorrelation function for PEO in water and isobutyric acid. The inset shows the schematic representation of the tail O-C-C-O vector for which autocorrelation function eq. 3.34 is calculated.

fastest component has a lifetime comparable to that of a hydrogen bond, while the main relaxation time is about 50ps, demonstrating that only a short time scale is sufficient to dissipate any correlations with initial tail conformation.

As for isobutyric acid, the tail orientation autocorrelation function, eq. 3.34, exhibits a noticeably slower decay compared to water (figure 3.36). As is seen in Table 3.34, The characteristic decay time for isobutyric acid is one order of magnitude larger than that for water which is consistent with both the slower solvent diffusion and longer residence time of hydrogen bonds in isobutyric acid. A higher rigidity of PEO helix in isobutyric acid has also been experimentally reported.[15,17]

Table 3.34: Fitting parameters of double exponential decay function for the PEO tail orientation autocorrelation function eq. 3.34 in water and isobutyric acid.

Solvent	**A_0**	**A_1**	**τ_1 (ps)**	**A_2**	**τ_2(ps)**
Water	0	0.30	5.6±0.2	0.70	49.2±0.3
Isobutyric acid	0.02	0.42	38.6±3.6	0.56	676.1±13.6

PEO in water/isobutyric acid mixed solvent

As is seen from the discussion above, the PEO chain conformation and its rotational segmental dynamics are dependent on solvent properties – in water PEO forms a coil-like structure, which is very flexible with a rather short residence time of hydrogen bonded water, while in isobutyric acid PEO exhibits a non-ideal helical structure with folds and distortions, with a considerably longer residence time of hydrogen bonded solvent and slower chain mobility, accordingly. Having this obvious difference in behavior, it is informative to analyze the PEO conformation in mixed water/isobutyric acid solvent. In accordance with experimental data[16,54–56] we observe that addition of up to about 10 wt.% of water to isobutyric acid results in homogeneously mixed solution, which

phase separates at any higher water content up to about 95wt% of water, when solution becomes miscible again (figure 3.37).At low water content (<10wt.%) the PEO conformation remains

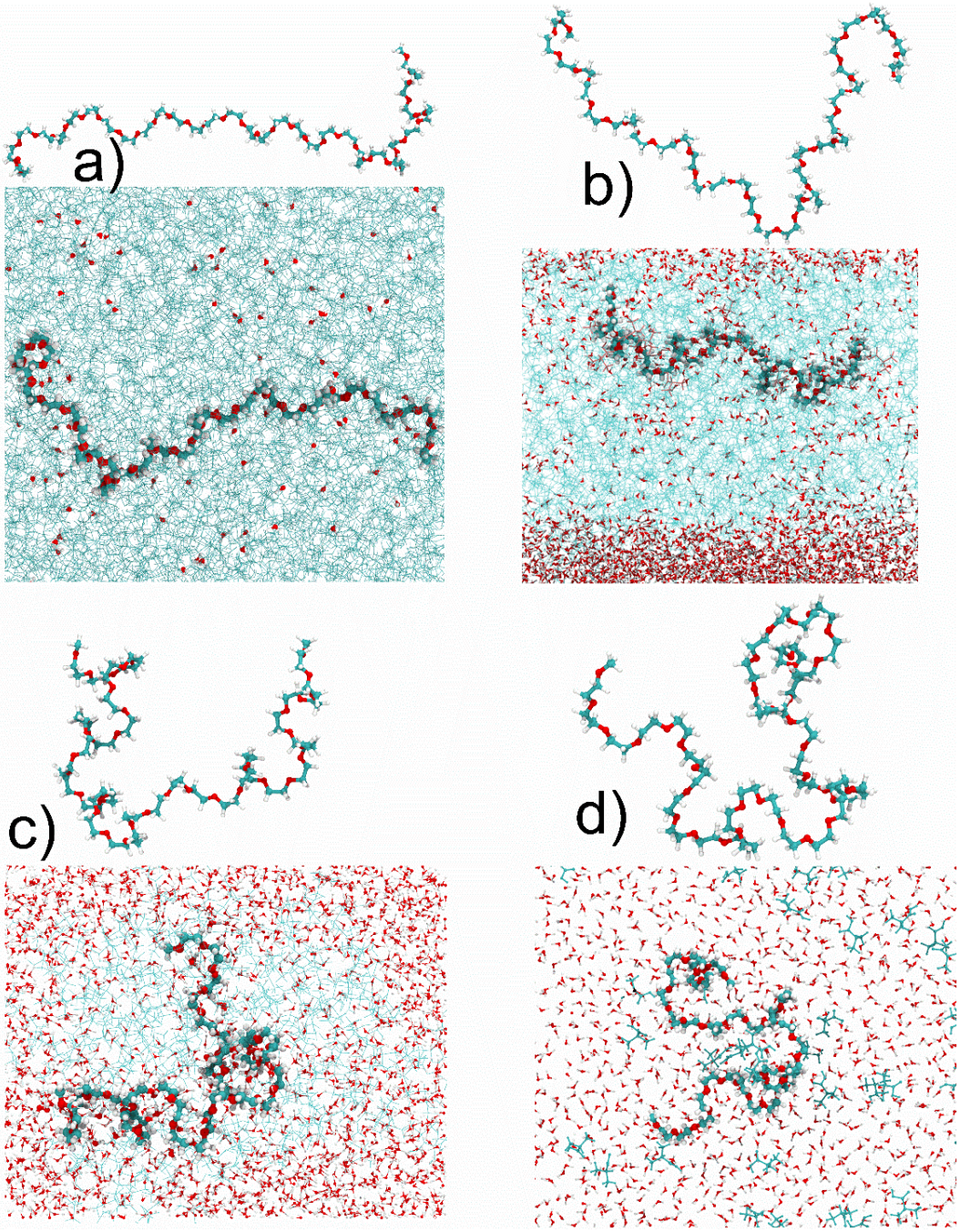

Figure 3.37: Computer simulations snapshots of PEO in mixed water/isobutyric acid solutions with weight fraction of water: 0.2 (a), 0.5 (b), 0.95 (c) and 0.98 (d). Isobutyric acid is shown in blue color.

helical and in general very similar to that in pure isobutyric acid (figure 3.37), i.e. R_g and R_{end} remain practically unchanged, as is seen in figure 3.38 and in supplemental material in ref 59.

In the phase-separation region (with water content between 10wt% and 95wt%), PEO resides in isobutyric-rich phase, as is seen in figure 3.37, in agreement with experimental observations.[16] With an increase in water content in phase separated region chain bending becomes more pronounced and defects in the helical regions become more common, as more water finds its way to the PEO vicinity (figures 3.37,3.38). Accordingly, the end-to-end distance (and R_g) of PEO decreases, as is seen in figure 3.38. At the upper boundary of phase-separated region (~90-95wt% of water), the PEO size becomes affected by the size of a droplet of the isobutyric-rich phase. Furthermore, upon development of phase separated phases from a homogeneous solution the PEO chain acts as a nucleating agent for the isobutyric-rich phase accelerating the process, as can be seen in supplementary of ref. 59. At high water content (>95wt%) the PEO chain retains no helical sections and behaves in a similar manner as in pure water.

To better understand solvent organization around the PEO molecules we analyzed the hydrogen bonding of isobutyric acid and water to PEO in mixed solvent. As is seen from figure 3.38, addition of a small amount of water to isobutyric acid, results in a corresponding substitution of isobutyric acid hydrogen bonded to PEO by water. The hydrogen bonded water mostly forms two hydrogen bonds with PEO oxygens (as usual, connecting the i and i+2 oxygens of PEO), as shown in figure 8a, to maintain the maximally possible degree of hydrogen bonding in this mixed solvent. An increase in water content systematically decreases the fraction of isobutyric acid molecules hydrogen bonded per repeat unit of PEO and stabilizes at about 0.2 molecules per repeat unit of PEO in the phase separated region. At the same time the fraction of hydrogen bonded water increases to 0.6 per repeat unit of PEO with the overall number of solvent molecules hydrogen

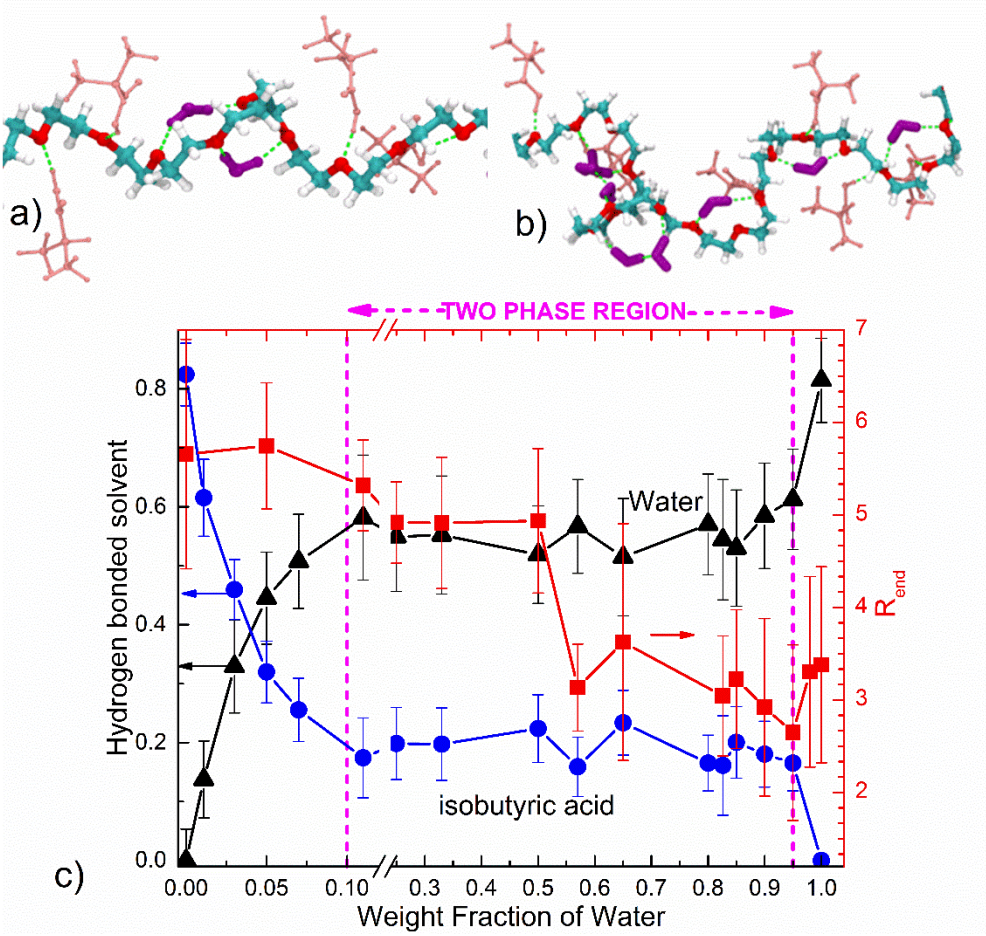

Figure 3.38: Molecular dynamics simulation snapshots of a section of PEO chain with hydrogen bonded water and isobutyric acid in a) one-phase region (~2 wt.% of water) and b) in phase separated region (50 wt% of water). c) Fraction of isobutyric acid and water hydrogen bonded to PEO and end-to end distance of PEO R_{end} as a function of the weight fraction of water in mixed water/isobutyric acid solvent. Phase separated region is indicated.

bonded to PEO remaining at about 0.8 per repeat unit. We note that in some cases hydrogen bonding of both water and isobutyric acid to the same oxygen of PEO is observed resulting in an increase of the number of hydrogen bonds per repeat unit from 0.85 in isobutyric acid to 1.12 in mixed water/isobutyric acid solution (supplementary in ref 59). In the phase separated region the fraction of both isobutyric acid and water hydrogen bonded to PEO remains practically unchanged, as is seen in figure 3.38. In this region, short sequences of water hydrogen bonded to PEO alternate

with sections of PEO with hydrogen bonded isobutyric acid, as is seen in figure 3.38b. Having a sequence of water hydrogen bonded to PEO increases chain bending and diminishes the PEO helicity, resulting a systematic decrease of the end-to-end distance (figure 3.38) and asphericity (supplementary in ref 59). At the upper boundary of the phase separated region, PEO exhibits only occasional helix-like sections with the overall size of the chain being close to that in aqueous solutions. In the water-rich solution with a small fraction of isobutyric acid (<5wt%) the fraction of isobutyric acid hydrogen bonded to PEO declines and fraction of water hydrogen bonded to PEO reaches the level observed in aqueous solutions. The PEO size, which is not limited anymore by the size of isobutyric-rich region, slightly increases and the chain assumes more spherically-symmetric form, as confirmed by further reduction in asphericity (supplementary in ref 59).

As the dynamic properties of PEO and hydrogen bonded solvents are found to be distinctly different for PEO in aqueous solution and in isobutyric acid (figures 3.34, 3.36), it is interesting to test how mixing of these solvents affects these dynamic properties. The residence time autocorrelation function for water and isobutyric acid hydrogen bonded to PEO in homogenous and phase separated mixed solvent is shown in figure 3.39a. As is seen at low water content (<10 wt.%) in the one-phase region the residence time of both solvents hydrogen bonded to PEO are rather similar to that for pure isobutyric acid. While this can be expected for the residence time of isobutyric acid, for hydrogen bonded water it is a surprising result, as water spends much less time interacting with PEO in aqueous solution (figure 3.34, Table 3.33). In the homogeneous mixed solvent, the residence time of water becomes even somewhat longer than that of isobutyric acid, as is seen in figure 3.39a. The main reason for this effect is that the low water concentration precludes rapid water diffusion through the solution; so, once water finds its way to PEO it remains

interacting with it for a prolonged period of time, comparable to that for isobutyric acid. With an increase of water content, the residence time for both solvents hydrogen bonded to PEO starts to decrease with the water residence time still exceeding that for isobutyric acid for the majority of the phase separated region (figure 3.39a). Only close to the upper boundary of the phase separated region, when the isobutyric-rich region becomes rather small thereby allowing prompt transport of water from the surrounding water-rich phase, does the residence time of water become smaller than that for isobutyric acid. The isobutyric acid residence time is also noticeably smaller than in pure solvent. Finally, in the homogeneous water-rich mixed solvent the residence time of water becomes comparable to that in aqueous solution, while the residence time for isobutyric acid is much smaller than that in pure isobutyric acid.

As discussed above, the overall segmental mobility of the chain is related to the residence time of hydrogen bonded solvent with PEO being very flexible in water and less so in isobutyric acid (figure 3.36). Thus, it comes as no surprise that in mixed solvent addition of water to the isobutyric acid results in a systematic enhancement of the PEO chain segmental mobility, as judged by the tail orientation autocorrelation function shown in figure 3.39b. As is seen from the fitting parameters for the bi-exponential decay function in the isobutyric-rich mixed homogeneous solution shown in Table 3.35, the main relaxation time is only slightly smaller than that in pure isobutyric acid, which is consistent with long residence time of both solvents hydrogen bonded to PEO (figure 3.39a). In the phase-separated region when the residence time for both hydrogen bonded solvents starts to decrease, the segmental mobility of PEO starts to increase and the main lifetime decreases by half in 50:50 (by weight) mixed solvent. At higher water content the residence time of both solvents become comparable to aqueous solution and accordingly the PEO segmental mobility approaches its level in aqueous solution as well. Thus, as is seen from figure

3.39 mixing two hydrogen bond-donating solvents affects both the chain conformation and its dynamic properties, demonstrating how addition of a solvent can be used to fine-tune the corresponding polymer properties.

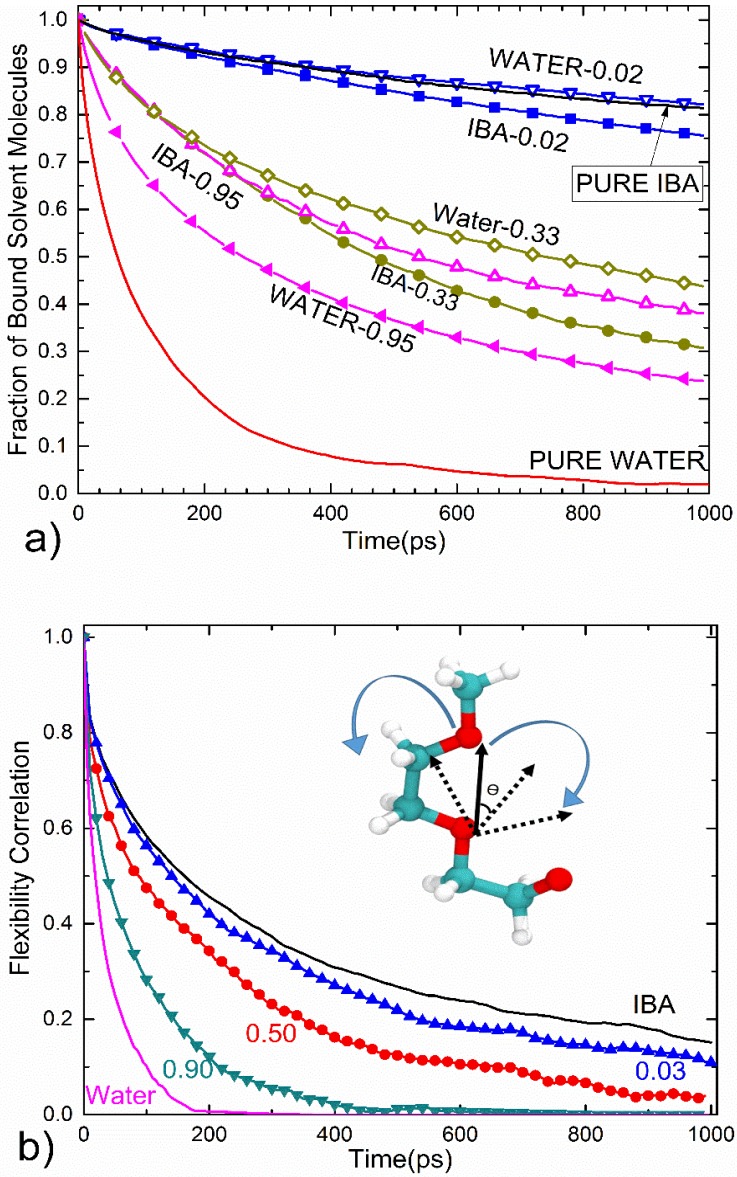

Figure 3.39: a) Residence time autocorrelation function for water and isobutyric acid (IBA) hydrogen bonded to PEO in mixed isobutyric acid/water solvent (water weight fraction is indicated near the curves) and corresponding pure solvents. b) Tail orientation autocorrelation function for PEO in mixed isobutyric acid/water solvent (water weight fraction is indicated near the curves) and corresponding pure solvents. The inset shows the schematic representation of the tail O-C-C-O vector for which autocorrelation function eq. 3.34 is calculated.

Table 3.35: Fitting parameters of double exponential decay function for the PEO tail orientation autocorrelation function eq. 3.34 in mixed water/isobutyric acid solution.

System	A_0	A_1	τ_1(ps)	A2	τ_2(ps)
Pure-IBA	0.02	0.42	38.6±3.6	0.56	676.1±13.6
3%Water	0	0.34	29.4±5.4	0.66	506.4±14.6
50%Water	0.03	0.30	12.9±1.1	0.67	254.1±4.9
90%Water	0	0.32	10.0±0.4	0.68	115.7±1.0
Pure-Water	0	0.30	5.6±0.2	0.70	49.2±0.3

3.4. Conclusions

Using atomistic molecular dynamic simulations, we investigated the role that hydrogen bonding plays in the conformational and segment dynamic behavior of polyethylene oxide in two hydrogen bonding–capable solvents, water and isobutyric acid. In agreement with experimental data,[15,16,29] we found that at room temperature PEO forms coil-like structure in aqueous solution and a rod-like 3_{10} helical structure in isobutyric acid, analogous to PEO helix formed in crystal state or under confinement in narrow carbon nanotube[19–21,51,52] (figure 3.31). The polymer conformation was characterized by calculating the radius of gyration, end to end distance and asphericity (Table 1), which confirm the different spatial arrangements of the polymer in these solvents. To obtain molecular insights into the origin of these differences in chain conformation we investigated the solvent arrangement near the polymer and characterized equilibrium and dynamic properties of hydrogen bonded solvent. We found that in both solvents there is on average about one solvent molecule hydrogen bonded to the repeat unit of the polymer, but the number of hydrogen bonds is 1.4 times larger in water since about 40% of hydrogen bonded water forms two hydrogen bonds (doubly bound water) with PEO (Table 2). The existence of doubly bound water was predicted in quantum mechanical calculations and suggested by experimental data.[41,57] The extent of PEO hydration can be defined in different ways: from directly hydrogen bonded (or bridged) water to

second shell water or water being in direct contact with polymer leading in agreement with experimental using different techniques.[1,4,45,48,49,58,5,7–9,33,36,43,44] While the number of solvent hydrogen bonded to PEO is comparable in isobutyric acid and water, the strength of hydrogen bonding and dynamics of hydrogen bonded solvent may not be the same. We demonstrate that the residence time of hydrogen bonded isobutyric acid exceeds that for water by more than 40 times (figure 3.34 and Table 3.33) leading to more stagnant environment for the polymer, which can be the key factor in stabilization of the helical structure, as our previous work on PEO helix stabilization under nanotube confinement shows.[21] We also characterized and compared segmental orientational dynamics for the PEO chain in isobutyric acid and water and found that the relaxation time for tail segment rotational autocorrelation function more than one order of magnitude larger in isobutyric acid than in water (figure 3.36, Table 3.34). This implies that the slower dynamics of the hydrogen bonded solvent, as evidenced by the longer residence time for isobutyric acid, affects both the overall polymer chain conformation and its dynamics including rotational mobility, which is important for interactions with other (bio)macromolecules.

Given the different conformation and dynamic behavior of PEO in pure isobutyric acid and water, it was informative to investigate PEO in isobutyric acid/water binary solutions. In agreement with experimental data,[16,54] we found that isobutyric acid and water are miscible only in a relatively narrow isobutyric acid -rich composition range and in the phase separated region PEO resides in the isobutyric acid – rich phase (figures 3.37-3.38). For most of the composition range, PEO conformation somewhat resembles that in pure isobutyric acid and exhibits obvious helical sections. However, with an increase of water content the residence time of both solvents starts to decline (figure 3.39) implying larger segmental mobility and a more noticeable chain bending/distortion of the helical structure. Perhaps the most interesting result is recruitment of a larger than composition-average fraction of water molecules to the vicinity of PEO - as is seen in figure 3.38 the fraction of hydrogen bonded water more than twice exceeds that of isobutyric acid in the phase separated region even though PEO resides with isobutyric acid-rich phase. This implies that polymer behavior in mixed solvent is far more complex and does not necessary is an extrapolation of what can be expect based on its behavior in each individual solvent. This is an interesting area of research, which deserves further attention in the future.

These results demonstrate the importance of not only the equilibrium hydrogen bonding properties, but also the dynamics of the hydrogen bonded solvent in determining polymer equilibrium properties (e.g. conformation, size, solubility) and polymer dynamics. Thus, to achieve a better understanding of the behavior of any hydrogen bonding-capable polymer system and to be able to predict and design new materials with desired properties, it is important in future research to characterize experimentally and to predict theoretically not only equilibrium properties, but also dynamics of hydrogen bonding.

3.5. References

(1) Sagawa, N.; Shikata, T. *J. Phys. Chem. B* **2013**, *117* (37), 10883–10888.

(2) Ono, Y.; Shikata, T. *J. Am. Chem. Soc.* **2006**, *128* (31), 10030–10031.

(3) Shang, B. Z.; Wang, Z.; Larson, R. G. **2008**, 2888–2900.

(4) Dormidontova, E. E. *Macromolecules* **2004**, *37* (20), 7747–7761.

(5) Dormidontova, E. E. *Macromolecules* **2002**, *35* (3), 987–1001.

(6) Duan, Y.; Wu, C.; Chowdhury, S. S.; Lee, M. C.; Xiong, G.; Zhang, W.; Yang, R.; Cieplak, P.; Luo, R.; Lee, T.; Caldwell, J.; Wang, J.; Kollman, P. *J. Comput. Chem.* **2003**, *24* (16), 1999–2012.

(7) Żwirbla, W.; Sikorska, A.; Linde, B. B. J. *J. Mol. Struct.* **2005**, *743* (1–3), 49–52.

(8) Smith, G. D.; Bedrov, D. *Macromolecules* **2002**, *35* (14), 5712–5719.

(9) Branca, C.; Magazù, S.; Maisano, G.; Migliardo, F.; Migliardo, P.; Romeo, G. *J. Phys. Chem. B* **2002**, *106* (39), 10272–10276.

(10) Samanta, S.; Hezaveh, S.; Milano, G.; Roccatano, D. *J. Phys. Chem. B* **2012**, *116* (17), 5141–5151.

(11) Fuchs, P. F. J.; Hansen, H. S.; Hünenberger, P. H.; Horta, B. A. C. *J. Chem. Theory Comput.* **2012**, *8* (10), 3943–3963.

(12) Shikata, T.; Okuzono, M.; Sugimoto, N. *Macromolecules* **2013**, *46* (5), 1956–1961.

(13) Borodin, O.; Bedrov, D.; Smith, G. D. *J. Phys. Chem. B* **2002**, *106* (20), 5194–5199.

(14) Deshmukh, S. A.; Sankaranarayanan, S. K. R. S.; Suthar, K.; Mancini, D. C. *J. Phys. Chem. B* **2012**, *116* (9), 2651–2663.

(15) Alessi, M. L.; Norman, A. I.; Knowlton, S. E.; Ho, D. L.; Greer, S. C. *Macromolecules*

2005, *38* (22), 9333–9340.

(16) Castellanos, P.; Norman, A. I.; Greer, S. C. *J. Phys. Chem. B* **2006**, *110* (44), 22172–22177.

(17) Norman, A. I.; Fei, Y.; Ho, D. L.; Greer, S. C. *Macromolecules* **2007**, *40* (7), 2559–2567.

(18) Seebach, D.; Zass, E.; Bernd Schweizer, W.; Thompson, A. J.; French, A.; Davis, B. G.; Kyd, G.; Bruno, I. J. *Angew. Chemie - Int. Ed.* **2009**, *48* (51), 9596–9598.

(19) French, A. C.; Thompson, A. L.; Davis, B. G. *Angew. Chemie Int. Ed.* **2009**, *48* (7), 1248–1252.

(20) Maranski, K.; Andreev, Y. G.; Bruce, P. G. *Angew. Chemie Int. Ed.* **2014**, *53* (25), 6411–6413.

(21) Dahal, U. R.; Dormidontova, E. E. *Phys. Rev. Lett.* **2016**, *117* (2), 027801.

(22) Toumi, A.; Bouanz, M.; Gharbi, A. *Chem. Phys. Lett.* **2002**, *362* (August), 567–573.

(23) Ouerfelli, N.; Kouissi, T.; Zrelli, N.; Bouanz, M. *J. Solution Chem.* **2009**, *38* (8), 983–1004.

(24) Jorgensen, W. L.; Maxwell, D. S.; Tirado-Rives, J. *J. Am. Chem. Soc.* **1996**, *118* (15), 11225–11236.

(25) Horta, B. A. C.; Fuchs, P. F. J.; van Gunsteren, W. F.; Hünenberger, P. H. *J. Chem. Theory Comput.* **2011**, *7* (4), 1016–1031.

(26) Arkın, H.; Janke, W. *J. Chem. Phys.* **2013**, *138* (5), 054904.

(27) Humphrey, W.; Dalke, A.; Schulten, K. *J. Mol. Graph.* **1996**, *14* (1), 33–38.

(28) Devanand, K.; Selser, J. C. *Nature* **1990**, *343* (6260), 739–741.

(29) Harris, J. M. In *Poly(Ethylene Glycol) Chemistry*; Springer US: Boston, MA, 1992; pp 1–14.

(30) Bailey, F. E.; Koleske, J. V. In *Poly (ethylene Oxide)*; Elsevier, 1976; pp 29–86.

(31) Harris, J. M.; Chess, R. B. *Nat. Rev. Drug Discov.* **2003**, *2* (3), 214–221.

(32) Devanand, K.; Selser, J. C. *Macromolecules* **1991**, *24* (22), 5943–5947.

(33) Hezaveh, S.; Samanta, S.; Milano, G.; Roccatano, D. *J. Chem. Phys.* **2012**, *136* (12), 124901.

(34) Lee, H.; Venable, R. M.; MacKerell, A. D.; Pastor, R. W. *Biophys. J.* **2008**, *95* (4), 1590–1599.

(35) Shikata, T.; Takahashi, R.; Sakamoto, A. *J. Phys. Chem. B* **2006**, *110* (18), 8941–8945.

(36) Huang, L.; Nishinari, K. *J. Polym. Sci. Part B Polym. Phys.* **2001**, *39* (5), 496–506.

(37) Van Der Spoel, D.; Van Maaren, P. J.; Larsson, P.; T??mneanu, N. *J. Phys. Chem. B* **2006**, *110* (9), 4393–4398.

(38) Wada, R.; Fujimoto, K.; Kato, M. *J. Phys. Chem. B* **2014**, *118* (42), 12223–12231.

(39) Sasanuma, Y.; Sugita, K. *Polym. J.* **2006**, *38* (9), 983–988.

(40) Fischer, J.; Paschek, D.; Geiger, A.; Sadowski, G. *J. Phys. Chem. B* **2008**, *112* (8), 2388–2398.

(41) Begum, R.; Hiroatsu Matsuura, and. *J. Chem. Soc. Faraday Trans.* **1997**, *93* (21), 3839–3848.

(42) Hey, M. J.; Ilett, S. M. *J. Chem. Soc. Faraday Trans.* **1991**, *87* (22), 3671–3675.

(43) Lüsse, S.; Arnold, K. *Macromolecules* **1996**, *29* (12), 4251–4257.

(44) Wu, J.; Chen, S. *Langmuir* **2012**, *28* (4), 2137–2144.

(45) Hey, M. J.; Ilett, S. M.; Mortimer, M.; Oates, G. *J. Chem. Soc. Faraday Trans.* **1990**, *86* (14), 2673–2674.

(46) Kaatze, U.; Gottmann, O.; Podbielski, R.; Pottel, R.; Terveer, U. *J. Phys. Chem.* **1978**, *82* (1), 112–120.

(47) Bieze, T. W. N.; Barnes, A. C.; Huige, C. J. M.; Enderby, J. E.; Leyte, J. C. *J. Phys. Chem.* **1994**, *98* (26), 6568–6576.

(48) Hager, S. L.; Macrury, T. B. *J. Appl. Polym. Sci.* **1980**, *25* (8), 1559–1571.

(49) Sato, T.; Niwa, H.; Chiba, A.; Nozaki, R. *J. Chem. Phys.* **1998**, *108* (10), 4138–4147.

(50) Rapaport, D. C. *Mol. Phys.* **1983**, *50* (5), 1151–1162.

(51) Takahashi, Y.; Tadokoro, H. *Macromolecules* **1973**, *6* (5), 672–675.

(52) Seebach, D.; Zass, E.; Schweizer, W. B.; Thompson, A. J.; French, A.; Davis, B. G.; Kyd, G.; Bruno, I. J. *Angew. Chemie Int. Ed.* **2009**, *48* (51), 9596–9598.

(53) Torchilin, V. P.; Trubetskoy, V. S. *Adv. Drug Deliv. Rev.* **1995**, *16* (2–3), 141–155.

(54) Greer, S. C. *Phys. Rev. A* **1976**, *14* (5), 1770–1780.

(55) Zhuang, Z.; Casielles, A.; Cannell, D. *Phys. Rev. Lett.* **1996**, *77* (14), 2969–2972.

(56) Venkataraman, T. S.; Narducci, L. M. *J. Phys. C Solid State Phys.* **1977**, *10* (15), 2849–2861.

(57) Wahab, S. A.; Harada, T.; Matsubara, T.; Aida, M. *J. Phys. Chem. A* **2006**, *110* (3), 1052–1059.

(58) Branca, C.; Magazù, S.; Maisano, G.; Migliardo, P.; Villari, V. *J. Phys. Condens. Matter* **1998**, *10* (45), 10141–10157.

(59) Dahal, U. R.; Dormidontova, E. E. *Phys. Chem. Chem. Phys.* **2017**, *19* (15), 9823–9832.

Chapter 4

Polyethylene Oxide Under Nanoconfinement

4.1. Introduction

With the rapid development of nanotechnology, the exposure of macromolecules to nanoconfinement becomes more common. Many material properties, such as biodegradability, ionization, charge transport etc., are affected by water mobility and accessibility to the polymer under confinement. A better understanding of interactions and conformational changes for macromolecules under nanoconfinement is required to improve nanomaterial design and to anticipate the effect of nanomaterials on the environment. The effect of confinement on the behavior of biopolymers has been actively discussed, as nanopores and nanoconfinement are commonly encountered in biology.[1–11] However a complete understanding has not been achieved so far due both to the complexity of the systems and variations in the outcome of nanoconfinement of biopolymers, e.g. in some cases a helical structure is stabilized and in others it is destabilized.[4,6,12,13] Biopolymer hydration is recognized as an important factor affecting their secondary and ternary structure with a few reports discussing hydration effects under confinement.[6,14] In contrast to biopolymers, synthetic polymers, which are commonly used in nanomaterial design, do not exhibit a secondary structure, but some can form hydrogen bonds with water which ensure their solubility.[15–17] The effect of hydration on polymer conformation under confinement has not been considered so far, as theoretical discussion was focused on conformational limitations imposed on polymer/biopolymer by confinement [3,18,19] with only a few computer modeling reports of non-polar polymers entering carbon nanotubes (CNTs) from solution.[20,21] Since the structure and properties (e.g. diffusion) of water under confinement, e.g. inside CNTs, is quite different from bulk solution,[22–26] it is logical to expect that hydration of

water-soluble polymers will be different under confinement. Polyethylene oxide, PEO, which is considered in this Letter, is a water-soluble polymer actively used in biomedical applications due to its biocompatibility and propensity to inhibit protein adsorption.[27,28] Understanding of PEO behavior under nanoconfinement can also be important for developing PEO-based nanocomposites, separation/sensing membranes and energy applications.[29,30] Elucidation of the water arrangement around the polymer can be challenging to achieve experimentally due to the required sub-nanoscale resolution. Atomistic molecular dynamic simulations can provide the necessary level of molecular detail to address this issue and make experimentally-testable predictions, therefore stimulating and guiding future experimental research.

In this Letter, we present a systematic investigation by means of atomistic molecular dynamic simulations of spontaneous PEO chain insertion into CNTs from aqueous solutions. We explain the key role that water plays in this phenomenon and investigate the equilibrium polymer conformation inside the CNTs as a function of nanotube diameter. We analyze the water arrangement around the confined polymer and explain the physical origin of unusual PEO helix formation and its stability inside the CNT. We also make experimentally-testable predictions regarding the conditions under which water-soluble polymers can be encapsulated into nanochannels and the PEO helix can be observed. More generally, we demonstrate why hydration under nanoconfinement is important for predictions of polymer properties essential for nanomaterial design and applications.

4.2. Simulation Details

All MD simulations were performed using the GPU version of GROMACS 4.6.5.[31] with OPLS all atom force field[32,33] Unless otherwise specified the methyl-terminated polyethylene oxide contained 36 repeat units. In all simulations CNTs were of finite length (typically 15nm) oriented in the z-direction, neutral and fixed (frozen). Carbon nanotubes of different chirality/size listed in Table 4.21 were generated using VMD[34] and placed inside a box containing PEO and SPC/E water molecules. The carbon nanotubes had open ends and were neutral with interactions described by LJ parameters ($\sigma_{c-c} = 0.355nm, \epsilon_{C-C} = 0.292KJ/mol$). In all simulations CNTs were fixed (frozen) in order to avoid any deformation of the tube during energy minimization. The smallest nanotube used in the simulation was 7-7 (0.949 nm in diameter) and contained ~36000 atoms (including PEO and water), while the largest nanotube was 20-20 (2.71nm in diameter) and contained ~40000 atoms. In all cases CNTs were oriented along the Z-direction and the length of nanotubes was not less than 15nm. Periodic boundary conditions were implemented in all dimensions with the box size chosen to accommodate CNTs and polymer in solution, surrounded by water from all sides. Periodic boundary conditions were implemented in all dimensions with the box size (typically 4nm×4nm×25nm) chosen to accommodate CNTs and polymer, surrounded by SPC/E (extended simple point charge model) water from all sides. All simulations were performed at T=288K using the Berendsen thermostat. To calculate hydrogen bonding between PEO and water we used geometric criteria: r≤3.5A for the distance between donor and acceptor groups and θ≤30^o for hydrogen-donor-acceptor angle. All visualizations were done using Visual Molecular Dynamics[34].

Table 4.21: Diameter of the Carbon Nanotube (CNT) corresponding to the chiral indices $(n-m)$ using the equation $d = 0.783\sqrt{n^2 + nm + m^2}$

Chiral Indices (n-m)	Diameter of Tube (nm)
7-7	0.95
7-8	1.02
4-11	1.05
8-8	1.09
8-9	1.15
9-9	1.22
9-10	1.29
10-10	1.36
11-11	1.49
12-12	1.63
14-14	1.90
15-15	2.03
20-20	2.71

4.3. Result and Discussion

To study the interactions between the CNT and PEO in aqueous solution the chain was placed and equilibrated in the vicinity but outside the nanotube. When a polymer chain finds itself in the vicinity of the outer surface of the CNT a weak polymer adsorption without wrapping around the CNT is observed, in agreement with results of previous MD simulations.[35] When one of the ends of the PEO chain finds its way into a nanotube a spontaneous and rapid insertion of PEO into the

nanotube occurs.[44] figure 4.31 shows change in PEO coordinates upon insertion into a 8-8 CNT of 1.085nm diameter d ($d=(n^2+m^2+nm)^{1/2}\times 0.0783$nm with n=8 and m=8 being the chiral indices). After about 1ns from the beginning of the process a portion of the chain containing 8 repeat units (out of a total 36) have entered into the CNT and assumed a helical conformation (figure 4.31b). After another 1ns the majority of the chain (24 repeat units) was inside the CNT in a helical conformation (figure 4.31c). The whole process of PEO encapsulation into the CNT took about 3.5ns. Additional simulation runs showed qualitatively and quantitatively similar results with the characteristic encapsulation time being approximately the same: 3.5ns±0.5ns. The same

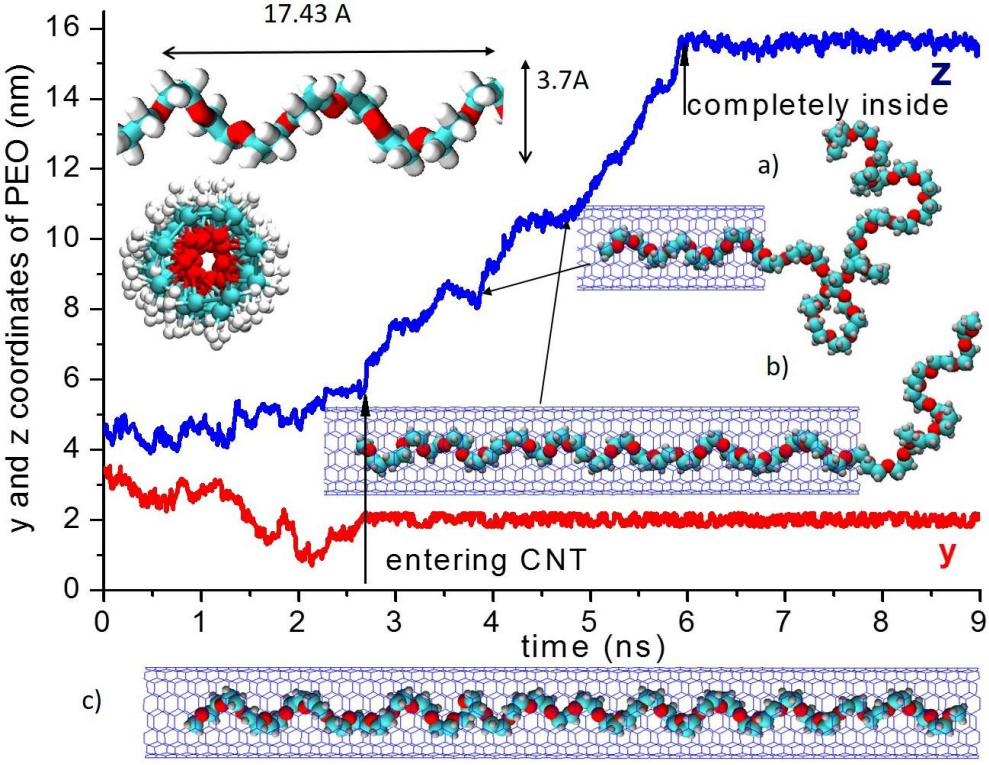

FIG. 4.31. The coordinates (y – perpendicular and z - along the CNT) of the PEO center of mass (N=36) as a function of time and simulation snapshots showing chain conformation (a) 1ns, (b) 2 ns (c) 3.5ns after entering the CNT with a zoom-in view of the helix period and a rear-view (inset). In all snapshots water is removed for clarity, oxygens and carbon atoms are shown as red and cyan balls, respectively; hydrogens as small grey or white balls.

phenomenon of spontaneous chain insertion was observed for PEO of different lengths (e.g. PEO chain of 18 repeat units took 1.4ns ±0.5ns to enter the same CNT) and for CNTs of different diameters. Insertion of PEO (N=36) into the narrow tubes (0.95nm≤d≤ 1.15nm) occurs more rapidly (i.e. with a larger velocity) once the process started than that for wider tubes. This result may seem surprising taking into account that entering a narrow tube requires a more dramatic change of polymer conformation. However, the dynamics of water in narrow tubes is known to be very facile due to single file diffusion[22–24] and, as will be discussed below, water substitution by PEO is one of the important factors in the process.

After the complete encapsulation the PEO chain remains in a helical conformation inside the 8-8 CNT without exiting the tube. We characterized the properties of the helix and arrived at a diameter of 3.7A (from carbon to carbon) with about 7 repeat units per period of 17.43A (figure 4.31) leading to 2.49A for the helix rise (i.e. the pitch per repeat unit), which corresponds to the so-called 3_{10} helix in Bragg's nomenclature. The properties of the helix are close to that for the PEO helix formed in the crystal state, a 7/2 helix with 7 repeat units per 19.48A helix period and a diameter of 3.3-3.5A,[36–38] except the PEO helix inside the 8-8 CNT containing water is somewhat shorter and wider. The difference is most likely attributed to the water associated with a helix inside the CNT, as in a narrower CNT (4-11) with less water the helix structure (period 18.2A, diameter 3.5A) is closer to that in crystal state, while in CNTs of larger diameters (1.2-1.3nm for 9-9, 9-10) containing more water the PEO helix becomes even shorter (period 15.4-15.8A) and wider (4.8-5.4A) with 9-10 repeat units per period.

To investigate PEO conformation under nanoconfinement we studied a range of CNTs of different diameters *d* from 0.95nm (7-7) to 2.7nm (20-20) into which the PEO chain spontaneously

infiltrates. To characterize the chain conformation, we analyzed the average end-to-end distance R_{end}, radius of gyration, R_g, and their ratio, R_{end}/R_g, which are shown (except for R_g) as a function of CNT diameter in figure 4.32. As is seen, in the narrowest CNTs (7-7, 7-8) PEO is strongly stretched (e.g. R_{end} =12.8 nm in CNT 7-7 is nearly 3 times larger than the solution value of $R_{end\text{-}solution}$=4.1nm) forming a rod-like conformation, with R_{end}/R_g approaching $\sqrt{12}$. Obviously, such chain stretching is highly unfavorable entropically leading to an estimated conformational free energy loss of about 13kT, (based on the simple Flory-like expression $3kTR^2_{end}/(2R^2_{end\text{-}solution})$, where k is the Boltzmann constant), not to mention the loss in the energy of hydrogen bonding[39] between PEO and water (1.2 hydrogen bonds with energy about 19kJ/mol per oxygen in solution vs. no hydrogen bonds in CNT 7-7). For this conformation to be thermodynamically stable there has to be some strong counter-balancing benefit for the system, which can be the liberation of water that gains 0.8 hydrogen bonds (i.e. about 11.4kJ/mol) per molecule moving from CNT to solution. As a PEO chain of 36 repeat units replaces approximately 65 water molecules inside the nanotube (nearly independently of the CNT diameter) the free energy change due to the water gain and PEO loss in hydrogen bonding is about -55.8kJ/mol or -23.3kT (at T=288K), as shown in the supplemental material of ref. 40.[40] This exceeds the loss in conformational entropy of the chain at least for narrow CNTs (7-7, 7-8), and can explain the observed spontaneous chain insertion. We note that PEO-CNT,[35] water-CNT interactions and translational entropy of water,[41,42] also contribute to the chain insertion free energy making its calculation rather challenging and requiring further detailed investigation.

In CNTs of larger diameter (*d*=1.05-1.3 nm) water forms a shell well interconnected by hydrogen bonding at a level approaching the bulk solution value.[23,24] In these CNTs PEO forms a helix with

R_{end}/R_g remaining close to the rigid rod value of $\sqrt{12}$ despite the intrinsic flexibility of PEO (persistence length 3.7A).[43] As the CNT diameter increases the helix becomes noticeably shorter and wider to accommodate the increasing number of water molecules participating in PEO hydration and R_{end} starts to decline. The decrease of R_{end} with CNT diameter does not follow any classical models,[3,11,18] but can be well described (somewhat in the spirit of eq.10 of ref.[44]) by:

$$\frac{R_{end}}{R_{end-solution}} = \frac{1.1}{d_{eff}} = \frac{1.1}{(d-0.6)}, \qquad (4.31)$$

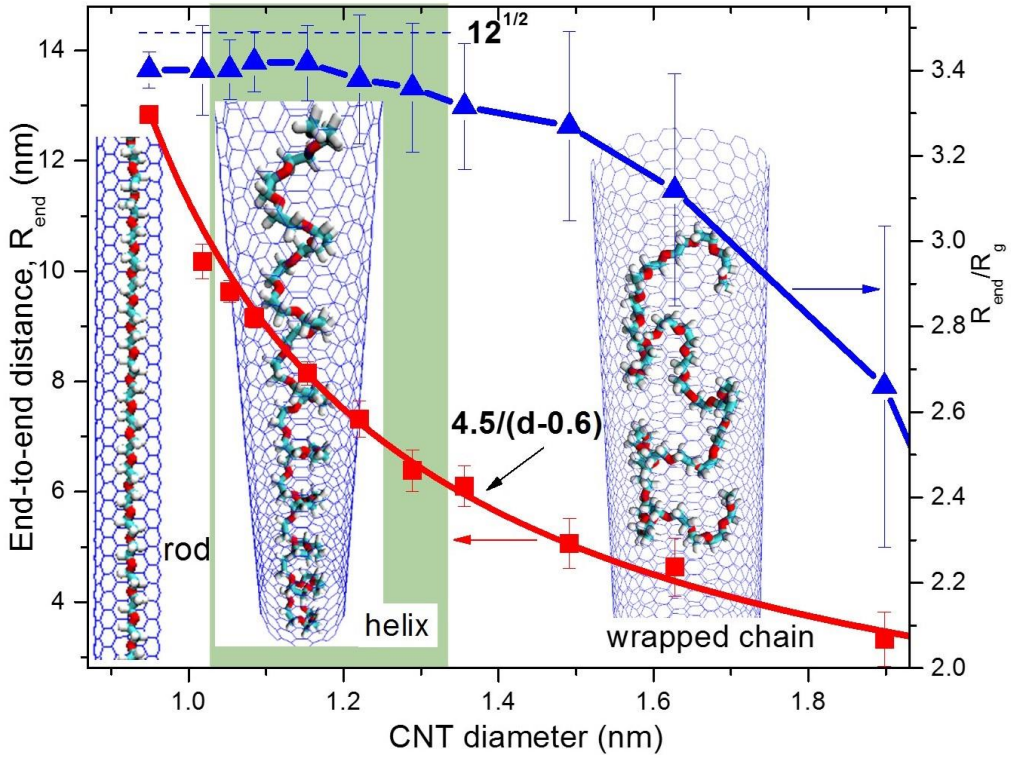

FIG. 4.32. The average end-to-end distance R_{end} (squares) fitted by eq. 4.31 (with $R_{end-solution}$=4.1nm) and the ratio R_{end}/R_g (triangles) for PEO chain inside the CNT as functions of the CNT diameter, d. The horizontal dashed line indicates $R_{end}/R_g=\sqrt{12}$, the expected value for a rigid rod. Snapshots of PEO chain inside the CNT representing three conformational regimes: rod, helix and chain wrapped along the inner CNT surface (representation similar to Fig. 4.31).

with $d_{ef} \equiv 2r_{efff} = d - 0.6nm$ being the polymer-accessible radius of the tube. r_{eff} corresponds to the CNT radius reduced by an exclusion zone width, 0.3nm, which is the average separation of the PEO hydrogens from the CNT inner surface.[40] The implication of eq. 4.31, which remains valid over the whole studied d range, is that the effective surface area of PEO-CNT contact, $2\pi r_{eff} R_{end}$, remains constant with an increase of CNT diameter.

To understand the origin of helix formation we characterized PEO hydration inside the CNT by calculating the average number of hydrogen bonds per oxygen of PEO, n_{hb}, which is shown in figure 4.33. As is seen, for 4-11 (d=1.053nm) and 8-8 CNTs (d=1.085nm), n_{hb} and correspondingly, the number of water molecules hydrogen bonded to PEO, N_w^{hb}, is noticeably smaller than in aqueous solution, while in 8-9, 9-9 and 9-10 CNTs (d=1.153-1.29nm), n_{hb} and N_w are close to the solution values. To gain further insights into water arrangements around the PEO helix, we categorized water hydrogen bonded to PEO into two classes: "singly-bonded water" forming a single bond with PEO and "doubly-bonded water" having two hydrogen bonds with two different oxygens of PEO, usually the *i* and *i+2* oxygens of PEO, as is seen in figure 4.33c. The doubly-bound water is of particular interest in understanding the physical origin of helix stabilization inside the CNT, as it brings together a section of the PEO chain in the TGT conformation which favors helix formation. In 9-9 and 9-10 CNTs the fraction of doubly bound water (relative to the total number, N_w), n_{db}, exceeds that for aqueous solution, resulting in an average of 4 double-bonded waters per helix period (figure 4.33c). These doubly bound waters play a role analogous to intramolecular hydrogen bonding in biopolymers that are responsible for their helical structure. In 8-9 CNT (d=1.153nm) there are on average 3 doubly bonded waters per helix period with n_{db} comparable to bulk solution where PEO does not form a helix. In the narrow 4-11 and 8-8 CNTs, there is insufficient space to form multiple bridges between the *i* and *i+2*

oxygens by doubly bonded water, so singly bonded water dominates, as is seen in figure 4.33a,b. While there are some hydrogen bonded bridges between singly bonded waters, as is seen in Figure 4.33b, that can help to hold together the helix structure, where must be some additional factor(s) that plays a role in helix structure stabilization.

One possible reason for helix stabilization is a higher stability of the PEO hydration shell inside the CNT compared to solution. To quantify this effect we selected water hydrogens bonded to PEO inside the CNT at *t=0*, $N_w(0)$ and calculated the following correlation function C(t):

$$C(t) = \left\langle \frac{N_w(t)}{N_w(0)} \right\rangle \qquad (2)$$

where $N_w(t)$ is the number of water molecules among the initially selected ones that remain, hydrogen bonded (but not necessarily to the same PEO oxygen) at time *t* and <…> denotes averaging over different initial states. Thus, the larger is C(t), the larger is the fraction of long-lasting waters in the hydration shell of PEO, even though this water may not be continuously bound to PEO. As is seen from figure 4.34, for a given CNT diameter C(t) firstly abruptly decreases and then stabilizes at some plateau-like level. In the narrow CNTs (4-11, 8-8, 8-9) more than 70% of the water remains in the PEO hydration shell for more than 1ns (for comparison the characteristic lifetime of a PEO-water hydrogen bond is about 4-5ps.[45]). This result is not that surprising, as pure water diffusion inside the corresponding CNTs is known to be rather limited, based on results of MD simulations.[23–25] The presence of PEO is likely to further slowdown the water diffusion inside the CNT. Thus, the stability of the PEO hydration shell is likely to be the main factor in helix stabilization inside the CNTs, as near the chain ends where water moves more freely the helical conformation is noticeably less stable compared to the middle of the chain.[40] Since the contribution of chain ends is larger for shorter chains, one should expect that short PEO chains are

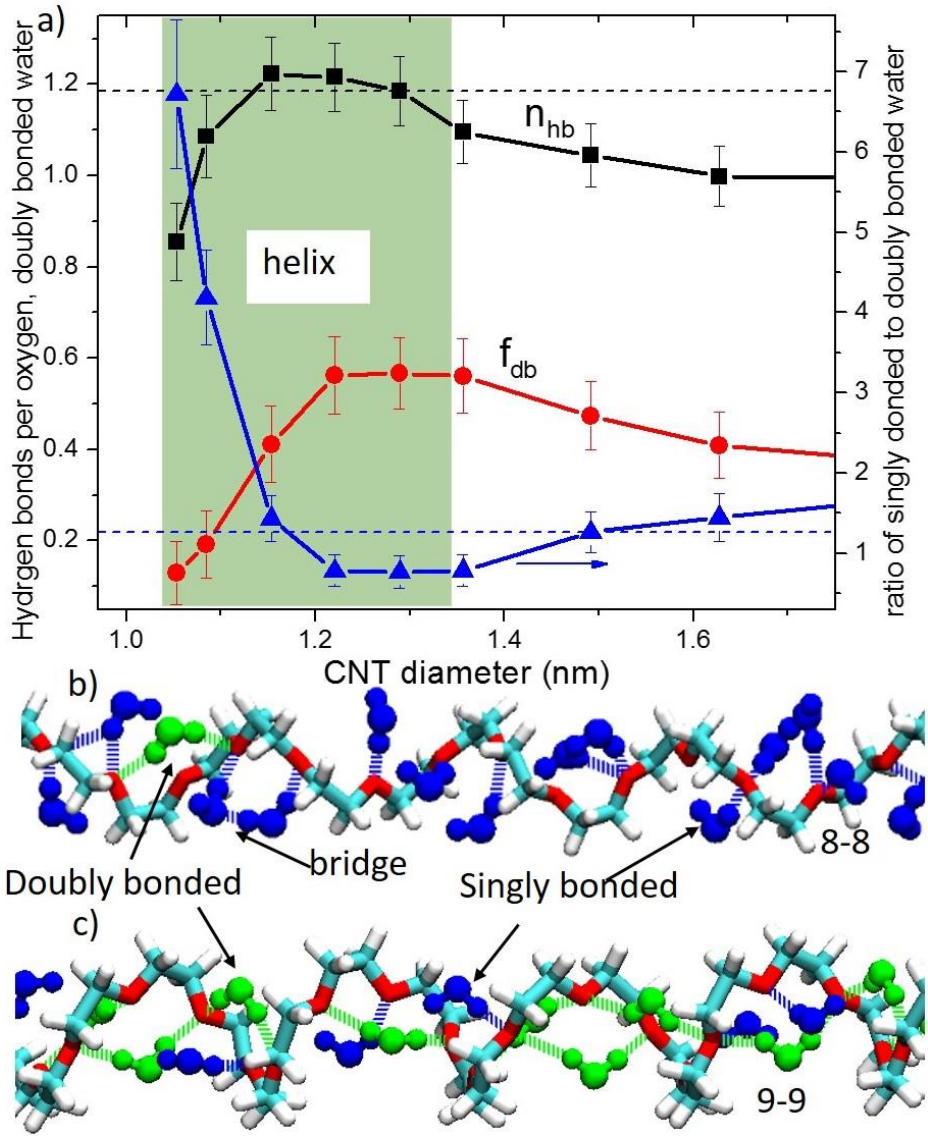

FIG. 4.33. (a) The average number of hydrogen bonds per oxygen of PEO, n_{hb} (squares), the fraction of water doubly bound to PEO, f_{db} (circles), and the ratio of singly- to doubly- bonded water (triangles) vs. the CNT diameter. The horizontal dashed lines mark n_{hb} and the ratio of singly- to doubly-bonded water for aqueous solutions of PEO. Simulation snapshots (same representation as in fig.1) of sections of the PEO helix with singly bonded (blue) and doubly bonded (green) water molecules together with the corresponding hydrogen bonds for 8-8 (b) and 9-9 (c) CNTs.

less likely to form a stable helix, as is indeed the case.[40] For CNTs of somewhat larger diameter, such as 9-9 and 9-10 (d=1.22nm and d=1.29nm) the fraction of long-lasting water in hydration shell decreases to 40-50%, but recall that the fraction of doubly-bonded water acting as

intramolecular crosslinks for the helix is larger in this case, so the helical structure remains stable. Since the decay in C(t) is associated with the exchange of water hydrogen bonded to PEO and free water in its vicinity, the plateau value of the fraction of long-lasting water in the hydration shell

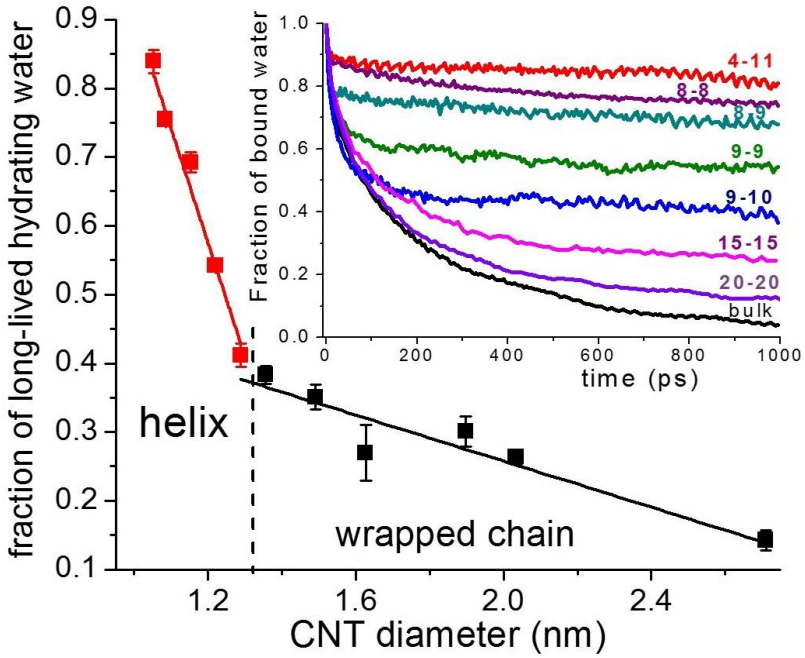

FIG. 4.34. The average fraction of long-lasting water in PEO hydration shell corresponding to the plateau value of the correlation function C(t) (eq. 4.32), (shown in the inset as a function of time for different CNTs), as a function of CNT diameter. The best linear fits to the data for helices and wrapped chains respectively are shown as solid lines. The vertical dashed line indicates the boundary between helix and wrapped chain regimes.

should linearly decrease with the amount of free water, which in turn scales with CNT diameter, as indeed is seen in Figure 4, where the plateau value of C(t) is plotted as a function of CNT diameter.

In CNTs with a diameter exceeding 1.3 nm the number of free waters exceeds those hydrogen bonded to PEO, so the waters initially in the hydration shell of PEO can now diffuse away from the polymer almost as easily as in solution. Accordingly, the correlation function C(t) exhibits a somewhat different pattern with a more continuous decay and a smaller fraction of long-lasting

waters in the hydration shell (figure 4.34) which is insufficient to support the helix structure and consequently the PEO chain wraps along the inner surface of the CNT, as is seen in figure 4.32. The fraction of long-lasting water in the hydration shell of wrapped PEO systematically decreases following a somewhat different linear dependence on the CNT diameter than for the PEO helices (figure 4.34), since now the most stable water is that in the layer interfacing with the CNT with the degree of hydrogen bonding between PEO and water being somewhat smaller than in aqueous solution. The observed change in slopes seen in figure 4.34 is indicative of different water dynamics inside the CNT and delineates the transition from helix to wrapped chain regimes. For the wider CNTs the dominant factor for water replacement by PEO becomes the minimization of less favorable water-CNT contacts. In the limit of wide CNTs we expect that any preference for the PEO chain wrapping the inner compared to the outer CNT surface will vanish.

4.4. Conclusions

In summary, based on the results of our atomistic molecular dynamics simulations we show that a polyethylene oxide chain spontaneously enters carbon nanotubes of different sizes from aqueous solution. Rapid chain insertion occurs for narrow CNTs ($0.95\text{nm} \leq d \leq 1.15\text{nm}$) with highly mobile structured water inside and slows down with increasing tube diameter. Inside CNTs PEO forms a rod-like, helical or wrapped (along the inner CNT surface) chain conformation depending on the CNT diameter (figure 2). We show that the high stability of the PEO hydration shell inside the CNT is a key factor in helix formation (figure 4), with doubly bound water playing the role of intramolecular crosslinks (figure 3). These results provide molecular level insights into the role of water in PEO helix formation and imply that relatively immobile water (or other hydrogen bond-donating solvents) is necessary for helix formation. The obtained results suggest a new method of

PEO (or other amphiphilic water-soluble polymer) encapsulation in nanopores and demonstrate the importance of understanding hydration for predicting the behavior of macromolecules under nanoconfinement, which can be further explored in future experimental and theoretical research and used in designing nanomaterials for biomedical, sensing and energy applications.

4.5. References

(1) Dill, K. A.; Bromberg, S.; Yue, K.; Chan, H. S.; Ftebig, K. M.; Yee, D. P.; Thomas, P. D. *Protein Science*. 1995, pp 561–602.

(2) Tian, J.; Garcia, A. E. *J. Am. Chem. Soc.* **2011**, *133* (38), 15157–15164.

(3) Reisner, W.; Pedersen, J. N.; Austin, R. H. *Reports Prog. Phys.* **2012**, *75* (10), 106601.

(4) Ziv, G.; Haran, G.; Thirumalai, D. *Proc. Natl. Acad. Sci.* **2005**, *102* (52), 18956–18961.

(5) Gumbart, J.; Chipot, C.; Schulten, K. *Proc. Natl. Acad. Sci.* **2011**, *108* (9), 3596–3601.

(6) Ulmschneider, M. B.; Koehler Leman, J.; Fennell, H.; Beckstein, O. *J. Membr. Biol.* **2015**, *248* (3), 407–417.

(7) White, S. H.; von Heijne, G. *Annu. Rev. Biophys.* **2008**, *37* (1), 23–42.

(8) White, S. H. *FEBS Lett.* **2003**, *555* (1), 116–121.

(9) Muthukumar, M.; Kong, C. Y. *Proc. Natl. Acad. Sci.* **2006**, *103* (14), 5273–5278.

(10) Muthukumar, M. *Annu. Rev. Biophys. Biomol. Struct.* **2007**, *36* (1), 435–450.

(11) Reisner, W.; Morton, K. J.; Riehn, R.; Wang, Y. M.; Yu, Z.; Rosen, M.; Sturm, J. C.; Chou, S. Y.; Frey, E.; Austin, R. H. *Phys. Rev. Lett.* **2005**, *94* (19), 1–4.

(12) O'Brien, E. P.; Stan, G.; Thirumalai, D.; Brooks, B. R. *Nano Lett.* **2008**, *8* (11), 3702–3708.

(13) Zhou, H.-X. *J. Chem. Phys.* **2007**, *127* (24), 245101.

(14) Xue, Y.; Chen, M. *Nanotechnology* **2006**, *17* (20), 5216–5223.

(15) Dormidontova, E. E. *Macromolecules* **2002**, *35* (3), 987–1001.

(16) Dormidontova, E. E. *Macromolecules* **2004**, *37* (20), 7747–7761.

(17) Molyneux, P. *Water-Soluble Synthetic Polymers: Properties and Behavior*; 1985; Vol. 16.

(18) Odijk, T. *Macromolecules* **1983**, *16* (8), 1340–1344.

(19) Gennes, P.-G. de. *Scaling Concepts in Polymer Physics*; Cornell University Press:

Ithaca,NY, 1979.

(20) Wei, C.; Srivastava, D. *Phys. Rev. Lett.* **2003**, *91* (23), 235901.

(21) Wanjari, P. P.; Sangwai, A. V.; Ashbaugh, H. S. *Phys. Chem. Chem. Phys.* **2012**, *14* (8), 2702.

(22) Alexiadis, A.; Kassinos, S. *Chem. Rev.* **2008**, *108* (12), 5014–5034.

(23) Mashl, R. J.; Joseph, S.; Aluru, N. R.; Jakobsson, E. *Nano Lett.* **2003**, *3* (5), 589–592.

(24) Ye, H.; Zhang, H.; Zheng, Y.; Zhang, Z. *Microfluid. Nanofluidics* **2011**, *10* (6), 1359–1364.

(25) Kolesnikov, A. I.; Zanotti, J.-M.; Loong, C.-K.; Thiyagarajan, P.; Moravsky, A. P.; Loutfy, R. O.; Burnham, C. J. *Phys. Rev. Lett.* **2004**, *93* (3), 035503.

(26) Striolo, A. *Nano Lett.* **2006**, *6* (4), 633–639.

(27) Harris, J. M. In *Poly(Ethylene Glycol) Chemistry*; Springer US: Boston, MA, 1992; pp 1–14.

(28) Lee, J.; Lee, H.; Andrade, J. *Prog. Polym. Sci.* **1995**, *20* (6), 1043–1079.

(29) Zhang, Q.; Archer, L. A. *Langmuir* **2002**, *18* (26), 10435–10442.

(30) Honma, I.; Nomura, S.; Nakajima, H. *J. Memb. Sci.* **2001**, *185* (1), 83–94.

(31) Van Der Spoel, D.; Lindahl, E.; Hess, B.; Groenhof, G.; Mark, A. E.; Berendsen, H. J. C. *J. Comput. Chem.* **2005**, *26* (16), 1701–1718.

(32) Jorgensen, W. L.; Maxwell, D. S.; Tirado-Rives, J. *J. Am. Chem. Soc.* **1996**, *118* (15), 11225–11236.

(33) Damm, W.; Frontera, A.; Tirado-Rives, J.; Jorgensen, W. L. *J. Comput. Chem.* **1997**, *18* (16), 1955–1970.

(34) Humphrey, W.; Dalke, A.; Schulten, K. *J. Mol. Graph.* **1996**, *14* (1), 33–38.

(35) Rouhi, S.; Alizadeh, Y.; Ansari, R. *Brazilian J. Phys.* **2015**, *45* (1), 10–18.

(36) Takahashi, Y.; Tadokoro, H. *Macromolecules* **1973**, *6* (5), 672–675.

(37) Maranski, K.; Andreev, Y. G.; Bruce, P. G. *Angew. Chemie Int. Ed.* **2014**, *53* (25), 6411–6413.

(38) Seebach, D.; Zass, E.; Bernd Schweizer, W.; Thompson, A. J.; French, A.; Davis, B. G.; Kyd, G.; Bruno, I. J. *Angew. Chemie - Int. Ed.* **2009**, *48* (51), 9596–9598.

(39) Rubinstein, M.; Colby, R. H. *Polymer International*. 2003, p 440.

(40) Dahal, U. R.; Dormidontova, E. E. *Phys. Rev. Lett.* **2016**, *117* (2), 027801.

(41) Pérez-Hernández, G.; Schmidt, B. *Phys. Chem. Chem. Phys.* **2013**, *15* (14), 4995.

(42) Pascal, T. A.; Goddard, W. A.; Jung, Y. *Proc. Natl. Acad. Sci.* **2011**, *108* (29), 11794–

11798.

(43) Lee, H.; Venable, R. M.; MacKerell, A. D.; Pastor, R. W. *Biophys. J.* **2008**, *95* (4), 1590–1599.

(44) Tree, D. R.; Wang, Y.; Dorfman, K. D. *Phys. Rev. Lett.* **2013**, *110* (20), 208103.

(45) Borodin, O.; Bedrov, D.; Smith, G. D. *J. Phys. Chem. B* **2002**, *106* (20), 5194–5199.

Chapter 5.

Planar PEO brushes

5.1. Introduction

Polymer brushes remain the subject of continuous interest in the scientific community due to both fundamental aspects of polymer behavior and the practical importance for improving material properties in various applications.[1,2] In particular, polyethylene oxide is one of the most commonly used polymers in brush formation due to its water solubility, biocompatibility and capability to inhibit protein adsorption.[3,4] PEO grafting on surfaces, such as gold or silica, ensures particle solubility, prevents aggregation and provides protection from undesirable interactions.[5,6] PEO brushes are commonly relied on in antifouling applications and are essential in biosensing, scaffolding and drug/gene delivery and imaging applications.[4–6] Despite numerous reports on the successful use of PEO grafted layers, a complete understanding of the fundamental behavior of PEO brushes has not been achieved so far. There are still ongoing debates regarding whether PEO becomes more hydrophobic when present in a brush compared to solution,[7–9] does the PEO brush phase separate into a dense dehydrated zone and hydrated layer upon stretching or temperature increase,[10–12] and what properties of a PEO brush (grafting density, overall mass, brush height) determine its anti-fouling capability.[13–15] One of the major obstacles is the difficulty to experimentally probe the detailed molecular organization of a brush, which would require highly sophisticated and high resolution experimental or computer modeling techniques. Furthermore, the overall interpretation of experimental results is often based on the assumption that changing the polymer grafting density has no impact on the polymer-solvent interactions, which is obviously not the case for PEO which is known for its concentration (and temperature) dependence of hydrogen bonding with water.[16,17] Besides thermodynamic structural aspects of PEO brushes,

chain flexibility in the brush is equally or perhaps even more important for antifouling applications, which so far has been studied to much less extent.[18–20] Molecular dynamics simulations is a powerful tool to study this range of problems.[21–23] In this paper we apply atomistic molecular dynamic simulations to gain insights into molecular level details of PEO brush structure, hydration and analyze the dynamic properties of PEO chains (of constant length) attached to gold surface with different grafting densities.

One of the experimental challenges in polymer brush formulation is achieving a high density of grafting, brush monodispersity and homogeneous surface coverage,[14,15,24,25] which can strongly affect brush properties and makes it difficult to compare results obtained by different experimental groups. Thus, incomplete surface coverage by PEO brush is considered to be one of the major factor affecting protein and bacterial adhesion.[13,15] Several reports show that high molecular weight of PEO or high grafting density is required to ensure inhibition of protein adsorption,[14,15,18] while other papers suggest that too high a grafting density may not be the best for protein adsorption inhibition[9,19] and what is important is the total mass of PEO brush.[13] These requirements for PEO brush properties may be related to achievement of complete surface coverage and certainly affect brush hydration, which is considered as one of the important factors in protein adsorption inhibition. However, the relation of PEO hydration to the grafting density is not readily available from experimental data, which may explain some of the contradiction in results between different groups. Furthermore, the molecular mobility of PEO tails is another important factor in protein adsorption,[18,19] which is relatively rarely considered and studied to much less extent compared to static properties of the brush. Some reports indicate that high molecular weight of PEO is important to achieve high mobility and inhibition of protein adsorption,[18] but other data show that high molecular weight alone cannot guarantee adsorption inhibition.[15] The effect of

grafting density on PEO mobility and protein inhibition is also unclear with some intermediate grafting densities indicated as being preferable.[19] Interestingly, high mobility of PEO tails is found to be beneficial for both inhibition of non-specific adsorption and achieving high biorecognition.[18,19]

Another factor that can influence properties of the PEO brush at low grafting density is the interaction of water and PEO with the substrate. While such molecular level details are hard to assess experimentally, it has been studied in atomistic molecular dynamics simulations for graphite, oil and siloxane (silica) surfaces.[21–23] It was found that PEO adsorbs on these surfaces at low grafting densities replacing water, which in absence of polymer forms a layered structure near the surface and can interact (including formation of hydrogen bonds) with the siloxane surface. With an increase of grafting density PEO absorption on the surface decreases as polymer forms a stretched brush. It was determined that the polymer density profile exhibits classical brush behavior and was largely independent of the PEO-surface interaction at high grafting densities,[21] except for the average PEO brush height on siloxane surface,[22] which was found to follow the scaling dependence $h \sim \sigma^{1/2}$ instead of $h \sim \sigma^{1/3}$, where σ is the grafting density (i.e. number of chains per unit area). The PEO-water hydrogen bonding near the siloxane surface is found to be suppressed relative to hydrogen bonding between a free PEO chain in aqueous solution, but the number of hydrogen bonds increases away from the surface where chains become more accessible to the water medium.[23] At higher grafting densities in the brush regime the number of hydrogen bonds decreases due to the lateral overcrowding.[23] A similar result was obtained based on a molecular SCMF approach assuming hydrogen bonding in the brush follows the same concentration dependence as in solution.[26] It was shown that a polymer brush with hydrogen

bonding interactions is more swollen at low temperature, but can become dehydrated and perhaps even phase separate at elevated temperatures,[26] as expected in the n-cluster model.[10–12]

In this paper using atomistic molecular dynamics simulations we will investigate the molecular organization of PEO brushes on a planar gold surface. Gold surfaces and gold nanoparticles are actively used in biomedical applications with PEO grafting commonly used to ensure antifouling.[4,27,28] For a constant length of PEO chain (of 20 repeat units, N=20), we investigate the influence of grafting density on the extent of PEO hydration and compare the obtained results with PEO hydrogen bonding in aqueous solutions. We will also analyze the mobility of PEO tails in the bush for different grafting densities and study the local organization of PEO chains near the gold surface. To assess the solvent-induced changes to PEO brush structure and surface interactions, we will also study pure THF and a mixed THF/water solution and compare the results to that obtained in pure water. Our results provide molecular-level insights on the structural organization of PEO brushes and contribute to the resolution of outstanding questions regarding the impact of grafting on PEO hydration and tail mobility in a brush. These predictions can be experimentally tested and used as guidance in designing new materials of biomedical relevance. results with PEO hydrogen bonding in aqueous solutions. We will also analyze the mobility of PEO tails in the bush for different grafting densities and study the local organization of PEO chains near the gold surface. To assess the solvent-induced changes to PEO brush structure and surface interactions, we will also study pure THF and a mixed THF/water solution and compare the results to that obtained in pure water. Our results provide molecular-level insights on the structural organization of PEO brushes and contribute to the resolution of outstanding questions regarding the impact of grafting on PEO hydration and tail mobility in a brush. These predictions

can be experimentally tested and used as guidance in designing new materials of biomedical relevance.

5.2. Simulation Details

We performed all-atom molecular dynamics simulation using OPLS-AA force field to investigate the hydration behavior of PEO chains grafted to a gold surface. The gold surface was obtained by packing uncharged gold atoms on FCC lattice with lattice parameter of $0.408\,nm$.[29] The gold surface was 5 gold atoms thick and had surface area of $\sim 54\,nm^2$, i.e. $7.34nm\ \times 7.34\,nm$, which was kept constant in all simulations. The box size in z-direction normal to the gold surface was varied depending on the system size, exceeding the maximum brush height by at least$3\,nm$. PEO chains of 20 repeat units ($CH3-[O-CH2-CH2]_{20}-S$-) were homogeneously grafted to the gold surface via the sulfur bond with gold atoms on the surface. We note that as the sulfur bond with gold atoms is relatively weak and allows bond stretching leading to some fluctuation of the sulfur atom positions. The grafting densities that we model range from $\sigma = 0.167\,nm^{-2}\ to\ \sigma = 4.18\,nm^{-2}$ covering the whole range from the beginning of brush regime to highly dense and stretched brushes. To model PEO chains we used slightly modified OPLS model, as was previously used for polymer solutions.[30,31] PEO brushes were solvated with water, for which SPCE model was used. For comparison we also solvated the PEO brush with THF and mixed (80:20 by volume fraction) THF:water solution for grafting density $\sigma = 0.91\,nm^{-2}$. The details for THF model used are discussed in supporting information.

All simulations are carried out using the GPU version of GROMACS-4.6.5. The NPT ensemble is applied to equilibrate the system initially at 340K for about 20-35ns depending on the system size to speed-up system relaxation from the initial state and achieve a uniform water molecule

distribution in the system followed by equilibration at 310K for not less than an additional 20ns. All results presented in the paper are obtained at the temperature 310K and have more than 50 ns equilibration time in total. A semi-isotropic pressure coupling (i.e. x and y direction kept constant with the z-direction pressure coupled to 1 bar) was applied using Berendsen barostat at 1 bar with compressibility $4.5e^{-5}\ bar^{-1}$ and coupling time constant of 5 ps. V-rescale thermostat was used for temperature coupling with the coupling time constant of 1 ps. Electrostatic interactions were calculated using PME method with integration time step of 1 fs.

The volume fraction of PEO, water and THF were calculated using 0.3 nm wide bin zones in z-direction normal to the gold surface using 0.03 nm^3 for water molecule volume and 0.02 nm^3 for CH_2 group and O atom volumes each.[32] We note that since no atoms were found closer than 1.5 Å from the gold surface, this area was excluded from volume fraction calculations. For hydrogen bond analysis, we used the same bin sizes as for volume fraction calculation (when accounting for position of oxygen donors) and applied a geometrical criterion for donor-acceptor distance $r_{DA} \leq$ 3.5Å and (hydrogen-donor-acceptor) $angle$ $(H-D-A) \leq 30°$. For calculation of the residence time of water hydrogen bonded to PEO we extracted our data for the analysis every 10 ps. For visualization of chain conformation and hydration Visual Molecular Dynamics (VMD)[33] has been used.

5.3. Result and Discussion

To investigate PEO hydration in a polymer brush we varied the grafting density of polymer on gold surface from a moderate $\sigma = 0.67nm^{-2}$ to higher values, with a maximum $\sigma = 4.18\ nm^2$. Experimentally, high grafting density of polymer corresponds to approximately $1nm^{-2}$ for planar surfaces,[14,15,25] which is limited by the surface accessibility for polymer grafting with a much

higher grafting density achievable for curved surfaces.[24] Grafting from approach can provide a higher local polymer density, but results in a high polydispersity of polymer lengths obtained and inhomogeneous coverage.[34] We note that our polymer brush was monodisperse with respect to PEO molecular weight, which was kept at $N = 20$ repeat units in all cases. Figure 5.31 (upper row) shows the typical PEO conformation and structure of the brush obtained at five different grafting densities. As is seen, at lower σ the PEO conformation remains coil-like, except for the region in the immediate vicinity of the gold surface where some polymer adsorption is observed in agreement with experimental data[35] due to the more favorable interactions between PEO and gold compared to water-gold interactions. Correspondingly, for smaller σ we observe a depletion of water in the gold surface vicinity, as is seen in figure 5.31 (lower row). Overall the polymer orientation remains mostly random in the range of moderate grafting densities with only a slight preference in orientation in z-direction perpendicular to the gold surface. With an increase in grafting density the PEO orientation in z-direction increases and chains start to stretch away from the surface. We note that accumulation of PEO near the gold surface persists until rather high grafting densities. As is seen in figure 5.31, at the highest grafting density studied, $\sigma = 4.18\ nm^{-2}$, PEO forms a very dense highly stretched and dehydrated brush. Thus, the grafting densities considered cover the range from a fully hydrated PEO brush at lower σ to a nearly dehydrated brush at high σ through the intermediate range of nearly equal volume fraction of PEO and water.

A closer analysis of PEO behavior in these brushes will be informative to understand the interconnection of chain crowding and stretching with hydration.

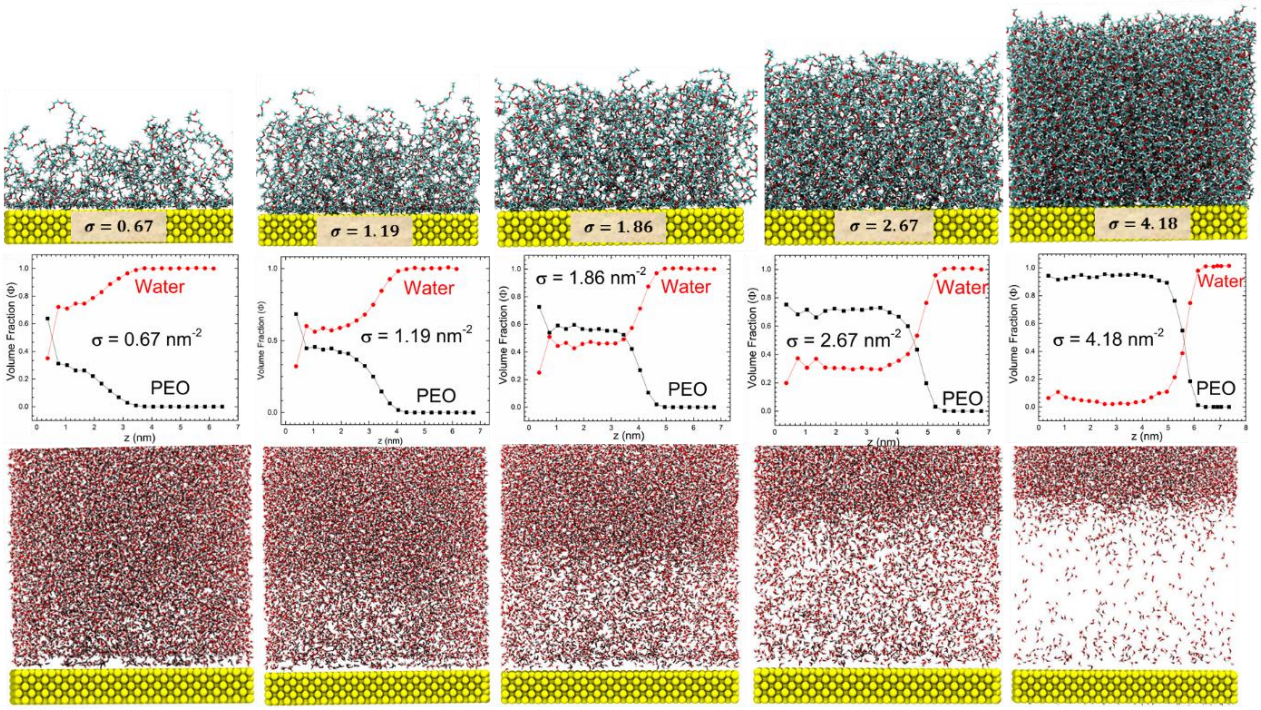

Figure 5.31. Computer simulation snapshots of grafted PEO chains (upper row) and complementary water (lower row) obtained for different grafting densities from left to right: $\sigma = 0.67\ nm^{-2}, 1.19\ nm^{-2}, 1.86\ nm^{-2}, 2.67\ nm^{-2}\ and\ 4.18\ nm^{-2}$. Corresponding volume fraction distribution of PEO and water are shown in the middle row.

To characterize chain conformation, we calculated the average end to end distance, R_{end} and the radius of gyration, R_g. The ratio R_{end}/R_g, which reflects the changes in the chain shape/conformation upon an increase in PEO grafting density, is shown in figure 5.32. As is seen at low grafting density polymer has close to a random coil conformation with the ratio R_{end}/R_g being only slightly larger than that for an ideal chain, $\sqrt{6} \approx 2.45$. With an increase in grafting density beyond 1 nm^{-2} the ratio R_{end}/R_g rapidly increases until about $\sigma = 2.7nm^{-2}$ when ratio R_{end}/R_g starts to saturate approaching the limit corresponding to a rod-like chain conformation

$\sqrt{12} \approx 3.46$ in strongly stretched brush. At the highest grafting density $\sigma = 4.18 nm^{-2}$ chain stretching reaches $R_g^2 \approx 3(R_g^2)_o$, where $(R_g)_o \approx 0.938\ nm$ corresponds to the R_g for solution.

To describe the chain orientation, we calculated the orientational order parameter:

$$S = \frac{1}{2}\langle(3\,\mathrm{Cos}^2\,\theta - 1)\rangle \qquad (5.31)$$

where θ is the angle between the end-to-end vector for the middle 10 repeat units of grafted PEO chains and z-direction perpendicular to the gold surface. We use middle 10 repeat units of PEO chain instead of the whole chain for the order parameter calculation to exclude the influence of the surface and the randomness of chain end orientation. At low grafting densities, there is no preferable orientation for the grafted PEO chains and the order parameter remains close to zero (figure 5.32). With an increase in grafting density the order parameters systematically increase and

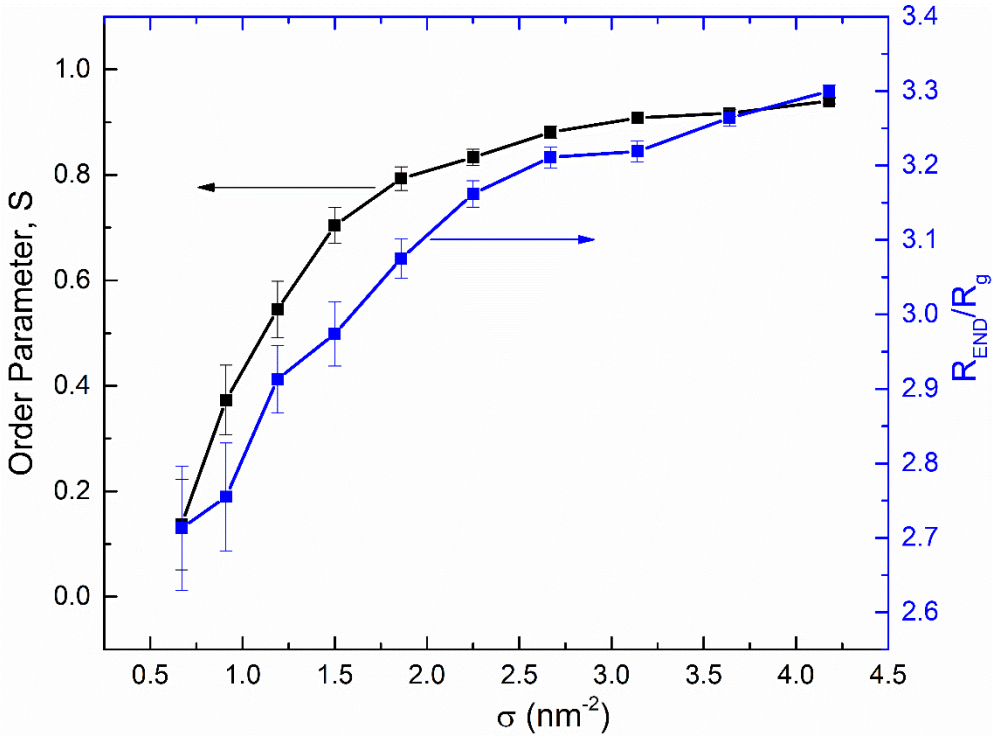

Figure 5.32. The average ratio of R_{end}/R_g and the orientational order parameter S (with respect to z-direction normal to the surface) for the PEO chains as functions of grafting density.

already at $\sigma \geq 1.2\ nm^2$ the order parameter reaches 0.5 indicating a preference in orientation away from the surface. At $\sigma \geq 2.2\ nm^{-2}$ the order parameter reaches rather high values $S \approx 0.8 - 0.94$ indicating that chains are strongly oriented and aligned along the z-direction, as expected for a strongly stretched brush.

To characterize the overall properties of the brush, we calculated and plotted in figure 5.33 the monomer volume fraction of polymer (accounting for CH_2 groups and O, as discussed in the simulation details) as a function of the distance from the surface for different grafting densities. At low grafting densities, there is polymer adsorption to the surface, as evidenced by the enhancement of polymer density in the vicinity of the surface. This adsorption is primarily caused by the tendency of PEO to substitute for the layered water in the vicinity of the gold surface. Indeed water layering near the gold surface has been previously reported in computer simulations and experimentally.[36–39] PEO adsorption on gold surfaces from aqueous solution has also been observed experimentally.[35] While such attraction can be caused by somewhat hydrophilic nature of the gold itself, we believe that PEO-gold contact is simply more favorable than water-gold contact, as water has to be re-structured into layers from normal bulk arrangement to sustain normal level of hydrogen bonding. Similar PEO adsorption on graphite surface in aqueous media has been previously reported.[21] The results of THF and THF/water solutions discussed below support this conclusion. Away from the gold surface (located at z=0), at $z > 1nm$, the polymer volume fraction follows parabolic profile, as expected for a brush.[40,41] With an increase in grafting density, the average volume fraction of polymer in the brush increases and correspondingly water content decreases figure 5.33). Polymer extends further away from the surface and the density

profile becomes closer to a step-function. At $\sigma \geq 2.7nm^{-2}$, the average polymer density in the brush becomes comparable to that near the surface indicating that polymer is stretching away from the surface throughout the brush. These are the cases of highly stretched and mostly dehydrated brush with density profile described by a step-like function.

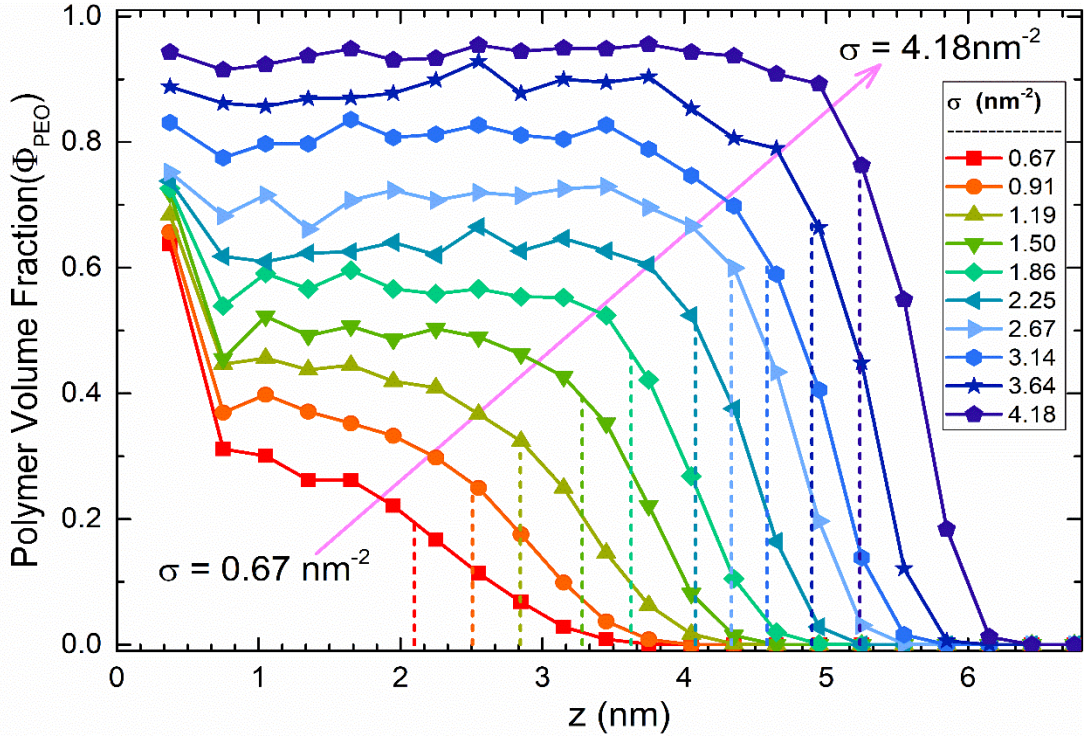

Figure 5.33. Polymer volume fraction as a function of the distance from the gold surface for the following grafting densities from top to bottom: $\sigma = 4.18, 3.64, 3.14, 2.67, 2.25, 1.86, 1.50, 1.19, 0.91\ and\ 0.67\ nm^{-2}$. The z coordinate corresponding to the maximum of end-group distribution is indicated by vertical dashed lines.

The average brush height, h, was calculated as [42–44]

$$h = \frac{\int z\, \Phi_{PEO}(z)\, dz}{\int \Phi_{PEO}(z)\, dz} \qquad (5.32)$$

where $\Phi_{PEO}(z)$ is the PEO volume fraction profile shown in figure 5.33, as a function of distance z from the gold surface. For a classical polymer brush composed of sufficiently long polymer chains, the brush height should scale with grafting density as[2,41–43]

$$h \sim \sigma^{1/3} \qquad (5.33)$$

The average brush height, h, is shown as a function of $\sigma^{1/3}$ in figure 5.34 (inset). As is seen, the brush height consistently increases with grafting density, qualitatively following the dependence of eq. (3). Furthermore, the maximum brush height, h_{max} , can also be estimated from the peak position of the end-group distribution (shown in supporting information).[43] The results are shown in figure 5.34 (inset). As is seen, h_{max}, exceeds more than twice the average brush height and similarly increases with σ. Thus, overall the properties of PEO brush follow the expected scaling

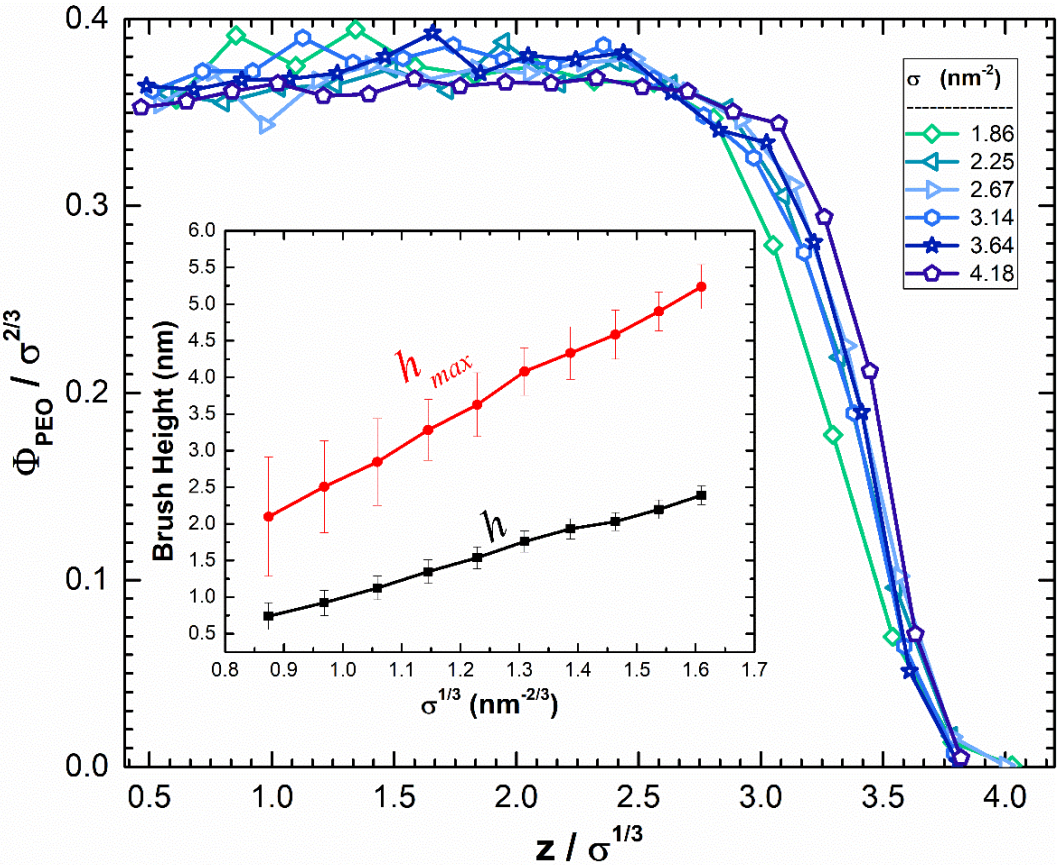

Figure 5.34. Re-scaled polymer volume fraction $\Phi_{PEO}(z)/\sigma^{2/3}$ as a function of reduced distance from the surface $z/\sigma^{1/3}$ for high grafting densities: $\sigma = 1.86,2.25,2.67,3.14,3.64\ and\ 4.18\ nm^{-2}$. The inset shows the average brush height, h, obtained using eq. (2) and the maximum brush height, h_{max} , corresponding to the maximum of end-group distribution, as functions of $\sigma^{1/3}$.

behavior for $\sigma > 1.8nm^{-2}$ when the surface influence becomes negligible and the PEO density profiles depicted in figure 5.33 can be all collapsed into one curve as shown in figure 5.34 by normalizing $\Phi_{PEO}(z)$ by $\sigma^{2/3}$ and z by $\sigma^{1/3}$. [42]

Brush hydration.

Knowing the polymer conformation and density distribution, we can now address polymer hydration in the brush. The PEO hydration shell can be characterized via the solvent accessible surface area (SASA) as shown in figure 5.35. As is seen, SASA considerably decreases with an increase of grafting density as water content declines inside the brush. Another measure of water surrounding PEO is the hydration number, which can vary considerably depending on definition and experimental technique which is used to assess it.[30] Counting all water molecules inside 3.5Å of PEO chain in the brush we arrived at the dependence shown in figure 5.35 per repeat unit of PEO. At $\sigma \leq 1.5nm^{-2}$ the average number per repeat unit of PEO remain unchanged and equal

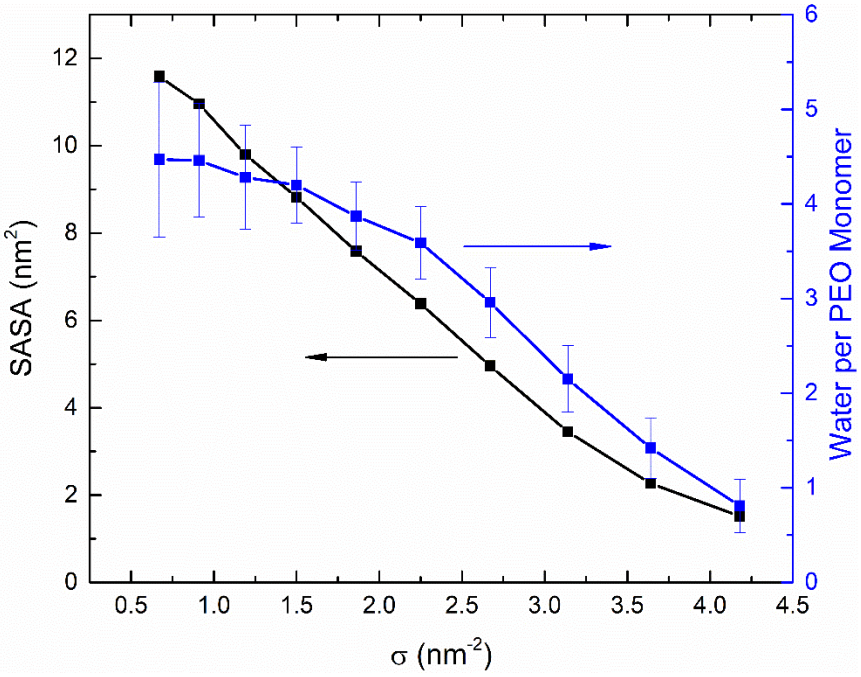

Figure 5.35. Solvent accessible surface area (SASA) per PEO chain and hydration number (i.e. the number of water molecules inside the distance 3.5A of PEO) per repeat unit of PEO as functions of grafting density.

to about 4.3 water molecules, which is smaller than that in solution, 5.9, likely due to PEO adsorption on the gold surface. At larger grafting densities, when PEO chains become more stretched (figure 5.32) the hydration number systematically declines following the SASA decrease with less than 1 water molecule remaining per repeat unit of PEO at the highest grafting density considered. More detailed information about PEO-water interaction in the polymer brush can be obtained from the analysis of the hydrogen bonding.

We analyzed the degree of hydrogen bonding between water molecules and PEO oxygens as a function of the distance from the gold surface for different grafting densities of PEO. The results are shown in figure 5.36a. As is seen, for $\sigma \leq 1.5\ nm^{-2}$ PEO is fully hydrated, similar to that in dilute solutions,[30] except for the first 0.8nm closest to the surface, where the polymer is present at high concentration and correspondingly water concentration is low (figure 5.36b). It is interesting to note that for small σ even though the water concentration decreases with an increase in grafting density, it does not affect the level of hydration in this region. A further increase in grafting density beyond $\sigma = 1.5nm^{-2}$, when the volume fraction of polymer starts to exceed that of water, results in a decrease in the average number of hydrogen bonds per oxygen of PEO as is seen in figure 5.36. For a given σ the hydration remains nearly constant throughout the brush except for the area near the gold surface and the outer surface of the brush, interfacing with water. When the grafting density exceeds $2.7nm^{-2}$ and volume fraction of water declines below 0.3, we start to observe considerable dehydration of the polymer brush with hydrogen bonding reduced by 50% or more. At these grafting densities polymer becomes strongly stretched, as discussed above (figure 5.34). At the highest grafting density considered, $\sigma = 4.18nm^{-2}$, less than 0.1 volume fraction of water remains in the brush and accordingly less than 10% of hydrogen bonds survive. This is a dehydrated strongly stretched PEO brush.

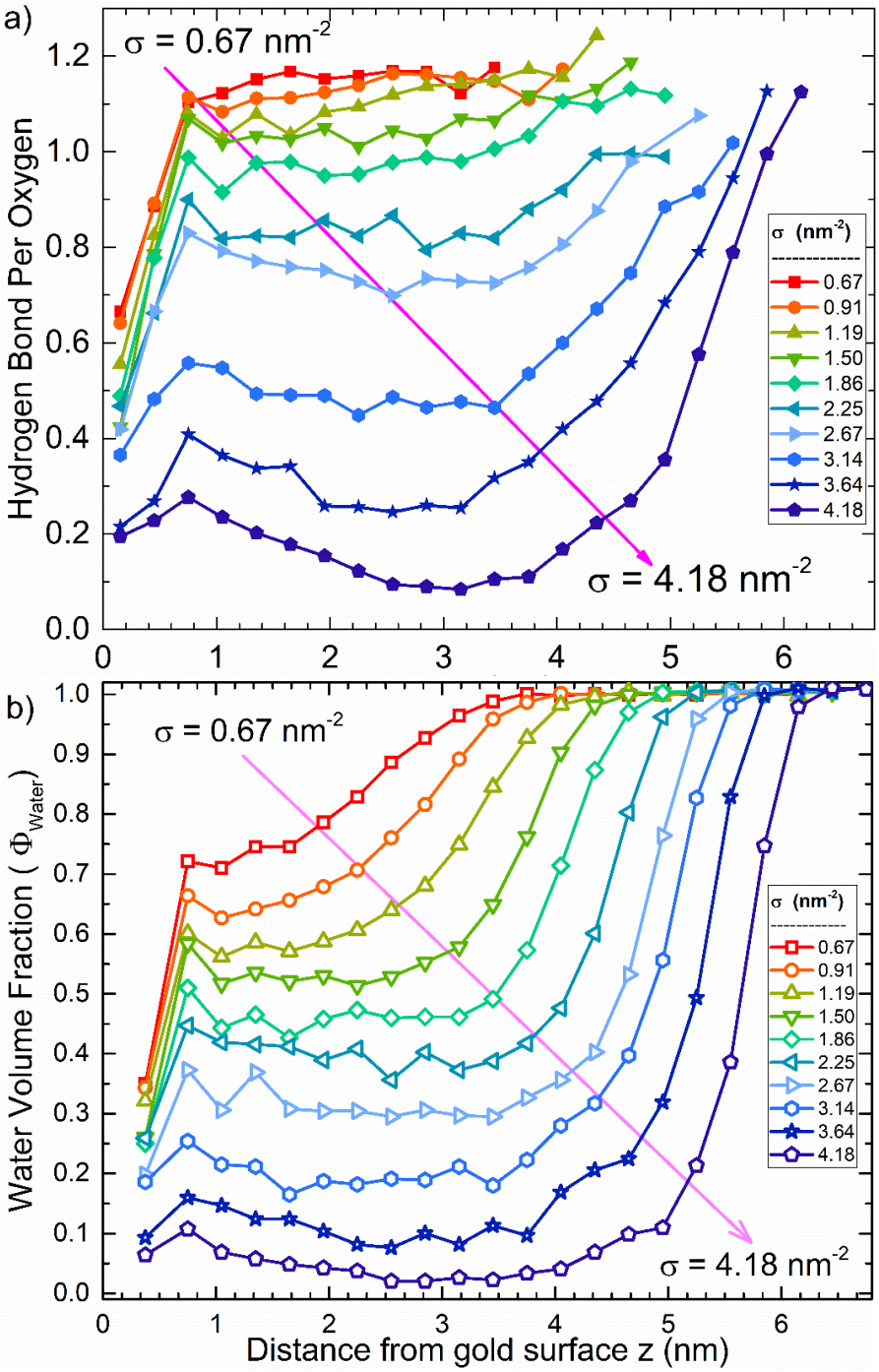

Figure 5.36. The average fraction of water –PEO hydrogen bonds per oxygen of PEO (a) and volume fraction of water (b) as a function of the distance from the gold surface for the following grafting densities from top to bottom: $\sigma = 0.67,\ 0.91,\ 1.19,\ 1.50,\ 1.86,\ 2.25,\ 2.67,\ 3.14,\ 3.64,\ 4.18\ nm^{-2}$.

As the polymer hydration changes with the volume fraction of water available to interact with the polymer, which in turn depends on grafting density of polymer, it is informative to plot the average number of hydrogen bonds per oxygen of PEO as a function of local PEO volume fraction. The results are shown in figure 5.37. As is seen, the results obtained for different polymer grafting densities and different distances from the surface (except for the very vicinity of the gold surface, which was excluded from calculations) fall into one curve. Hydrogen bonding between water molecules inside the polymer brush (shown in supporting information) also follows the same pattern and forms water-water hydrogen bonding curve in figure 5.37. The fact that both water-PEO and water-water hydrogen bonding in a brush follow a common pattern independent of grafting density, but dependent on the local polymer/water volume fraction, indicates that hydration simply depends on local water availability for hydrogen bonding. Furthermore, comparing the results obtained for hydrogen bonding inside the brush, shown as symbols in figure 5.37 with that obtained for PEO aqueous solutions at different water content, shown as lines in figure 5.37, one can see a complete agreement. This implies that PEO hydration in the polymer brush is exactly the same as it would be in a solution with the same volume fraction of polymer/water. The obtained dependences of the degree of hydrogen bonding as a function of volume fraction of PEO closely resemble theoretical dependences derived by one of us in earlier work for PEO solutions.[17]

Dynamic properties of PEO brush. Besides the equilibrium hydration properties of PEO chains in the brush, dynamic properties are also of interest for e.g. antifouling properties of PEO. [18–20] We'll first analyze the dynamics of hydration by calculating the residence time for hydrogen bonded water.[30,31] To this end we selected waters hydrogen bonded to a given PEO chain at time $t = 0$ and monitored the fraction of water that remain hydrogen bonded to the polymer chain (not necessary to the same oxygen) at time t. The results for different chains at a given grafting density and the different initial time were averaged to obtain the correlation function

$$C_{hb}(t) \equiv \langle \frac{N_w(t)}{N_w(0)} \rangle \qquad (5.34)$$

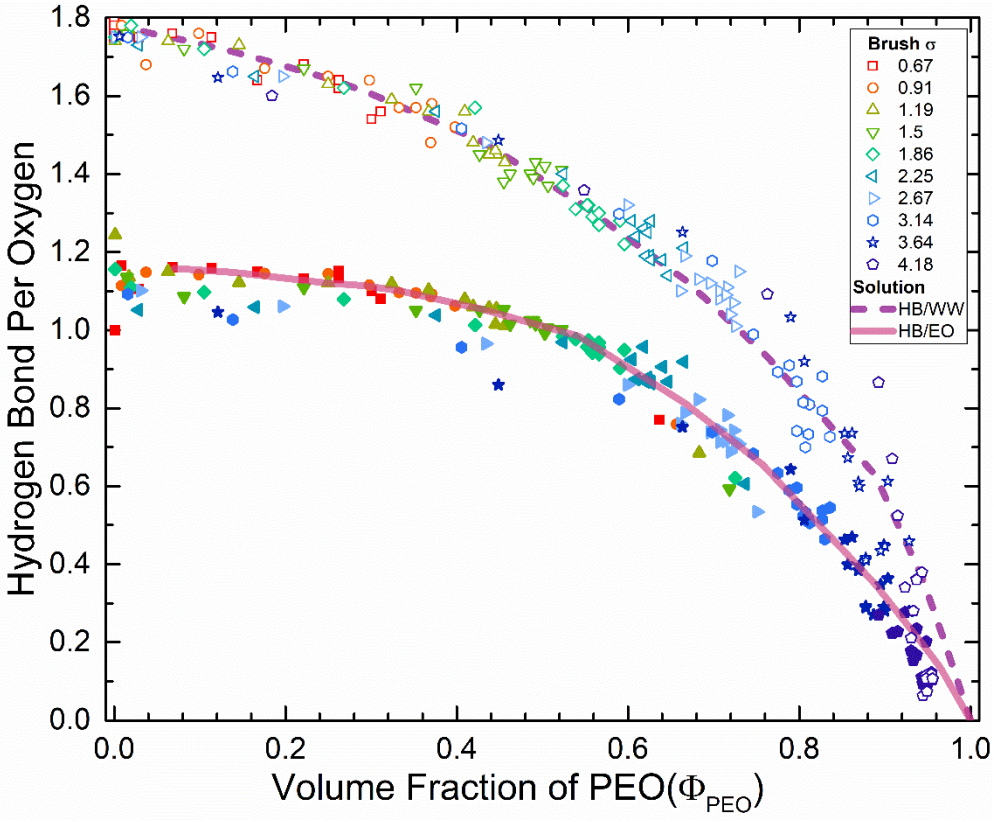

Figure 5.37. The average number of water hydrogen bonds per oxygen of PEO (solid symbols and solid line) and per oxygen of water (open symbols and dashed line) in polymer brush (symbols) and in aqueous solutions (lines) as functions of volume fraction of PEO. Data obtained for different grafting densities of PEO are shown in different color, as in Figures 5.33 and 5.36.

where $N_w(t)$ is the number of water hydrogen bonded to PEO at time t and $N_w(0)$ is the number of water at initial time $t = 0$. The results for $C_{hb}(t)$ obtained for different PEO grafting densities are shown in figure 5.38a. As is seen, exchange of water molecules hydrogen bonded to PEO considerably slows down as grafting density increases. Indeed, in the brush with $\sigma = 1.5nm^{-2}$ less than 10% of original hydrogen bonded water remains interacting with the polymer after 5 ns, while for $\sigma = 3.14nm^{-2}$ nearly 85% of water is still hydrogen bonded to the polymer after the same time period. This result is not unexpected, as high grafting density results in a denser brush with a lower fraction of water available (figure 5.34) and therefore less opportunity for water exchange.

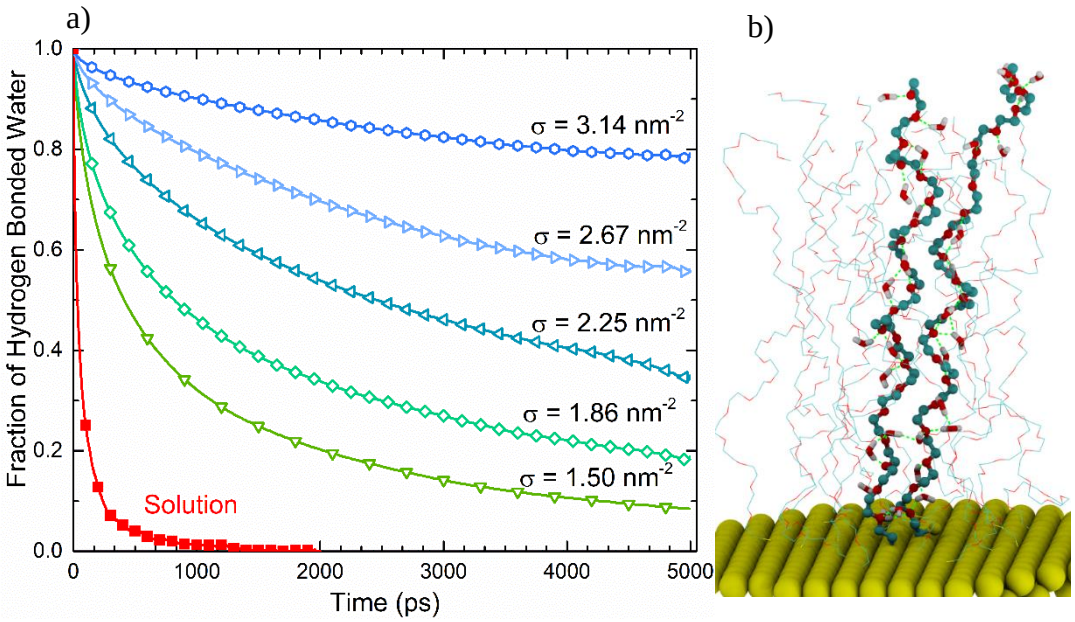

Figure 5.38. (a) The hydrogen bonded water fraction autocorrelation function, $C_{hb}(t)$, eq (4), for a PEO chain in a brush obtained at different grafting densities and in solution. (b) Polymer conformation containing helical portion for PEO brush at $\sigma = 2.25nm^{-2}$. Surrounding (non-helical) chains are shown as lines.

In order to numerically characterize the residence time of hydrogen bonded water we fit the $C_{hb}\ (t)$ correlation function with a triple exponential function (see supporting information for details),

which was required due to the presence of singe-bonded, double bonded and long-lived hydrogen bonded water, as discussed in ref.31.

Table 5.31. Orientational order parameter eq (1), R_{end}/R_g , the average number of hydrogen bonds per PEO oxygen, n_{hb} cumulative residence time of hydrogen bonded water, τ_{hb} and the tail orientation relaxation time for PEO chains in a brush, τ_{flex}.

$\sigma\ (nm^{-2})$	Order Parameter, S	R_{end}/R_g	n_{hb}	τ_{hb}(ns)	τ_{flex}(ns)
0.67	0.14 ± 0.04	2.71 ± 0.06	1.10 ± 0.04	--	--
0.91	0.37 ± 0.03	2.76 ± 0.06	1.09 ± 0.02	--	--
1.19	0.55 ± 0.03	2.91 ± 0.03	1.09 ± 0.03	--	0.38
1.50	0.70 ± 0.02	2.97 ± 0.04	1.04 ± 0.02	1.22	0.46
1.86	0.79 ± 0.02	3.08 ± 0.02	0.95 ± 0.02	1.50	0.52
2.25	0.83 ± 0.01	3.16 ± 0.01	0.89 ± 0.02	2.39	0.74
2.67	0.88 ± 0.01	3.21 ± 0.01	0.74 ± 0.04	2.47	0.94
3.14	0.91 ± 0.01	3.22 ± 0.01	0.55 ± 0.04	3.05	0.96
3.64	0.92 ± 0.00	3.26 ± 0.01	0.35 ± 0.06	--	1.02
4.18	0.94 ± 0.00	3.30 ± 0.01	0.16 ± 0.07	--	1.18

The cumulative residence time obtained using the sum of weighted relaxation times is shown in Table 1. As is seen, the cumulative residence lifetime of water $\sim 1.2ns$ for $\sigma = 1.5nm^{-2}$ and increases nearly linearly with σ reaching $\sim 3.0ns$ at $\sigma = 3.14\ nm^{-2}$. As discussed above, at the highest grafting densities the PEO brush becomes significantly dehydrated (figure 5.34), which slows down or totally precludes water exchange. We have not attempted to calculate the corresponding residence time, as the number of water molecules hydrogen bonded per chain becomes rather small to produce statistically meaningful results.

As previously discussed, the longevity of hydrogen bonded water interacting with a PEO chain is one of the necessary conditions to observe a helical or partially helical chain conformation.[30,31] The other condition is sufficiently high degree of hydrogen bonding with water. Analyzing the results shown in figure 5.37 and 5.38a, one can conclude that close to $\sigma = 2.24\, nm^{-2}$ both conditions can be satisfied, as at lower grafting density residence time of water is relatively short and at higher σ hydration is too low. Looking closely at PEO chain conformations in the brush we indeed spotted a couple of chains having a helical or partially helical conformation, as shown in figure 5.38b, even though the majority of the chains remain in a more random (and statistically preferable) non-helical conformation. Experimentally a helical conformation of PEO in a brush has also been occasionally observed under the right conditions.[14]

To further characterize the dynamics of surface grafted PEO chains, we calculated the tail flexibility correlation function. The segmental mobility of PEO chain ends is believed to be a contributing factor of PEO capability to prevent protein adsorption.[18–20] In our analysis we considered the PEO tail of three repeat units and calculated the autocorrelation orientational order parameter:

$$C_{tail}(t) = \langle \frac{1}{2}(3\,\mathrm{Cos}^2\,\theta - 1) \rangle \qquad (5.35)$$

where $Cos\theta = [\vec{r}_i(0).\vec{r}_i(t)] \,/\, |\vec{r}_i(0)|\,|\vec{r}_i(t)|$ and $\vec{r}_i(t)$ is the three segments tail vector at time t, as shown in the figure 5.39a and $\vec{r}_i(0)$ is the vector at $t = 0$. This function goes to zero when there is no correlation with the original orientation of the chain tail. The results for the tail autocorrelation function $C_{tail}(t)$ for PEO chains in a brush obtained at different grafting densities are shown in figure 5.39a.

As is seen, the correlation with the initial tail orientation dissipates rather quickly for low grafting densities of PEO. As the PEO brush becomes denser the correlation in orientation starts to become more obvious and persists for longer time. To obtain characteristic time we fitted the curves with triple exponential function as discussed in supporting information and calculated cumulative relaxation time by using a weighted sum of relaxation times shown in Table 1. As is seen, the characteristic relaxation times for PEO tail varies from $0.4ns$ at low grafting densities to about $1.2ns$ at the highest grafting density studied. This change in PEO tail flexibility originates from the increased density and decreased hydration of the polymer brush occurring upon increased σ. To connect the obtained results for $C_{tail}(t)$ with actual changes in PEO chain conformation, we traced a PEO chain conformation with time up to $2.5ns$ and show it for a few grafting densities in figure 5.39b along with the residual autocorrelation $C_{tail}(t \to \infty)$ dependence on σ. As is seen, at low σ, when the average distance between chains is considerable, PEO chains can freely change conformation with negligible tail orientation self-correlation. At intermediate grafting densities, chain motion is much more restricted and we start to observe a residual tail orientation self-correlation. At high σ only minor chain motion is observed leading to significant (up to 80%) residual tail orientation self-correlation. Thus, while a high grafting density of PEO chains may be beneficial for protecting underlying surface from contacts with surrounding media, the resulting PEO brush is very dense, highly stretched and dehydrated with very little chain flexibility remaining, which may lead to protein adsorption on top of the brush.

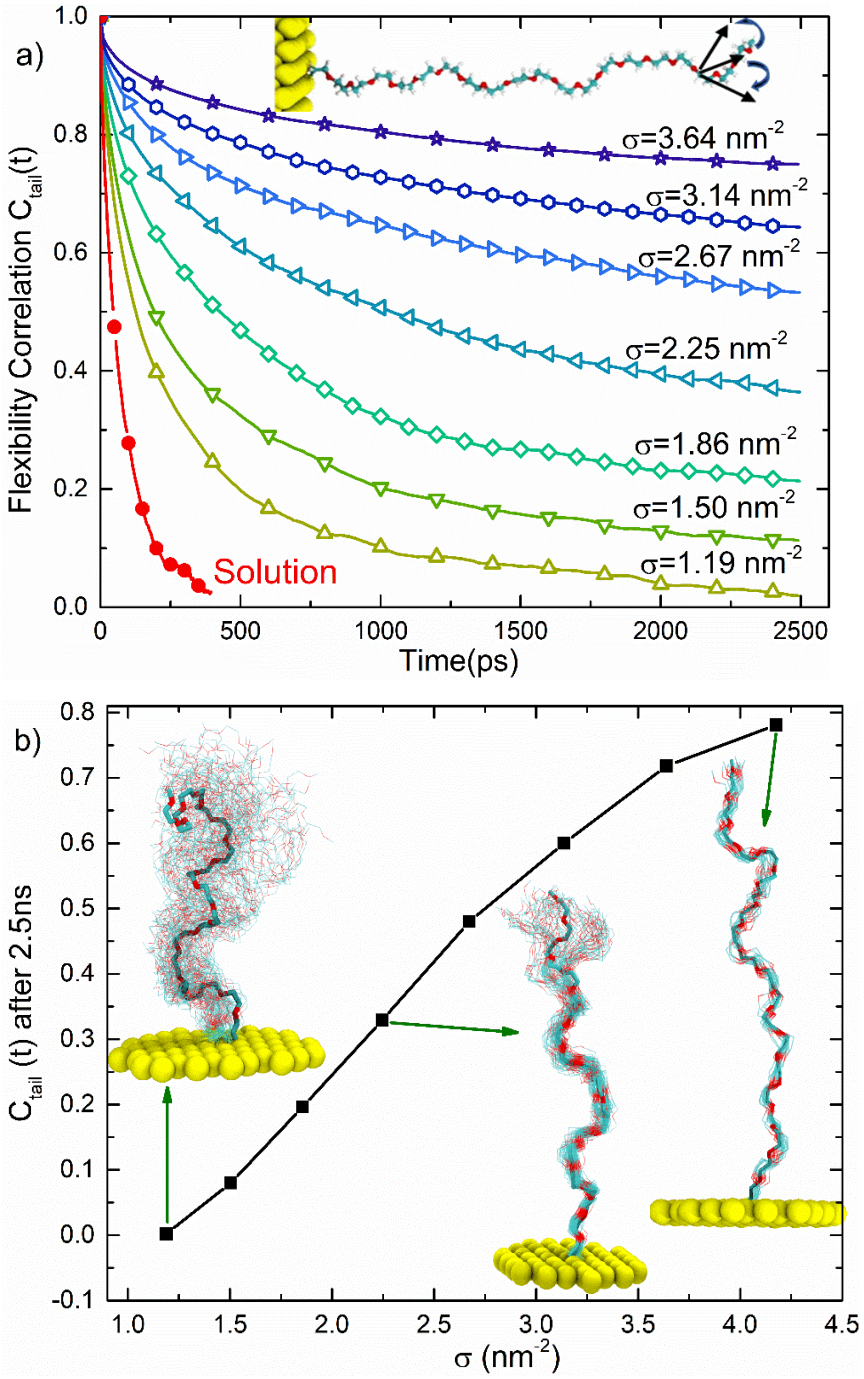

Figure 5.39. (a) PEO tail orientation autocorrelation function $C_{tail}(t)$ eq (5) obtained for different grafting densities. Simulation snapshot of PEO chain grafted to gold surface indicating tail orientation vector used in calculations is shown. (b) Residual PEO tail orientation autocorrelation function $C_{tail}(t \to \infty)$ as a function of grafting density. Simulation snapshots show the time evolution of PEO chain conformation for the following grafting densities: $\sigma = 1.19, 2.25\ and\ \ 4.18\ nm^{-2}$.

PEO brush in THF solution.

As discussed above, at low grafting densities PEO tends to adsorb on gold surface releasing water from the layers adjacent to the gold surface (figure 5.31, 5.32). It is informative to compare the behavior of PEO brush in a different solvent. We have chosen THF in which PEO is soluble (at least to some extent),[45] but which is not a proton donating solvent like water, so there is no hydrogen bonding in a PEO solution in THF. For comparison, we selected a relatively low grafting density of $0.91 nm^{-2}$ for which we observe noticeable PEO adsorption on gold surface in aqueous solution (figure 5.32). The PEO density profile and snapshot of PEO brush conformation in THF are shown in figure 5.310. In agreement with experimental observations[46] we observe THF adsorption onto gold surface with formation of high density (~0.8 volume fraction) THF layer, shielding the gold surface. No PEO adsorption is observed, confirming that PEO-gold interactions are favorable only compared to water-gold interactions, but not compared to THF-gold contacts. In fact, THF layering near the gold surface results in stretching of PEO chain away from the gold surface (figure 5.310). Despite this local chain stretching in the vicinity of gold surface, no significant changes observed in the overall PEO brush height, even though the PEO density is distributed differently in THF and PEO solutions (inset of figure 5.310). As THF nearly completely covers the gold surface, we expect that very similar results should be expected for PEO brush on e.g. an alkane monolayer-modified surface.

We also investigated the behavior of PEO brush (at $\sigma = 0.91\, nm^{-2}$) in THF:water mixture. A simulation snapshot of the brush and volume fraction profiles for PEO, THF and water are shown in figure 5.311 for 80:20 THF:water mixture (by volume), which was chosen for computational convenience. As is seen, THF/gold contacts are the most favorable, so we observe layering of THF in the vicinity of gold surface similar to that in pure THF (figure 5.310). There is also PEO

stretching away from the gold surface as in pure THF with practically no water being in contact with the gold surface. At larger distances from the surface, $z > 0.8nm$ the distribution is reverse – there is less than 10% of THF present inside the PEO brush, which is saturated with water. This preferential accumulation of water inside the PEO brush is consistent with water being a better

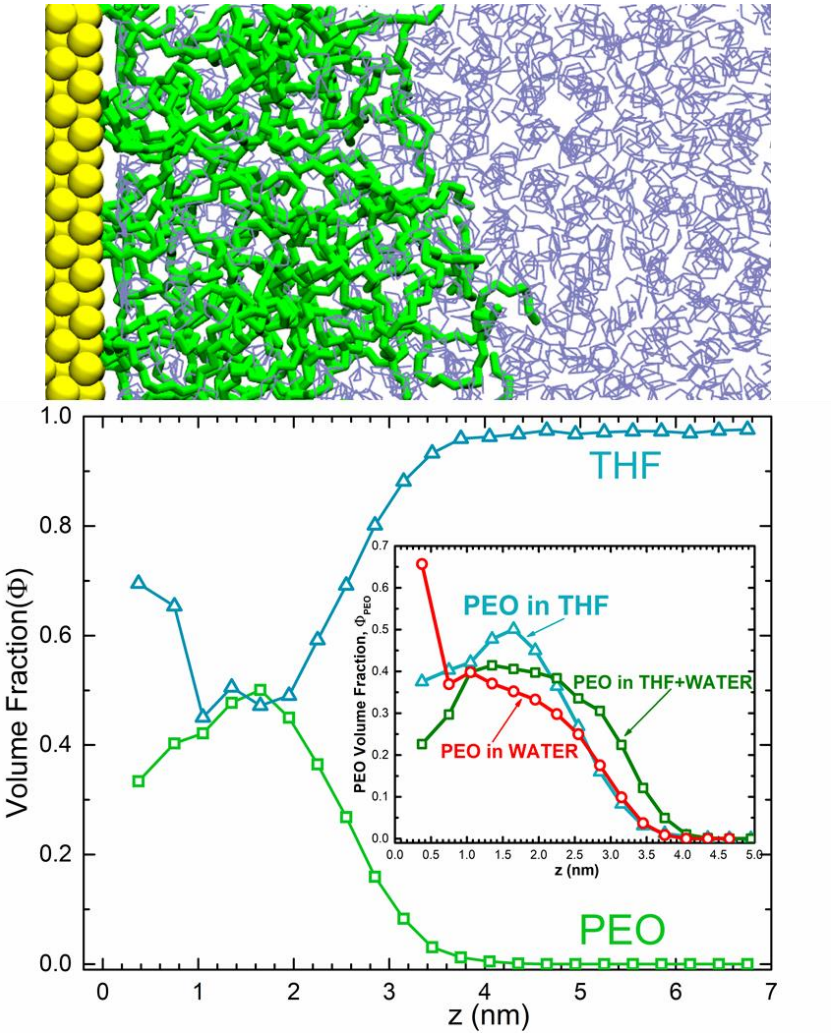

Figure 5.310. (top) Computer simulation snapshot of PEO brush grafted to gold surface ($\sigma = 0.91\ nm^{-2}$) in THF. PEO chains are shown in green, THF in blue. (bottom) Volume fraction of PEO and THF as a function of the distance away from the gold surface, z. Inset shows PEO volume fraction profile in the brush in THF (triangles), water (circles) and in 80:20 (by volume) THF/water mixture (squares).

solvent for PEO than THF. The overall height of the PEO brush is somewhat larger in this case compared to pure THF or pure water solvents, as is seen in figure 5.310 (inset). This is a result of PEO extension away from the surface compared to adsorption observed in water and more expanded PEO conformation in an aqueous surrounding compared to THF. Away from the PEO brush we observe (e.g. an inhomogeneous water density profile) a local clustering of water in the THF media in agreement with experimental observations[47] indicating that the miscibility of these

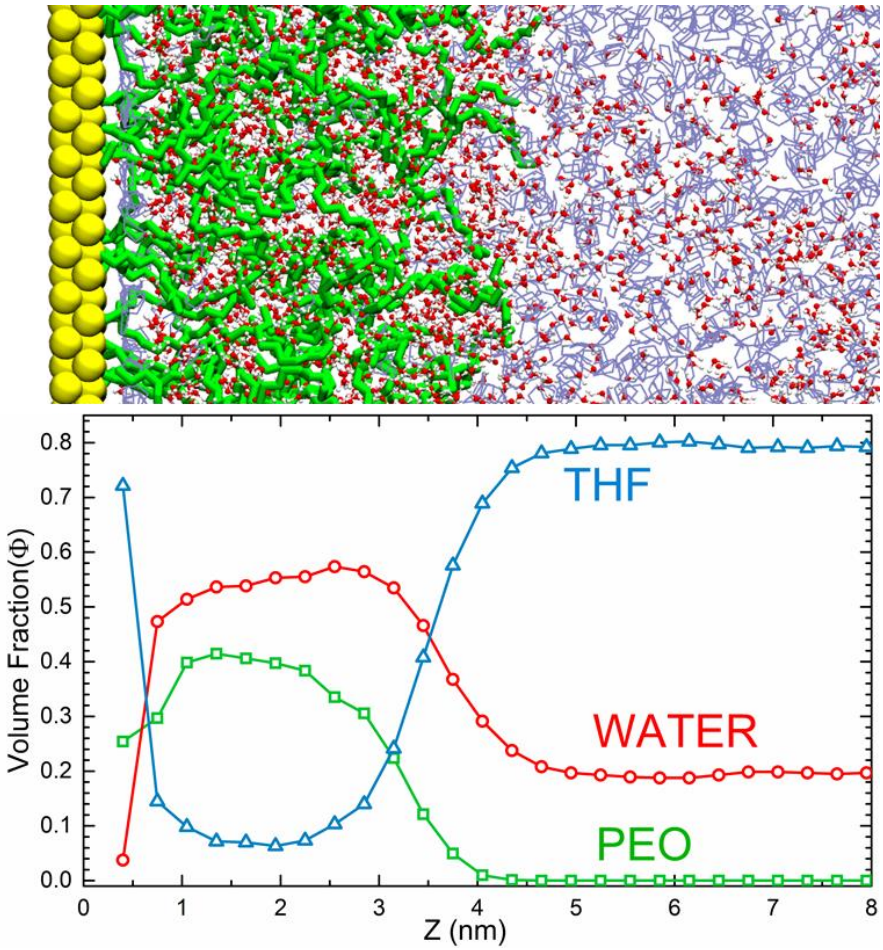

Figure 5.311. (top) Computer simulation snapshot of PEO brush grafted to gold surface ($\sigma = 0.91\, nm^{-2}$) in mixed 80:20 (by volume) THF:water solvent. PEO chains are shown in green, THF in purple, water in red. (bottom) Volume fraction of PEO, THF and water as functions of the distance away from the gold surface, z.

two solvents is somewhat limited. Extrapolating the results presented in figure 5.311 one can anticipate that PEO brush grafted to e.g. an alkane-functionalized surface would be somewhat more expanded in aqueous surrounding than gold-functionalized PEO brush (except for high grafting densities when adsorption on the surface or further PEO expansion is not possible) and that PEO brush can be used as effective separation media for extraction of water from some mixed solvents.

5.4. Conclusions

Using atomistic molecular dynamics simulations, we investigated the hydration, static and dynamic properties of PEO chains (of 20 repeat units) grafted to a planar gold surface. The effect of grafting density (ranging from $\sigma = 0.67nm^{-2}$ to $\sigma = 4.18nm^{-2}$) has been investigated. We found that at low grafting densities PEO chains are fully hydrated and retain a conformation similar to that in solution, except for the area in the immediate vicinity of the gold surface, where PEO adsorption is observed figure 5.33). In agreement with experimental observations,[35] PEO adsorption on gold is attributed to more favorable interactions between PEO and gold compared to water-gold interactions which leads to water layering near the gold surface. At higher grafting density the excluded volume interactions overcome the PEO attraction to gold resulting in PEO chains stretching away from the surface with the chain's aspect ratio R_{end}/R_g approaching a value of 3.3 similar to that expected for a rod-like conformation (figure 5.32, Table 1). The overall PEO monomer density profile (figure 5.33) follows the expected parabolic dependence[40,41] at low grafting density and a step function at higher grafting densities[41,48] with all curves collapsing into

a single dependence upon re-scaling[42] (figure 5.34). Accordingly, the polymer brush height increases with grafting density following the expected $h \propto \sigma^{1/3}$ scaling dependence.[41]

Hydration of a PEO brush depends on the accessibility of water inside the grafted layer. For lower grafting densities, $\sigma \leq 1.5nm^{-2}$ (i.e. $1/(R_g\sqrt{\sigma}) \geq 0.62$), the volume fraction of water exceeds that of polymer with the exception of the close vicinity of the gold surface (Figure 5.36) and as a result PEO is well-hydrated (figure 5.35). With an increase in the grafting density, the polymer volume fraction noticeably increases and accordingly PEO becomes dehydrated with only about 10% of hydrogen bonding remaining at the highest grafting density considered, $\sigma = 4.18nm^{-2}$, compared to polymer hydration in aqueous solutions or at the lowest grafting density considered. We found that PEO hydration inside the brush closely follows that for aqueous solutions at the corresponding polymer volume fraction (figure 5.37). This implies that hydrogen bonding is determined by the local concentration of water and adheres to the polymer density profile of the brush rather than *vice versa*. This property of a PEO brush makes it easier to anticipate the level of PEO hydration and design a PEO brush with desired properties.

The dynamic properties of PEO brush are somewhat more complex. At low grafting density PEO attachment to the surface does not strongly affect the dynamics of its hydration and its flexibility (figures 5.38 and 5.39). With an increase in grafting density the residence time of hydrogen bonded water noticeably increases and at a high grafting density of $\sigma = 3.64nm^2$ reaches nearly $10ns$, which is several orders of magnitude larger than a hydrogen bond life-time in bulk aqueous solution.[30] Such a long residence time of hydrogen bonded water is attributed to the low volume fraction of water inside the PEO brush and limited water diffusion due to the presence of the gold surface. The analysis of the PEO tail orientation autocorrelation function also shows a noticeable enhancement in the residual "orientational memory" and corresponding decrease in tail flexibility

with an increase in σ (figure 5.39). These findings are consistent with the general idea that dense PEO brushes are not only dehydrated but also lose flexibility, which may compromize their capability to inhibit protein adsorption.

To test the effect of solvent quality we compared properties of PEO brush at $\sigma = 0.91\ nm^{-2}$ in THF and a mixed water/THF solvent (figures 5.310 and 5.311). In pure THF we observed that the solvent prefers contacts with gold surface, while the overall brush height remains comparable to that observed in water, implying a less expanded PEO conformation in THF, which is known to be a marginal solvent for PEO. In the mixed THF/water solution THF forms a thin layer near the gold surface, but otherwise is practically excluded from the PEO brush where water predominantly resides ensuring more expanded PEO conformation compared to pure THF or aqueous solutions.

The obtained results provide fundamental insights on the physical properties of a PEO brush grafted to gold surfaces, including experimentally testable predictions regarding PEO layer hydration and tail flexibility, as these are the key properties relevant for anti-fouling applications.

5.5. References

(1) Whiting, G. L.; Farhan, T.; Huck, W. T. S. Polymer Brushes: Towards Applications. In *Polymer Brushes*; Wiley-VCH Verlag GmbH & Co. KGaA: Weinheim, FRG, 2005; pp 371–380.

(2) Binder, K.; Milchev, A. Polymer Brushes on Flat and Curved Surfaces: How Computer Simulations Can Help to Test Theories and to Interpret Experiments. *J. Polym. Sci. Part B Polym. Phys.* **2012**, *50* (22), 1515–1555.

(3) Lee, J.; Lee, H.; Andrade, J. Blood Compatibility of Polyethylene Oxide Surfaces. *Prog. Polym. Sci.* **1995**, *20* (6), 1043–1079.

(4) Jokerst, J. V; Lobovkina, T.; Zare, R. N.; Gambhir, S. S. Nanoparticle PEGylation for Imaging and Therapy. *Nanomedicine (Lond).* **2011**, *6* (4), 715–728.

(5) Ratner, B. D.; Bryant, S. J. Biomaterials: Where We Have Been and Where We Are Going. *Annu. Rev. Biomed. Eng.* **2004**, *6* (1), 41–75.

(6) Harris, J. M.; Chess, R. B. Effect of Pegylation on Pharmaceuticals. *Nat. Rev. Drug*

Discov. **2003**, *2* (3), 214–221.

(7) Lee, H.; Kim, D. H.; Park, H. W.; Mahynski, N. A.; Kim, K.; Meron, M.; Lin, B.; Won, Y. Y. Reduced Water Density in a Poly(ethylene Oxide) Brush. *J. Phys. Chem. Lett.* **2012**, *3* (12), 1589–1595.

(8) Fuchs, C.; Hussain, H.; Schwieger, C.; Schulz, M.; Binder, W. H.; Kressler, J. Molecular Arrangement of Symmetric and Non-Symmetric Triblock Copolymers of Poly(ethylene Oxide) and Poly(isobutylene) at the Air/water Interface. *J. Colloid Interface Sci.* **2015**, *437*, 80–89.

(9) Tsukanova, V.; Salesse, C. On the Nature of Conformational Transition in Poly(ethylene Glycol) Chains Grafted onto Phospholipid Monolayers. *J. Phys. Chem. B* **2004**, *108* (30), 10754–10764.

(10) Halperin, A. Compression Induced Phase Transitions in PEO Brushes: The N-Cluster Model. *Eur. Phys. J. B* **1998**, *3* (3), 359–364.

(11) Wagner, M.; Brochard-Wyart, F.; Hervet, H.; de Gennes, P.-G. Collapse of Polymer Brushes Induced by N-Clusters. *Colloid Polym. Sci.* **1993**, *271* (7), 621–628.

(12) Leckband, D.; Sheth, S.; Halperin, A. Grafted Poly(ethylene Oxide) Brushes as Nonfouling Surface Coatings. *J. Biomater. Sci. Polym. Ed.* **1999**, *10* (10), 1125–1147.

(13) Gon, S.; Kumar, K.-N.; Nüsslein, K.; Santore, M. M. How Bacteria Adhere to Brushy PEG Surfaces: Clinging to Flaws and Compressing the Brush. *Macromolecules* **2012**, *45* (20), 8373–8381.

(14) Pop-Georgievski, O.; Verreault, D.; Diesner, M.-O.; Proks, V.; Heissler, S.; Rypáček, F.; Koelsch, P. Nonfouling Poly(ethylene Oxide) Layers End-Tethered to Polydopamine. *Langmuir* **2012**, *28* (40), 14273–14283.

(15) Emilsson, G.; Schoch, R. L.; Feuz, L.; Hook, F.; Lim, R. Y. H.; Dahlin, A. B. Strongly Stretched Protein Resistant Poly(ethylene Glycol) Brushes Prepared by Grafting-To. *ACS Appl. Mater. Interfaces* **2015**, *7* (14), 7505–7515.

(16) Dormidontova, E. E. Influence of End Groups on Phase Behavior and Properties of PEO in Aqueous Solutions. *Macromolecules* **2004**, *37* (20), 7747–7761.

(17) Dormidontova, E. E. Role of Competitive PEO−Water and Water−Water Hydrogen Bonding in Aqueous Solution PEO Behavior. *Macromolecules* **2002**, *35* (3), 987–1001.

(18) Otsuka, H.; Nagasaki, Y.; Kataoka, K. Characterization of Aldehyde-PEG Tethered Surfaces: Influence of PEG Chain Length on the Specific Biorecognition. *Langmuir* **2004**, *20* (26), 11285–11287.

(19) Ji, J.; Feng, L.; Qiu, Y.; Yu, X. Stearyl Poly(ethylene Oxide) Grafted Surfaces for Preferential Adsorption of Albumin Part 2. The Effect of Molecular Mobility on Protein Adsorption. *Polymer (Guildf).* **2000**, *41* (10), 3713–3718.

(20) Torchilin, V. P.; Trubetskoy, V. S. Which Polymers Can Make Nanoparticulate Drug Carriers Long-Circulating? *Adv. Drug Deliv. Rev.* **1995**, *16* (2–3), 141–155.

(21) Bedrov, D.; Smith, G. Molecular Dynamics Simulation Study of the Structure of Poly (Ethylene Oxide) Brushes on Nonpolar Surfaces in Aqueous Solution. *Langmuir* **2006**, *22* (14), 6189–6194.

(22) Benková, Z.; Szefczyk, B.; Cordeiro, M. N. D. S. Molecular Dynamics Study of Hydrated Poly(ethylene Oxide) Chains Grafted on Siloxane Surface. *Macromolecules* **2011**, *44* (9), 3639–3648.

(23) Benková, Z.; Cordeiro, M. N. D. S. Molecular Dynamics Study of Water Interacting with Siloxane Surface Modified by Poly(ethylene Oxide) Chains. *J. Phys. Chem. C* **2011**, *115* (38), 18740–18751.

(24) Sebby, K. B.; Mansfield, E. Determination of the Surface Density of Polyethylene Glycol on Gold Nanoparticles by Use of Microscale Thermogravimetric Analysis. *Anal. Bioanal. Chem.* **2015**, *407* (10), 2913–2922.

(25) Laradji, A. M.; McNitt, C. D.; Yadavalli, N. S.; Popik, V. V.; Minko, S. Robust, Solvent-Free, Catalyst-Free Click Chemistry for the Generation of Highly Stable Densely Grafted Poly(ethylene Glycol) Polymer Brushes by the Grafting To Method and Their Properties. *Macromolecules* **2016**, *49* (20), 7625–7631.

(26) Ren, C.; Nap, R. J.; Szleifer, I. The Role of Hydrogen Bonding in Tethered Polymer Layers. *J. Phys. Chem. B* **2008**, *112* (50), 16238–16248.

(27) Khlebtsov, N.; Dykman, L. Biodistribution and Toxicity of Engineered Gold Nanoparticles: A Review of in Vitro and in Vivo Studies. *Chem. Soc. Rev.* **2011**, *40* (3), 1647–1671.

(28) Boisselier, E.; Astruc, D. Gold Nanoparticles in Nanomedicine: Preparations, Imaging, Diagnostics, Therapies and Toxicity. *Chem. Soc. Rev.* **2009**, *38* (6), 1759.

(29) Tay, K. A.; Bresme, F. Wetting Properties of Passivated Metal Nanocrystals at Liquid−Vapor Interfaces: A Computer Simulation Study. *J. Am. Chem. Soc.* **2006**, *128* (43), 14166–14175.

(30) Dahal, U. R.; Dormidontova, E. E. The Dynamics of Solvation Dictates the Conformation of Polyethylene Oxide in Aqueous, Isobutyric Acid and Binary Solutions. *Phys. Chem. Chem. Phys.* **2017**, *19* (15), 9823–9832.

(31) Dahal, U. R.; Dormidontova, E. E. Spontaneous Insertion, Helix Formation, and Hydration of Polyethylene Oxide in Carbon Nanotubes. *Phys. Rev. Lett.* **2016**, *117* (2), 27801.

(32) Bondi, A. Van Der Waals Volumes and Radii. *J. Phys. Chem.* **1964**, *68* (3), 441–451.

(33) Humphrey, W.; Dalke, A.; Schulten, K. VMD: Visual Molecular Dynamics. *J. Mol. Graph.* **1996**, *14* (1), 33–38.

(34) Ma, H.; Hyun, J.; Stiller, P.; Chilkoti, A. "Non-Fouling" Oligo(ethylene Glycol)-Functionalized Polymer Brushes Synthesized by Surface-Initiated Atom Transfer Radical Polymerization. *Adv. Mater.* **2004**, *16* (4), 338–341.

(35) Huang, Y.; Gupta, V. K. Effects of Physical Heterogeneity on the Adsorption of Poly (Ethylene Oxide) at a Solid - Liquid Interface. *Macromolecules* **2001**, *34* (11), 3757–3764.

(36) Velasco-Velez, J.-J.; Wu, C. H.; Pascal, T. A.; Wan, L. F.; Guo, J.; Prendergast, D.; Salmeron, M. The Structure of Interfacial Water on Gold Electrodes Studied by X-Ray Absorption Spectroscopy. *Science (80-.).* **2014**, *346* (6211), 831–834.

(37) Stacchiola, D.; Park, J. B.; Liu, P.; Ma, S.; Yang, F.; Starr, D. E.; Muller, E.; Sutter, P.; Hrbek, J. Water Nucleation on Gold: Existence of a Unique Double Bilayer. *J. Phys. Chem. C* **2009**, *113* (34), 15102–15105.

(38) Corem, G.; Kole, P. R.; Zhu, J.; Kravchuk, T.; Manson, J. R.; Alexandrowicz, G. Ordered H 2 O Structures on a Weakly Interacting Surface: A Helium Diffraction Study of H 2 O/Au(111). *J. Phys. Chem. C* **2013**, *117* (45), 23657–23663.

(39) Cicero, G.; Calzolari, A.; Corni, S.; Catellani, A. Anomalous Wetting Layer at the Au(111) Surface. *J. Phys. Chem. Lett.* **2011**, *2* (20), 2582–2586.

(40) Milner, S. T.; Witten, T. A.; Cates, M. E. Theory of the Grafted Polymer Brush. *Macromolecules* **1988**, *21* (8), 2610–2619.

(41) Milner, S. T. Polymer Brushes. *Science (80-.).* **1991**, *251* (4996), 905–914.

(42) Laradji, M.; Guo, H.; Zuckermann, M. J. Off-Lattice Monte Carlo Simulation of Polymer Brushes in Good Solvents. *Phys. Rev. E* **1994**, *49* (4), 3199–3206.

(43) Murat, M.; Grest, G. S. Structure of a Grafted Polymer Brush: A Molecular Dynamics Simulation. *Macromolecules* **1989**, *22* (3), 4054–4059.

(44) Carignano, M. A.; Szleifer, I. Statistical Thermodynamic Theory of Grafted Polymeric Layers. *J. Chem. Phys.* **1993**, *98* (1993), 5006.

(45) Nayak, J.; Aralaguppi, M.; Naidu, B. V.; Aminabhavi, T. Thermodynamic Properties of Water + Tetrahydrofuran and Water + 1 , 4-Dioxane Mixtures at (303 . 15 , 313 . 15 , and 323 . 15) K. *J. Chem. Eng. Data* **2004**, *49*, 468–474.

(46) Barden, W. R. T.; Singh, S.; Kruse, P. Roughening of Gold Atomic Steps Induced by Interaction with Tetrahydrofuran. *Langmuir* **2008**, *24* (6), 2452–2458.

(47) Hao, J.; Cheng, H.; Butler, P.; Zhang, L.; Han, C. C. Origin of Cononsolvency, Based on the Structure of Tetrahydrofuran-Water Mixture. *J. Chem. Phys.* **2010**, *132* (15).

(48) Alexander, S. Adsorption of Chain Molecules with a Polar Head a Scaling Description. *J. Phys.* **1977**, *38* (8), 983–987.

Chapter 6.

Spherical PEO brushes

6.1. Introduction

Surface modification of organic and inorganic nanoparticles by polymers has gained considerable attention in a growing range of nanotechnological applications.[1–7] With the development of new synthetic grafting approaches the range of available polymers has expanded and the accessible window of grafting densities considerably increased. Unlike the planar brush for which the maximum experimental grafting density corresponds to approximately 1 chain per nanometer squared, for nanoparticles with a larger accessible volume the number of chains grafted per nm^2 can be as high as 4 and even higher numbers ($\sim 6\, nm^{-2}$) are experimentally reported.[8] A high grafting density can be desirable to achieve the complete coverage and protection of the nanoparticle surface from the surrounding media. These polymer grafting densities on nanoparticles are considerably higher than can be achieved by self-assembly of e.g. diblock copolymers and represent an interesting case to test classical theoretical predictions for polymer stars or spherical polymer brushes.[9–12] Despite the reports of high grafting densities for spherical polymer brushes on nanoparticles the majority of experimental measurements of the physical properties of these brushes, as well as theoretical and computation research, is limited to a low to moderate grafting densities,[12–15] with only a few recent publications discussing spherical polymer brushes of high grafting density.[8,16,17] One of the important applications of polymer grafted nanoparticles is in imaging and therapeutic applications in biomedicine.[6,18–20]. In particular gold nanoparticles grafted by polyethylene oxide to insure stability and prevent protein adsorption have been actively explored due to their low toxicity, ability to produce local heating, plasmonic properties making them desirable for photodynamic therapy, cell imaging and biosensing.[4,21,22]

The main functions of the grafted spherical PEO shell surrounding gold nanoparticle are to ensure a long circulation time and protect them from undesirable interactions which relies on the high solubility and mobility of PEO, which in turn depends on hydrogen bonding between PEO and water and PEO hydration in general. Experimental characterization of PEO hydration is a difficult task, which becomes almost impossible to achieve for a grafted spherical layer where the distribution of water significantly varies with the distance from the surface and depends on grafting density and nanoparticle radius of curvature. So far there have been no comprehensive studies, either experimental or by computer simulations, analyzing hydration of PEO grafted to a nanoparticle. In this work using atomistic molecular dynamic simulations we investigate a range of spherical gold nanoparticles varying in size and grafting densities of polyethylene oxide and analyze the scaling behavior, PEO conformation and hydration throughout the spherical layer. The results of this study on the effect of grafting density and nanoparticle radius of curvature on PEO hydration, water distribution and dynamics inside the layer can have important implications in designing of PEO-grafted nanoparticles for biomedical applications as well as for catalysis.

Experimentally, small angle neutron scattering (SANS) or small angle x-ray scattering (SAXS) are the common techniques used to characterize polymer-grafted nanoparticles with the intensity curve fitted to different models to obtain the polymer shell size, polymer density distribution and water fraction. Recently, Lennox et. al. studied PEO capped gold nanoparticles using transmission electron microscopy(TEM), thermogravimetric analysis(TGA), mass density, SANS and SAXS. They reported a rather high PEO grafting density,$\sigma = 5.83 \pm 0.5\ nm^{-2}$.[8] Using contrast matching the properties of the spherical PEO corona were analyzed using two-shell model with the inner dehydrated PEO shell of about 1.66 nm containing practically no water and the outer shell with a

polymer volume fraction ranging from 0.68 to 0.48. Similar conclusions on existence of concentrated inner PEO shell of constant density (of 1.1 nm width) were made in another recent study by Reimhult et. al. on PEO grafted iron-oxide nanoparticles.[16] Analyzing SAXS data the authors discussed the PEO brush density profile which in dilute regime for the outer shell is found to follow the classical model by Daoud and Cotton.[9] Since it is difficult to probe molecular level details of polymer conformation and hydration in experiment, which rely on assumptions of the model used for data fitting, computer simulation can be a very helpful tool to investigate the polymer conformational properties and organization inside the brush as well as to analyze water dynamics. Understanding the interfacial properties of polymer brush as well as polymer arrangement near the nanoparticle surface is essential to improve nanoparticle performance and broaden the application of nanomaterials in nanotechnology and biomedicine.

Experimental data are normally analyzed using Daoud and Cotton scaling model[9] which considers three regimes, the central rigid core of constant density, concentrated regime where volume fraction of polymer changes as $\Phi \propto r^{-1}$ and semi-dilute regime, $\Phi \propto r^{-4/3}$. Later, the scaling model was extended to consider polymer micelles and self-consistent mean filed approach was used to describe the structural properties of neutral and charged spherical polymer brushes.[10,11,23] These models recover Daoud-Cotton scaling, $\Phi \propto r^{-4/3}$ in semi-dilute good solvent conditions and predict the average brush height H (calculated as second moment of density distribution) to follow $H \propto \sigma^{1/5}$ dependence on polymer grafting density σ for small particles and converge to $H \propto \sigma^{1/3}$ for large particles and/or very high grafting densities.[11] Besides of being tested experimentally, the predicted scaling dependences have been probed in computer simulations. Monte Carlo and generic molecular dynamics (MD) simulations that have been used mainly

investigated spherical brushes of low grafting density.[12,15,24] Thus, recently Binder et. al. carried out coarse grained model simulation of polymer brushes on curved surfaces using MD simulation and density functional theory with the main focus on scaling behavior of curved brushes.[12] They found that polymer brush follows Daoud-Cotton scaling, $\Phi \propto r^{-4/3}$ but DFT shows brush height scaling on chain length as $N^{2/3}$ instead of star polymer scaling $N^{3/5}$. Several coarse-grained MD simulations and a few atomistic simulations of gold nanoparticles functionalized mainly by short alkane oligomers have been performed in recent years with the main purpose to understand their interactions with lipid bilayers and aggregates.[25] These studies have not analyzed properties of polymer brush nor studied polymer hydration. In general, we are not aware of any atomistic molecular dynamics simulations of PEO-grafted gold nanoparticles or any investigations by means of computer simulations of PEO hydration in a spherical polymer brush grafted to a nanoparticle computer modeling the equilibrium structure of spherical PEO brush. All-atom MD simulations are well-suited to obtain molecular level insights on polymer hydration and conformation inside the spherical brush, which as discussed above is of obvious fundamental and practical importance.

In this paper, using all-atom MD simulations we study the equilibrium properties and hydration of PEO brush grafted to spherical gold nanoparticles of different radii: r=1,2 and 3 nm, as shown in Figure 1.6.31. We investigate the polymer and water volume fraction distribution and test applicability of Daoud-Cotton scaling model. Varying polymer grafting density σ we analyze polymer conformation and orientation in the spherical layer and test theoretical predictions for the brush height. Furthermore, we investigate hydrogen bonding between polymer and water and compare the obtained results for the spherical brush to that for the planar PEO brush and PEO solutions to test whether the hydrogen bonding depends only on local polymer (water) content, as

has been previously seen for planar brushes.[26] We analyze hydration shell of PEO as a function of the radial distance from the gold nanoparticle surface and determine the zone of low hydration for nanoparticles of different sizes and for different PEO grafting densities. These results are compared to experimental observation for PEO grafted to gold and iron oxide nanoparticles. The overall effect of grafting density up to experimentally-relevant high values of σ=4.17 nm^{-2} on the structure properties and hydration of PEO in the spherical brush is elucidated. Comparison with previously done all-atom simulation on planar PEO brushes is carried out to better understand the curvature dependent hydration. Finally, we analyze water exchange within the polymer brush and with surrounding solution, which can have important implications for design of PEO-functionalized gold nanoparticles for biomedical applications and more generally for catalysis of PEO-grafted nanoparticles.

6.2. Model and Simulation Methods

We performed all-atom molecular dynamics simulations of spherical gold nanoparticles grafted with methyl terminated PEO chains of 20 repeat units. To investigate the curvature dependent hydration, we studied several systems ranging in the radius of gold nanoparticles: $r = 1nm, 2nm\ and\ 3nm$ and grafting densities σ= $0.17, 0.46, 0.91, 1.50, 2.25, 3.13, 4.17\ nm^{-2}$. To achieve an equilibrium structure of spherical PEO brush, we started with coarse-grained molecular dynamics simulations using Martini force field[27]. Gold nanoparticle was modelled as a spherical particle of inter-bonded coarse grained beads employing the force filed reported in ref.[28] PEO chains represented by sequence of coarse-grained beads[29] were homogeneously grafted to gold beads on nanoparticle surface to achieve a desired grafted density. The nanoparticle with grafted PEO chains was immersed in Martini water and the NPT coarse-grained simulations were run

using GPU version of GROMACS-4.6.5 for at least 100 ns to equilibrate the nanostructure. The obtained in coarse-grained simulations equilibrated structure of PEO-grafted gold nanoparticles was back-mapped[30] to atomistic structure. For atomistic simulations, gold nanoparticle was generated using FCC crystalline gold cut into a spherical shape of radii 1, 2 and 3nm. We used force-field for the gold reported in ref.[31] which we also employed in our previous paper on planar PEO brush.[26] PEO chains were roughly homogeneously attached to the surface of gold nanoparticle via sulfur bonds. The force field parameters for PEO and sulfur were same as in our previous papers.[26] SPCE model for water was used in all simulations. The periodic box sizes used in the simulations were 10 nm x 10 nm x 10 nm, 13 nm x 13 nm x 13 nm and 16 nm x 16 nm x 16 nm for gold nanoparticles of radii 1nm, 2nm and 3nm respectively. All simulations were carried out using GPU version of GROMACS-4.6.5. We used NPT ensemble to simulate the system using Berendsen barostat at pressure 1 atm and V-rescale thermostat at T=310 K to be consistent with previously done computer simulations.[26] The coupling time constants for temperature was 1ps while for pressure it was 2ps. Electrostatic calculation was done using PME method with Fourier spacing 0.12nm. The integration time step for the simulation was 2fs. Each system was equilibrated for not less than 20 ns with simulation time exceeding 70 ns for brushes of higher grafting density. The volume fractions of PEO and water were calculated using spherical layers of $0.3\,nm$ width in radial direction starting from the surface of gold nanoparticles. For volume fraction calculations we used $0.02\,nm^3$ for the volume of CH_2 group and PEO oxygen and $0.03\,nm^3$ for the water volume, similar to our previous paper.[26] The hydrogen bond calculation was performed using the geometrical criteria for the distance between oxygens of PEO and water $r_{oo} \leq 3.5\,nm$ and angle $\measuredangle HDA \leq 30^{\circ}$ between the vectors of hydrogen (H) to oxygen of (the same) water (D) (satisfying

the distance criterion) and oxygen of water (D) to oxygen of PEO (A) similar to what was used in our previous publications.[26,32,33]

6.3. Result and Discussion

To understand the effect of grafting density and nanoparticle radius curvature on PEO conformation and hydration inside the spherical brush, we studied three gold nanoparticles of radii 1nm, 2nm and 3nm and vary PEO grafting density from $\sigma = 0.16\, nm^{-2}$ to $\sigma = 4.18\, nm^{-2}$ for each nanoparticle. The representative set of the equilibrium PEO-grafted nanoparticles is shown in Figure 6.31. As is seen at low grafting densities PEO adsorbs on the gold surface primarily to substitute for water layering observed in the vicinity of planar and spherical gold surfaces.[31,34–36] With an increase of the grafting density σ the PEO adsorption diminishes and chains spread out forming a spherical shell. The overall shell size and density of PEO in the shell noticeably increases

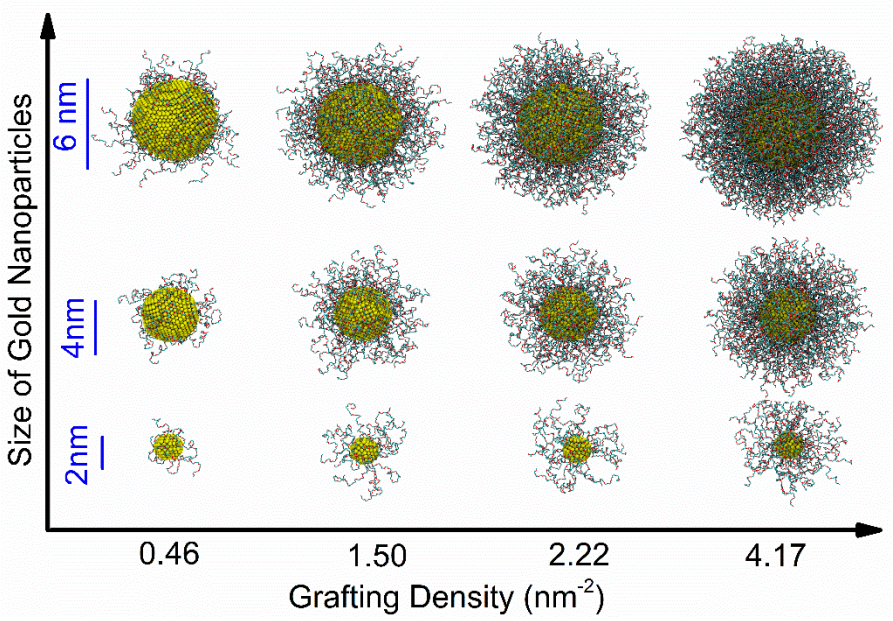

Figure 6.31: Computer simulation snapshots for the equilibrium structure of three gold nanoparticles studied of diameter 2nm, 4nm and 6nm grafted with PEO chains of 20 repeat units with grafting densities $\sigma \sim 0.46,\ 1.50,\ 2.24\ and\ 4.17\ nm^{-2}$ at T=310 K. and the column represents the varying particles with r = 3nm (upper row), 2nm(middle row) and 1nm (bottom row) respectively. Gold nanoparticle are shown in yellow and PEO represented as lines and water is not shown for clarity. The snapshots are obtained using VMD.

with an increase of both grafting density (for a given nanoparticle size) and an increase of nanoparticle radius (for a given grafting density) demonstrating that both effects play prominent role in PEO conformation and structure of the PEO layer, which we'll discuss below.

PEO grafting density effect.

To characterize the structure of grafted PEO layer we calculated the radial volume fraction profile of PEO, which is shown in Figure 6.32 for gold nanoparticle of radius 2nm as a function of radial distance from its center. As is seen, PEO volume fraction can be rather high in the immediate vicinity of the gold surface. At low PEO grafting density it is attributed to PEO adsorption on the gold to substitute for water layering[34]. As grafting density increases, chain crowding near the gold nanoparticle surface diminishes the tendency for PEO to adsorb with overall volume fraction of PEO continue to rise until it reaches about 0.7 at the highest grafting density considered, $\sigma = 4.17\ nm^{-2}$. Comparable PEO volume fraction (Φ~0.6) was reported experimentally for PB-PEO micelles[37] and even higher PEO volume fraction was obtained from fitting SANS data fitting for the dense region near the surface of gold nanoparticle of radius $r = 2.45 \pm 0.1nm$ at high grafting density $\sigma = 5.83 \pm 0.5\ nm^{-2}$.[38] Further away from gold nanoparticle surface the available area per chain increases and volume fraction of PEO decreases rapidly at lower grafting densities and somewhat slower for higher grafting densities.

It is informative to test classical scaling models for the polymer density profile behavior in a spherical brush. According to Daoud-Cotton model[9] supported by subsequent other analytical and SCF models,[10,11,39] the polymer volume fraction profiles scales as $\Phi(r) \sim r^{-\frac{4}{3}}$ for semi dilute spherical brush. As is seen from Figure 6.32b, which shows the log-log plot of PEO volume fraction as a function of radial distance from nanoparticle center, $\Phi(r)$ indeed follows the Daoud-Cotton model for experimentally-relevant grafting densities $\sigma \geq 1\ nm^{-2}$. Similar behavior is observed for other studied nanoparticle sizes (r=1nm, r=3nm).

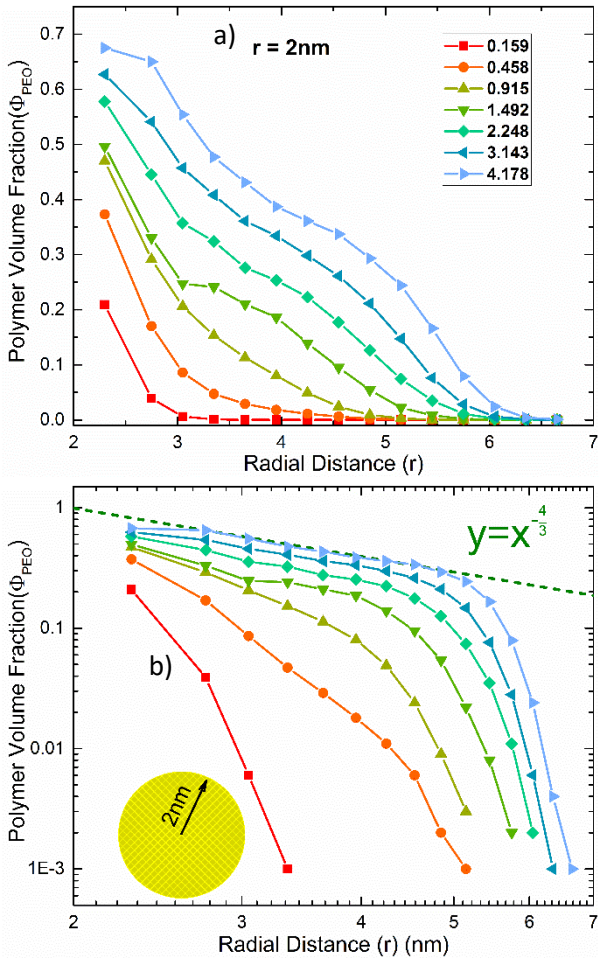

Figure 6.32: Volume fraction of PEO in a spherical layer surrounding gold nanoparticle as a function of the radial distance from the gold nanoparticle center plotted a linear (a) and logarithmic (b) scale for different grafting densities of PEO indicated in the plot. The gold nanoparticle radius r=2 nm, the number of repeat units of PEO is 20, T=310 K.

These results are consistent with recent SANS experimental data for PEO grafted ($\sigma = 3.5nm^{-2}$) on iron-oxide nanoparticles of 3.7-4.6nm in diameter,[16] which show $\Phi(r) \sim r^{-\frac{4}{3}}$ dependence for PEO volume fraction away from the nanoparticle but suggest a constant polymer density for concentrated polymer brush regime near the nanoparticle surface. Our simulation results indicate that in the immediate vicinity of the surface the decrease of polymer volume fraction seems less pronounced, but surface roughness and statistical variation of the data does not definitively support or contradict these experimental observations. At low grafting densities PEO

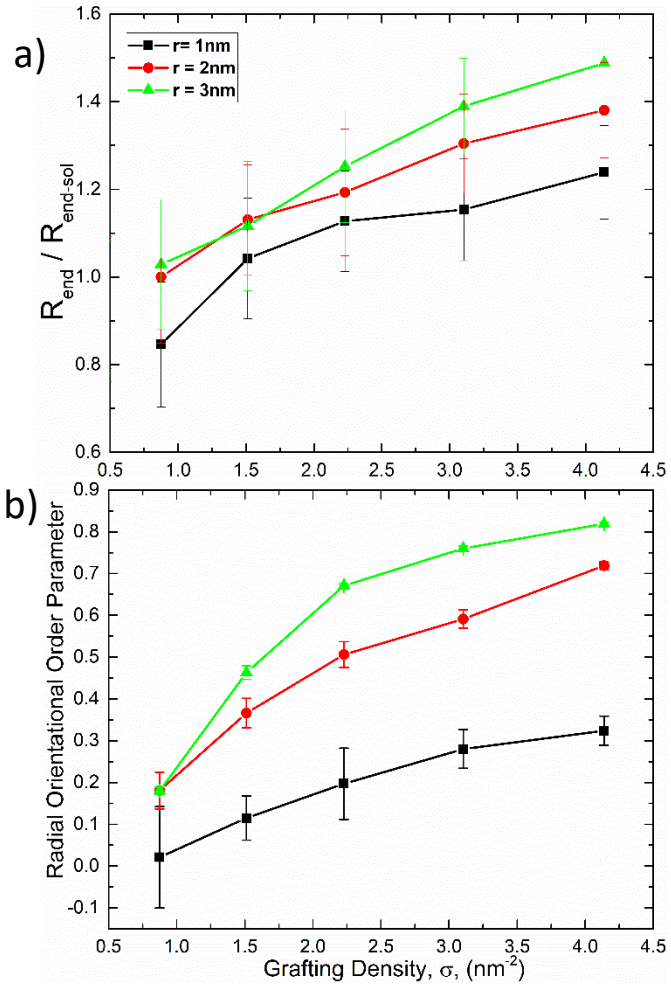

Figure 6.33: a) The ratio of the end-to-end distances for PEO grafted to gold nanoparticles of 1nm, 2nm and 3nm in radius to that in aqueous solution characterizing the chain extension and b) the orientational order parameter for the end-to-end vector with respect to radial direction as a function of grafting density σ.

adsorption on gold surface results in local polymer density enhancement leading to a stronger decay of Φ(r) dependence away from the surface.

To characterize the PEO stretching in the spherical brush we calculated and plotted in Figure 6.33a) the ratio of the end-to-end distance (R_{end}) for PEO chain grafted to gold nanoparticles to that in aqueous solution. As is seen, at low grafting density, σ~1nm^{-2}, the PEO conformation is comparable to that in aqueous solutions, implying that the PEO chains are in mushroom regime. With an increase in the grafting density, PEO chains started to stretch near the gold surface and the overall end-to-end distance increases compared to that in solution. This trend persists for different nanoparticle sizes, i.e. r=1n, 2nm and 3nm. For the larger nanoparticles PEO stretching is more pronounced at higher grafting densities reaching $1.2, 1.35$ and 1.5 times for gold nanoparticles of 1nm, 2nm and 3nm respectively. This demonstrates that the decrease in curvature

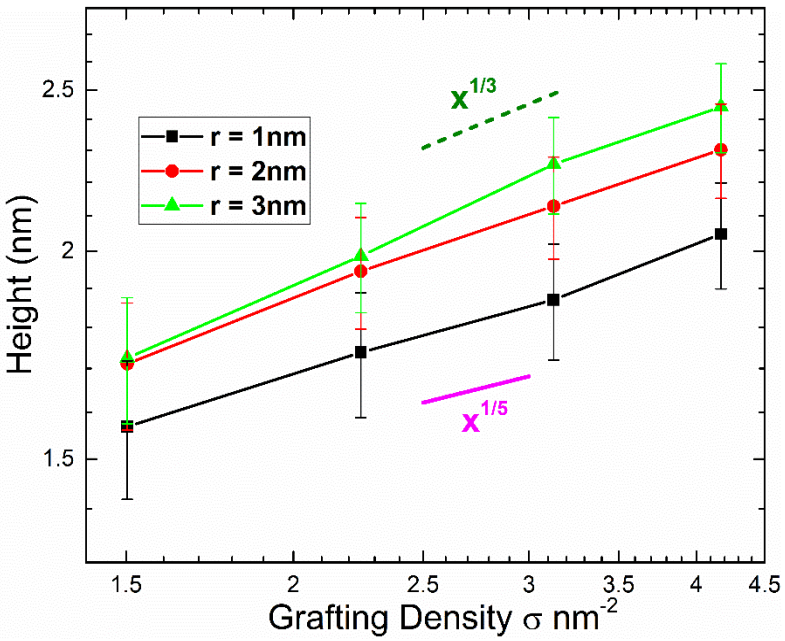

Figure 6.34: The average height of spherical PEO brush obtained using eq.6.32 as a function of polymer grafting density for gold nanoparticles of radius 1nm (squares), 2nm (circles) and 3nm (triangles). Slopes corresponding to the scaling dependences for spherical $H \sim \sigma^{\frac{1}{5}}$ and planar brushes $H \sim \sigma^{\frac{1}{3}}$ are shown.

enhances the chain crowding and stretching with highly stretched chain for planar brushes where the ratio reaches 2.2. Polymer crowding near the gold surface also leads to preferential chain orientation away from the surface, unless there is chain adsorption. To characterize chain orientation, we calculated the orientational order parameter of PEO end-to end vector with respect to the radial direction (normal to spherical surface):

$$S = \frac{1}{2}\langle(3\ Cos^2\theta - 1)\rangle \qquad (6.31)$$

where θ is the angle between the end-to-end vector of PEO chain and radial direction from center of gold nanoparticle to the grafting point of the chain. Figure 6.33b, shows the orientational order parameter as a function of grafting density for gold nanoparticles of varying size. As can be seen from the plot, there is a systematic increase in the order parameter with the grafting density, as well as the order parameter increases with particles size. For the smallest particle with r=1nm, the order parameter remains below 0.5 even for the highest grafting density. In contrast for nanoparticles with r=2nm and r=3nm the order parameter reaches 0.7-0.8 at high grafting densities, indicating that both, an increase of grafting density and a decrease in nanoparticle curvature enhances the chain stretching and orientation.

One of the general properties of polymer brushes is the brush height. The average height for PEO chains grafted to gold nanoparticles can be obtained from the volume fraction profile Φ(r) shown in Fig. 6.32, by calculating the second moment using equation:[11,12]

$$H^2 = \frac{\int r^2 dr\ \Phi(r)\ (r-R_c)^2}{\int r^2\ dr\ \Phi(r)} \qquad (6.32)$$

Figure 6.34 shows in logarithmic scale the spherical brush heights H for different nanoparticle size as functions of grafting density σ for four highest values of σ. As is seen, for the smallest nanoparticle studied, the heights of the spherical brush follows closely the expected $\sigma^{\frac{1}{5}}$ scaling predicted by Daoud-Cotton model[9] supported by subsequent other analytical and SCF models[10,11,39]. We note that at low grafting densities partial or complete polymer adsorption distorts the scaling. For the larger nanoparticles, the height of the spherical PEO brush increases somewhat quicker with grafting density, so the scaling shifts towards $\sigma^{\frac{1}{3}}$ expected for planar polymer brushes,[40,41] as the nanoparticle curvature decreases. These changes in scaling of PEO brush height are consistent with stronger chain stretching and orientation occurring at higher grafting densities and for nanoparticles of larger size, as we discussed above.

Hydration: Hydration plays an important role in PEO conformation and dynamics in aqueous solutions and in polymer brushes,[26,32,33,42–46] including important implications for protein inhibition.[3] And yet, there is a little known about PEO hydration in spherical brushes. To investigate hydration of PEO grafted to gold nanoparticles we calculated and plotted in Figure 6.35a) the average number of hydrogen bonds between PEO and water as a function of radial distance from the center of the gold nanoparticle. To identify hydrogen bonds we used the distance and angle criterions discussed in simulation details section. As is seen from Figure 6.35a), at low grafting densities $\sigma \leq 1.5\, nm^{-2}$ PEO chains achieve the solution level of hydrogen bonding (~ 1.2 hydrogen bonds per oxygen of PEO) already at distances exceeding $\sim 0.5 nm$ from the gold nanoparticle surface indicating that hydrogen bonding is restricted only in the immediate vicinity of gold surface. At higher grafting densities this zone of insufficient hydrogen bonding expands up to $\sim 1.5\, nm$ from the gold core surface for the highest grafting density. In this zone polymer

volume fraction exceeds that of water, similar to experimental observations of concentrated polymer area near the gold or iron oxide nanoparticle surface.[16,38]

While the average number of hydrogen bonds is a good measure of direct water-PEO interactions, it is not the only measure of hydration. Depending on experimental technique used, the hydration number of water molecules in direct contact with a PEO repeat unit in solution varies from 2 to 8.[42,47–55] [exp. Papers on hydration]. To quantify PEO hydration shell, we calculated the total number of water molecules within 3.5A of the polymer backbone per repeat unit of PEO as a function of the distance from the gold nanoparticle center (for calculation we used spherical shells of 3A width). The results of these calculations are shown in the Figure 6.35b for the gold nanoparticle of radius 2nm. As is seen, nearby the gold surface the hydration shell is very thin for all grafting densities considered. The number of water molecules in the hydration shell of PEO systematically increases with the radial distance as the area per chain expands and reaches the solution level, (~ 5.8) only at the periphery of the PEO layer.[33,56–58] It is interesting to note that comparing Figure 6.35 a) and b) one can notice that hydrogen bonding reaches the solution level at a rather short distance from the gold surface while incomplete hydration of PEO persists almost throughout the whole spherical layer (at least for PEO chains of 20 repeat units studied here). If one takes 2.5 water molecules per repeat unit of PEO as a satisfactorily hydrated state based on experimental reports using acoustic, DSC and IR measurements,[48,51,54,55] then the estimate of poorly hydrated zone based on the hydration shell and hydrogen bonding match with the maximum zone width of $\sim 1.5\, nm$ from the gold core surface achieved for the highest grafting density ($\sigma = 4.17\, nm^{-2}$).

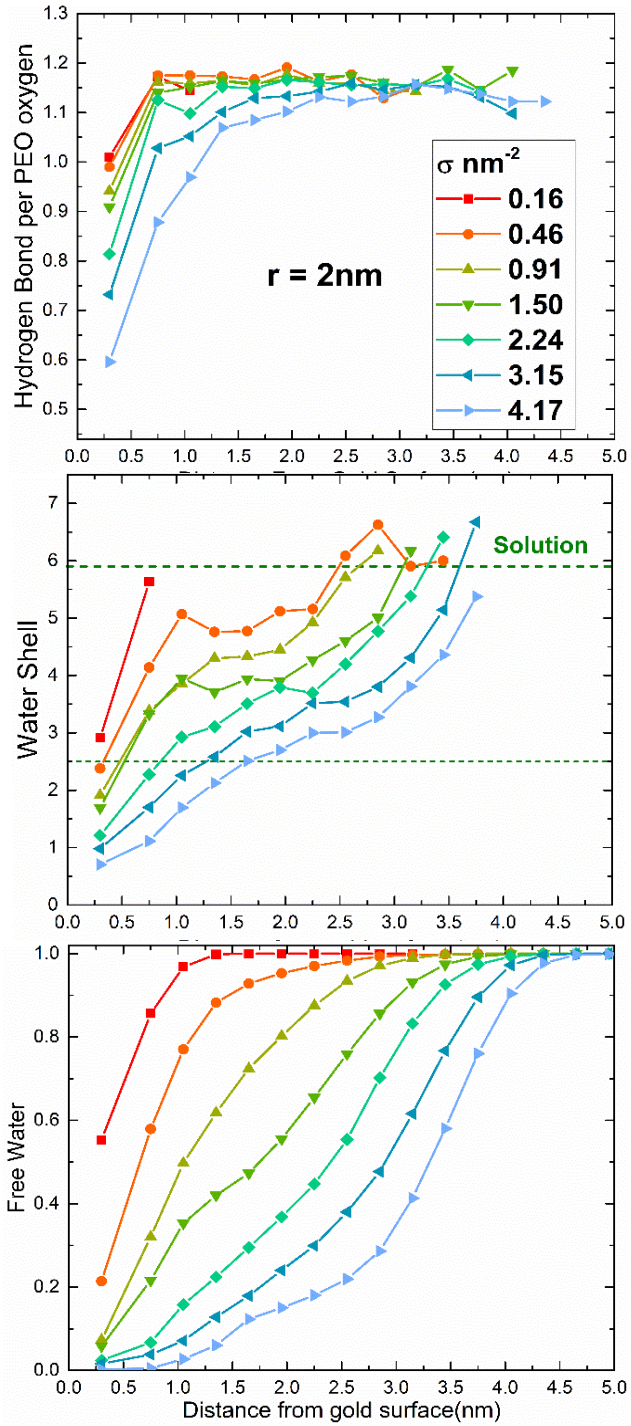

Figure 6.35: The average number of a) hydrogen bonds per oxygen of PEO; b) water molecules in the hydration shell per repeat unit of PEO and c) the fraction of water molecules which are not hydrogen bonded to PEO as functions of radial distance from nanoparticle center for gold particle of 2nm radius. Different grafting densities of PEO are indicated in the plot.

.

To understand the origin of incomplete hydration of PEO in the spherical brush, we calculated and plotted in Figure 6.35c the fraction of "free water", i.e. fraction of water that is not hydrogen bonded to PEO to all water present at a given radial distance r. As expected, near the gold surface the fraction of free water is low. In particular for PEO brushes at high grafting densities the fraction of free water is zero within some range of the surface, i.e. all water present there is hydrogen bonded to PEO and contributes the hydration shell. This range of bound water near the gold surface reaches 1nm at the highest grafting density ($\sigma = 4.17\ nm^{-2}$) considered. Further away from the gold surface fraction of free water rapidly increases. At low density of grafting PEO can be considered well-hydrated throughout the spherical layer, except for the immediate vicinity of gold surface. In contrast, PEO chains densely grafted to the gold nanoparticle exhibit dehydrated zone with lower degree of hydrogen bonding and thin hydration shell within up to 1.5nm zone from the surface and even at larger distanced from the surface PEO remains not fully hydrated.

As is seen from Figure 6.35c) for high grafting densities the fraction of free water dramatically changes throughout the spherical PEO brush from nearly zero level to dominance at the periphery of the layer. The free water distribution affects not only the equilibrium hydration discussed above, but also the dynamics of hydration and therefore segmental dynamics of grafted PEO, which is relevant for protein adsorption inhibition.[59] To quantify the dynamics of hydration, we subdivided spherical brush into spherical shells of 1nm width starting from the gold surface and calculated the water residence correlation function

$$C_{hb}(t) \equiv \langle \frac{N_w(t)}{N_w(0)} \rangle \qquad (6.33)$$

for the number of water molecules hydrogen bonded to PEO section inside the shell at time t, $N_w(t)$, compared to t=0, $N_w(0)$ for the first three shells, i.e. from 0-1nm, 1-2nm and 2-3nm from

the gold surface. We note that each shell contains approximately similar section of PEO chains and the averaging performed over different chains and different initial point of trajectory. $C_{hb}(t)$ is shown in Figure 6.36 for gold nanoparticle with radius 2nm at the highest PEO grafting density $\sigma = 4.17\ nm^{-2}$. As is seen, water hydrogen bonded to PEO in the first shell closest to the gold surface remains rather stable over the prolonged time period – even after 1ns more than 70% of water remain hydrogen bonded to PEO (not necessary at the initial location) inside the shell. This observation is consistent with practically zero free water present in this region according to Figure 6.35c). In the spherical shell from 1 to 2nm away from gold nanoparticle surface, hydrogen bonded water exchange more rapidly: only ~30% of the initial hydrogen bonded water retained after 1ns and for the shell further away from the nanoparticle surface 2-3nm almost all water initially bound

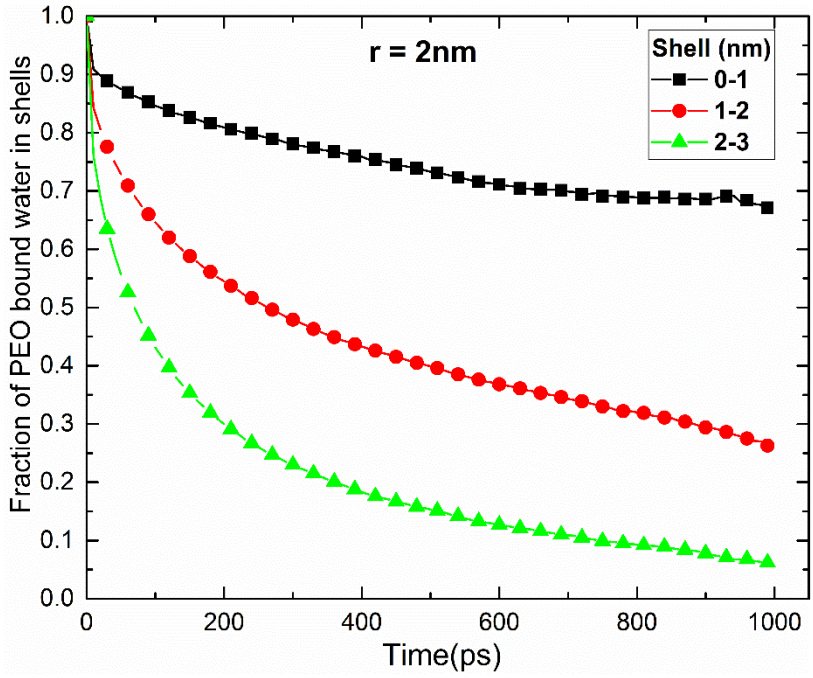

Figure 6.36: Water residence correlation function $C_{hb}(t)$ for PEO sections in the spherical shells: from the gold nanoparticle surface to 1nm in the radial direction (0-1), from 1 to 2 nanometer distance from the gold nanoparticle surface (1-2) and from 2 to 3 nanometer distance from the nanoparticle surface (2-3). Gold nanoparticle radius is 2nm, PEO grafting density is $\sigma = 4.17\ nm^{-2}$.

to PEO gets replaced by new water molecules, indicating quick free exchange of water with surrounding solution.

It is also informative to compare the water residence correlation function $C_{hb}(t)$ obtained for different grafting densities of PEO. Analyzing the grafting density effect for a given shell one can see that with an increase in σ stability of hydrogen bonded water increases. This is to be expected, as increase of local polymer concentration implies less available space for water and therefore slower exchange of water within and/or between shells. Comparing different spherical shells, one can see that the region closest to nanoparticle surface (0-1nm) is affected the most by the grafting density increase, the next shell (1-2nm) still shows a noticeable effect and only the most distance shell (2-3nm) exhibit a rather small influence of σ on dynamics of water exchange. Thus, there is systematic decrease in water stability away from the surface with relatively stagnant water zone extending up to 1.5-2nm from the surface depending on grafting density of PEO (for a given PEO degree of polymerization, N=20 considered here).

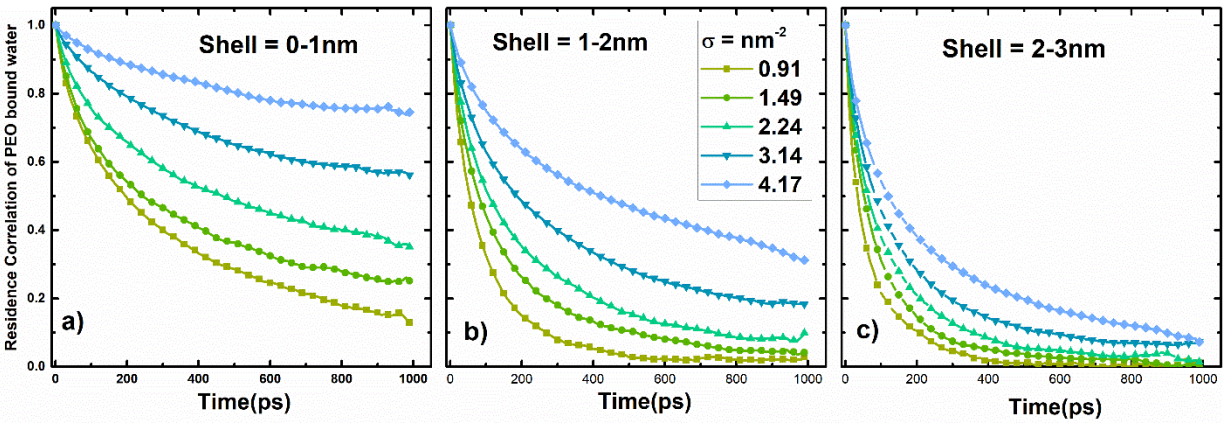

Figure 6.37: Water residence correlation function $C_{hb}(t)$ for PEO sections in the spherical shells: from the gold nanoparticle surface to 1nm in the radial direction (0-1), from 1 to 2 nanometer distance from the gold nanoparticle surface (1-2) and from 2 to 3 nanometer distance from the nanoparticle surface (2-3) obtained for different grafting densities for gold nanoparticle of radius 2nm.

Radius of curvature effect:

The area and volume available per PEO chain grafting to a nanoparticle varies dramatically with the distance away from the nanoparticle and obviously depends also on the grafting density as well as nanoparticle radius of curvature. Therefore, it is interesting to understand the radius of curvature effect on the volume fraction profile and hydration of spherical PEO brushes. In Figure 6.38 we compare PEO and water volume fraction profiles in spherical brushes grafted to nanoparticles of 1nm, 2nm and 3nm in radius and in planar PEO brush at the same grafting density, $\sigma = 4.17\text{nm}^{-2}$. As is seen an increase in the nanoparticle radius results in a smaller available space per PEO chain and results in a higher density polymer brush. In the limit of planar brush the PEO profile becomes step-like at this high grafting density. At low grafting densities the difference in the polymer density profiles is less pronounced, implying that the curvature effect is less important in mushroom or weakly overlapping brush regime. From these results we can infer that grafting density alone is not sufficient to characterize the polymer brush properties. Despite having identical grafting density, we find that the density profiles of polymer brush depend on nanoparticle curvature leading to different conformational properties, as shown in Figures 6.33 for the average chain stretching and orientation and Figure 6.34 for the brush height. To further understand the effect of curvature on hydration we compared In Figure 6.38b) the volume fraction profiles for PEO and water in spherical brushes grafted to nanoparticles of different curvature. The intersection between PEO and water volume fraction marks the point where volume fraction of both PEO and water reaches 0.5. For the highest grafting density $\sigma = 4.17nm^{-2}$, we find polymer dominates within 0.6nm, 1.2nm and 2nm of the nanoparticle surface for r=1nm, 2nm and 3nm gold particles, respectively. This systematic increase in the region of high polymer concentration in the vicinity of the nanoparticle surface show that both an increase in grafting density or decrease in

nanoparticle curvature can result in chain crowding and possible dehydration near the nanoparticle surface. This result is important for designing nanoparticles for e.g. biomedical applications as the nanoparticle protection and hydration of outer shell of PEO are essential for payload safety and prevention of undesirable interactions.

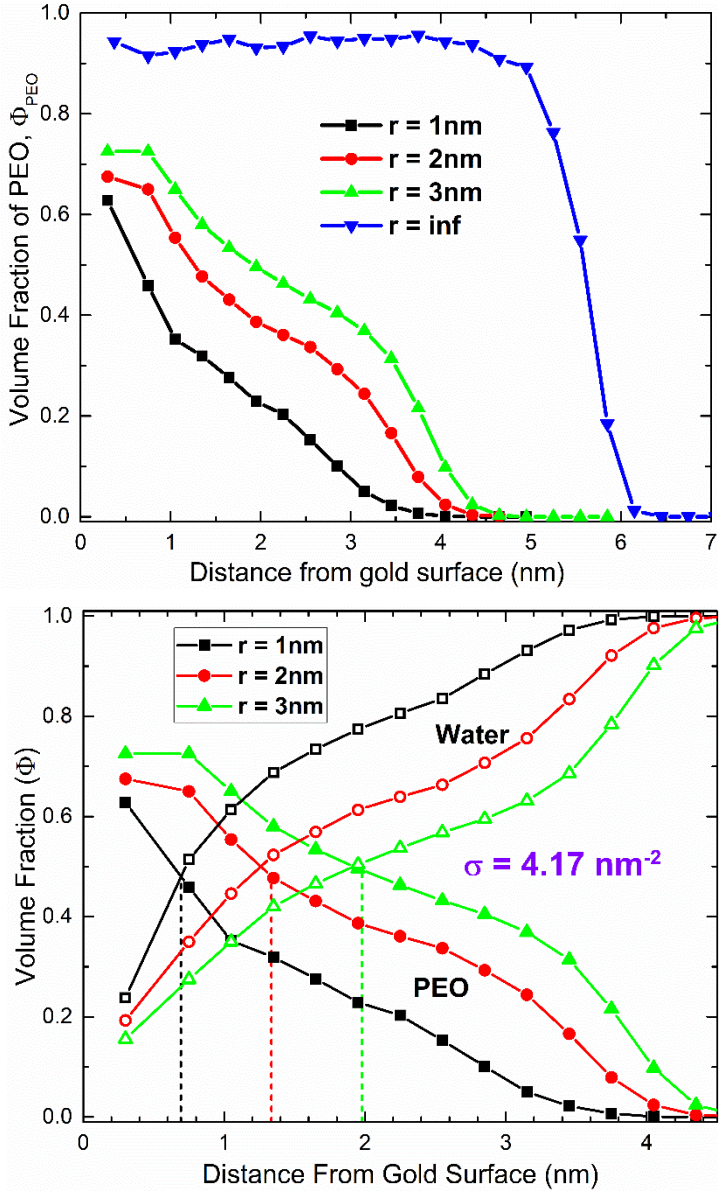

Figure 6.38: Volume fraction of PEO in spherical layers surrounding gold nanoparticles of different radii: 1nm (squares), 2nm (circles) and 3nm (up triangles) in comparison with a) that in the planar PEO layer (down triangles) and b) water volume fraction as functions of the (radial) distance from the gold (nanoparticle) surface at grafting density $\sigma = 4.17nm^{-2}$. The number of repeat units of PEO is 20, T=310K.

6.3Indeed, Figure 6.39a) shows the average number of water molecules hydrogen bonded to PEO calculated per oxygen of PEO as a function of radial distance from the gold surface. As is seen there is a systematic decrease in the degree of hydrogen bonding as nanoparticle size increases from 1nm to 2nm, to 3nm and there is a dramatic decrease in the average number of hydrogen bonds for the PEO brush grafted to a planar gold surface. In the latter case PEO brush is severely

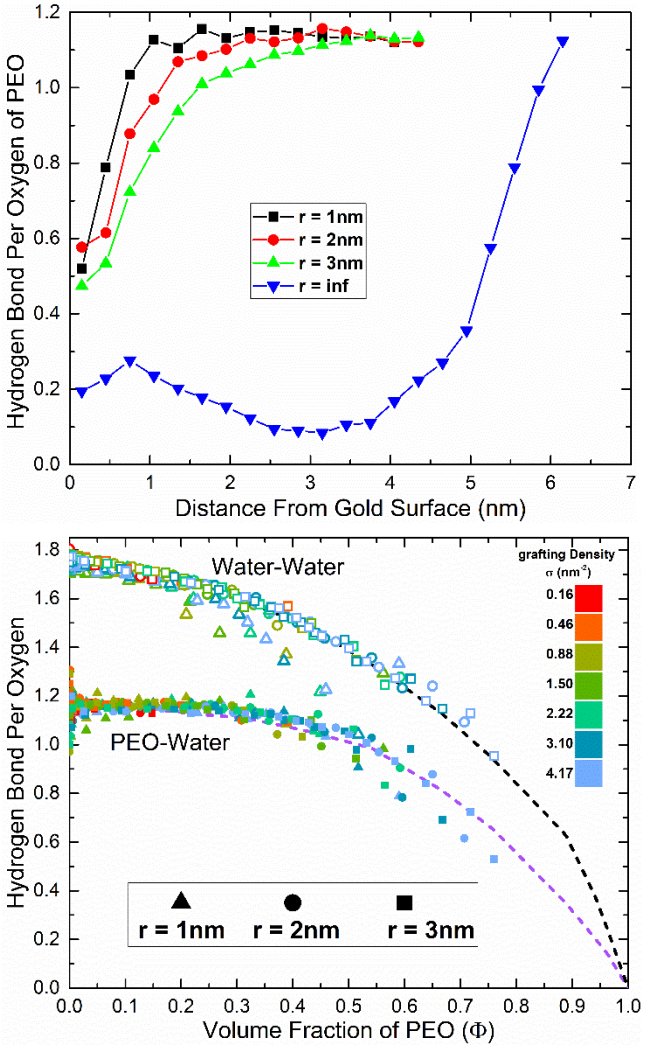

Figure 6.39: The average number of hydrogen bonds per oxygen of PEO a) as a function of radial distance from the gold nanoparticle surface for nanoparticles of different radius of curvature and planar gold surface at grafting density $\sigma = 4.17nm^{-2}$, b) as a function of local volume fraction of PEO (except for the area in the immediate vicinity of gold surface, where statistical errors are high) shown together with water-water hydrogen bonding (per water oxygen) obtained for all system studied. Dashed cures in b) show the results obtained for PEO solutions.

dehydrated leading to a very few hydrogen bonded water. In our preceding work on PEO brushes grafted to planar gold surface we found that the extent of hydrogen bonding depends primarily on local water content, so that the hydrogen bonding data obtained at different grafting densities can be all collapsed into one single curve.[26] Obviously the variation of water (and PEO) volume fraction is not as dramatic in the planar layers compared to the spherical brush studied here, so it is informative to plot the average number of water hydrogen bonded to PEO (per PEO oxygen) and water hydrogen bonded to water (per oxygen of water) for all cases studied here as a function of local volume fraction of PEO in a similar manner as we previously done for planar PEO brush. The result is shown in Figure 6.39b. As is seen for the spherical PEO brush obtained at different grafting densities and different nanoparticle radii of curvature, the average number of hydrogen bonded water follows the same dependence as in planar PEO brush[26] and in aqueous PEO solutions at the same local PEO content, in agreement with analytical model for PEO solutions.[45,46] This result confirms that hydrogen bonding depends primarily on the local water content inside the polymer brush.

As the number of hydrogen bonded to PEO water changes through the PEO brush depending on grafting density and nanoparticle curvature, so does the fraction of free water, i.e. water that is not hydrogen bonded to PEO. Figure 6.310a) shows the fraction of water that is no hydrogen bonded to PEO as a function of the distance from the gold surface for nanoparticles of different radii of curvature in comparison with that in planar PEO brush, all at the highest grafting density studied, ($\sigma = 4.17\text{nm}^{-2}$). As is seen the region near the gold surface containing no free water substantially expands from about 0.5nm to 1nm and 1.8nm for 1nm, 2nm and 3nm (in radius) nanoparticles and it expands to the whole PEO brush for the planar brush case. Indeed, with the decrease in the radius of curvature the area available for polymer and water reduces to such extent that practically all

water remained in a planar brush is bound to PEO by hydrogen bonding. This implies that the water exchange between the surrounding solution and the water within the brush slows down as the radius of curvature of the nanoparticle decreases. To quantify water exchange we compare in

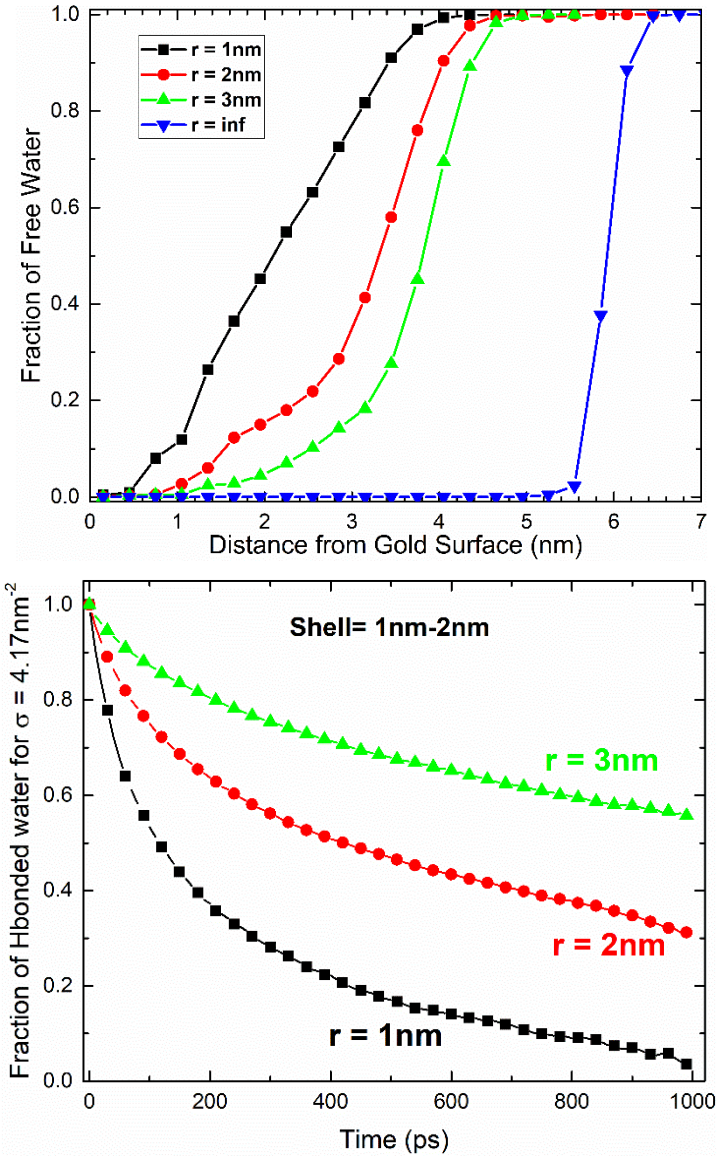

Figure 6.310: a) Fraction of free water, i.e. fraction of water molecules which are not hydrogen bonded to PEO as function of (radial) distance from the gold surface for spherical PEO brush grafted on nanoparticles of different radii and for planar PEO brush surface grafting density $\sigma = 4.17\text{nm}^{-2}$. b) Hydrogen bonded water residence correlation function $C_{hb}(t)$ for PEO spherical shell from 1 to 2 nanometer distance from the gold surface for the same grafting density ($\sigma = 4.17\text{nm}^{-2}$).

Figure 6.310b) the stability of water hydrogen bonded to PEO as a function of time $C_{hb}(t)$ in the shell from 1nm to 2nm from the gold surface calculated using eq. 6.33 for spherical PEO brushes grafted to nanoparticle of different radii in comparison to planar PEO layer. As is seen, with the decrease in the radius of curvature the stability of water hydrogen bonded to PEO increases with more than 50% of the water remain intact in the PEO hydration shell after 1ns for the gold nanoparticle of 3nm radius, while for nanoparticle of 2nm in radius only 30% of the water remains hydrogen boned to PEO and for the smallest nanoparticle of radius 1nm almost all water gets exchanged during the same time period. These results imply that water exchange between different regions of PEO shell significantly slows down, as PEO density increases (and water content decreases) as a result of grafting density increase or radius of curvature decrease.

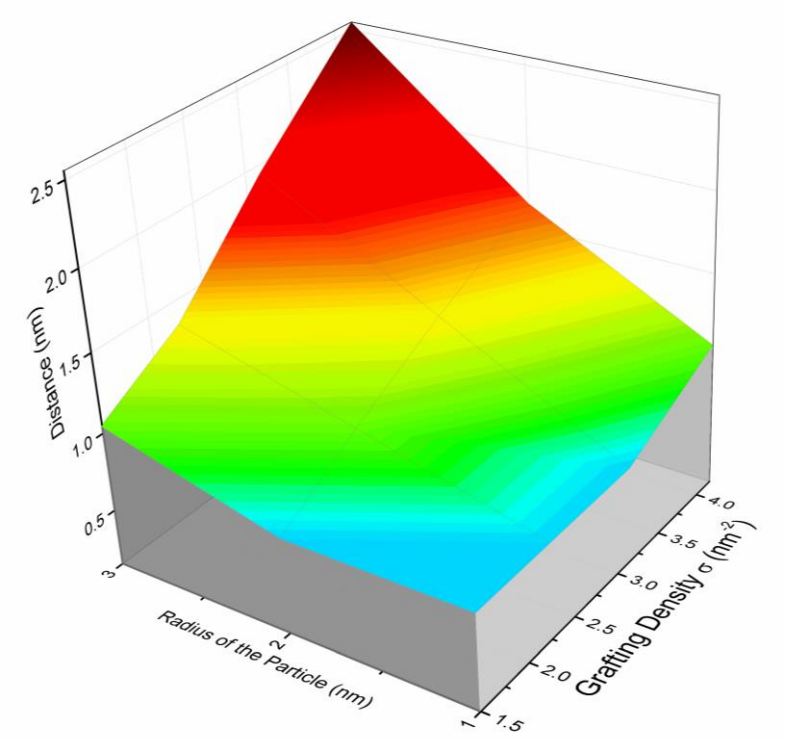

Figure 6.311: The thickness of low-hydration zone near the gold surface with less than 2.5 water molecules in a hydration shell per repeat unit of PEO as a function of PEO grafting density and nanoparticle radius.

As water exchange within the PEO brush and especially with surrounding solution is important for stability and protection of nanoparticles and payload from undesirable interactions, as well as for designing cleavable nanoparticles or for catalytic reactions in the core or on metallic surface, it is of obvious importance to understand the factors affecting dehydration and determine the dehydration zone width. There are different criteria that can be used to determine the low hydration zone. Using 2.5 water molecules in hydration shell of PEO, as often reported experimentally,[48,51,54,55] as satisfactory (but by no means complete[33,56–58]) level of hydration, we analyzed data for all nanoparticle sizes and grafting densities studied and determined the width of low hydration zone (with less than 2.5 water molecules per repeat unit of PEO) near the nanoparticle surface, as shown in Figure 6.311. As is seen, an increase in both nanoparticle radius and grafting density leads to an expansion of low hydration zone for PEO up to 2.5nm from the gold surface obtained for the highest grafting density and nanoparticle size. The plot shows that a different combination of grafting density and nanoparticle size may result in the same width of low hydration zone. Depending on practical applications one or another level of dehydration may be desirable – e.g. wider dehydration zone may be favorable for stability of the nanoparticle and payload but can be undesirable with respect to protein adsorption if the majority of the shell is dehydrated and stagnant or if drug release requires active water exchange.

6.4. Conclusions

Using all atom molecular dynamics simulations, we investigated the spherical brush of PEO chain of 20 repeat units in length grafted to gold nanoparticles of varying diameters and grafting densities. The radial volume fraction distribution for PEO chains were obtained for different grafting densities ranging from 0.16 nm^{-2} to 4.17 nm^{-2}. We found that the volume fraction profiles of PEO follow the expected scaling of Daoud-Cotton model $\Phi(r) \sim r^{-4/3}$ at high grafting

densities (Figure 6.32b). Polymer brush height was estimated from second moment of volume fraction profile using eq. 6.32. We found that for gold nanoparticle of 1nm in radius, the brush height H increases with grafting density following the expected H $\sim\sigma^{1/5}$ dependence, while with the nanoparticle size increase the dependence shifts towards H $\sim\sigma^{1/3}$ (Figure 6.34), even though limited range of high grafting densities and statistical errors precludes us from making definitive predictions of the exponent. When grafting density is low, we observe adsorption of PEO chains on gold surface consistent with experimental observations[36], which affect the polymer volume fraction profile and decreases the brush height. The PEO adsorption on gold originates from substitution for the water layering in the vicinity of gold surface.[26,34] Analyzing PEO conformation in a spherical brush, we found that PEO chains are somewhat stretched, especially in the case of high grafting densities and larger nanoparticle size when PEO end-to-end distance 1.5 times exceeds that in PEO solutions (Figure 6.33a). An increase of PEO end-to-end distance in the spherical PEO brush is also attributed to orientation of chain in the radial direction. We characterized the orientational order parameter for the end-to-end vector for the grafted PEO chains with respect to radial orientation and found that the orientation noticeably increases with nanoparticle size and PEO grafting density being attributed to the decreasing space available for chains and enhancement of chain crowding (Figure 6.33b). We note that the absolute value of the chain stretching and orientational order parameter may vary with PEO chain length, which will be a subject of our future work.

Having performed atomistic molecular dynamics simulations allowed us to investigate the details of water distribution throughout the PEO brush and calculate the degree of hydrogen bonding between PEO and water as well as water–water hydrogen bonding. We found that at low to moderate grafting densities the PEO chains fully hydrated and the average number of hydrogen

bonds per PEO oxygen reaches the level (1.2) observed for polymer solutions, except for the immediate vicinity of the gold surface, where chain adsorption and chain crowding prevents full hydration. With an increase of grafting density and nanoparticle size the average fraction hydrogen bond per PEO oxygen decreases and the zone of insufficient hydration near the gold surface expands (Figure 6.35a and Figure 6.39a). Analyzing the data for all nanoparticles and grafting densities studied, we found that the degree of hydrogen bonding between PEO and in between water follows the same common trend as in planar PEO brush, i.e. hydrogen bonding depends primarily on the local volume fraction of polymer (water) and can be predicted knowing degree of hydrogen bonding of polymer solutions of corresponding polymer content. We also analyzed the PEO hydration shell, i.e. the average number of water molecules located within of 3.5 of PEO backbone calculated per monomer of PEO. We found that achieving the full hydration shell for PEO is much more demanding than having hydrogen bonding at the solution level, so that the PEO chains have incomplete hydration shell for the most of the corona. Taking 2.5 water molecules (which is less than half of the complete hydration shell of 5.8) as a minimally acceptable hydration shell level, based on experimental data, we determined the zone of dehydration near the gold surface (Figure 6.35b). This dehydration zone considerably expands with an increase in PEO grafting density and especially nanoparticle size, reaching up to 2.5nm, the size comparable with a nanoparticle radius (Figure 6.311). The presence of dehydrated polymer-dominated regions of spherical PEO brush agrees well with recent experimental data on gold and iron oxide-grafted PEO brush.[8,16] Having a substantial dehydration zone raises the question about water distribution and mobility inside the spherical layer. We calculated the fraction of water which is not hydrogen bonded to polymer, I.e. free water, inside the spherical layer as a function of radial distance from the gold surface (Figure 6.35c). We found that in some vicinity of gold surface all water is bound

to polymer. This region significantly expands with an increase in grafting density (Figure 6.35c) and especially with decrease of nanoparticle curvature (Figure 6.310a) expanding to nearly the whole PEO brush in the limit of planar brush of high grafting density. We also analyzed the dynamics of water hydrogen bonded to PEO in different spherical layers of the corona and found that the hydrogen bonded water stability is the highest in the region closest to gold surface, which is to be expected. Hydrogen bonded water stability noticeably increases with grafting density and nanoparticle size (Figure 6.37 and 6.310b). It is interesting to note that water exchange is found to be somewhat limited even in the middle of the PEO brush and only the outer layer of the PEO brush exhibit a very minor dependence on grafting density indicating quick water exchange with surrounding media.

Thus, the analysis of equilibrium and dynamical properties of spherical PEO brush grafted on gold nanoparticles show that while the overall brush height and polymer distribution throughout the brush follow classical scaling dependences, the conformational properties and especially hydration of PEO chains inside the brush are less intuitive and strongly depend on both polymer grafting density and nanoparticle curvature. In particular, the presence of relatively wide zone of low polymer hydration near the nanoparticle surface and slow water exchange in the inner PEO brush region are important findings which expand current fundamental understanding of water-soluble spherical polymer brushes and have important implications for design optimization of PEO-grafted nanoparticles for biomedical applications or catalysis.

6.5. References

(1) Stuart, M. A. C.; Huck, W. T. S.; Genzer, J.; Müller, M.; Ober, C.; Stamm, M.; Sukhorukov, G. B.; Szleifer, I.; Tsukruk, V. V.; Urban, M.; Winnik, F.; Zauscher, S.; Luzinov, I.; Minko, S. Emerging Applications of Stimuli-Responsive Polymer Materials. *Nat. Mater.* **2010**, *9* (2), 101–113 DOI: 10.1038/nmat2614.

(2) Jokerst, J. V; Lobovkina, T.; Zare, R. N.; Gambhir, S. S. Nanoparticle PEGylation for Imaging and Therapy. *Nanomedicine (Lond).* **2011**, *6* (4), 715–728 DOI: 10.2217/nnm.11.19.

(3) Schöttler, S.; Becker, G.; Winzen, S.; Steinbach, T.; Mohr, K.; Landfester, K.; Mailänder, V.; Wurm, F. R. Protein Adsorption Is Required for Stealth Effect of Poly(Ethylene Glycol)- and Poly(Phosphoester)-Coated Nanocarriers. *Nat. Nanotechnol.* **2016**, *11* (4), 372–377 DOI: 10.1038/nnano.2015.330.

(4) Krishnamoorthy, M.; Hakobyan, S.; Ramstedt, M.; Gautrot, J. E. Surface-Initiated Polymer Brushes in the Biomedical Field: Applications in Membrane Science, Biosensing, Cell Culture, Regenerative Medicine and Antibacterial Coatings. *Chem. Rev.* **2014**, *114* (21), 10976–11026 DOI: 10.1021/cr500252u.

(5) Senaratne, W.; Andruzzi, L.; Ober, C. K. Self-Assembled Monolayers and Polymer Brushes in Biotechnology: Current Applications and Future Perspectives. *Biomacromolecules* **2005**, *6* (5), 2427–2448 DOI: 10.1021/bm050180a.

(6) Liu, H.; Doane, T. L.; Cheng, Y.; Lu, F.; Srinivasan, S.; Zhu, J.-J.; Burda, C. Control of Surface Ligand Density on PEGylated Gold Nanoparticles for Optimized Cancer Cell Uptake. *Part. Part. Syst. Charact.* **2015**, *32* (2), 197–204 DOI: 10.1002/ppsc.201400067.

(7) Müller, M. T.; Yan, X.; Lee, S.; Perry, S. S.; Spencer, N. D. Lubrication Properties of a Brushlike Copolymer as a Function of the Amount of Solvent Absorbed within the Brush. *Macromolecules* **2005**, *38* (13), 5706–5713 DOI: 10.1021/ma0501545.

(8) Maccarini, M.; Briganti, G.; Rucareanu, S.; Lui, X.; Sinibaldi, R.; Sztucki, M.; Lennox, R. B. Characterization of Poly (Ethylene Oxide) -Capped Gold Nanoparticles in Water by Means of Transmission Electron Microscopy , Thermogravimetric Analysis , Mass Density , and Small Angle Scattering. **2010**, 6937–6943.

(9) Daoud, M.; Cotton, J. P. Star Shaped Polymers : A Model for the Conformation and Its Concentration Dependence. *J. Phys.* **1982**, *43* (3), 531–538 DOI: 10.1051/jphys:01982004303053100.

(10) Dan, N.; Tirrell, M. Polymers Tethered to Curves Interfaces: A Self-Consistent-Field Analysis. *Macromolecules* **1992**, *25* (11), 2890–2895 DOI: 10.1021/ma00037a016.

(11) Wijmans, C. M.; Zhulina, E. B. Polymer Brushes at Curved Surfaces. *Macromolecules* **1993**, *26* (26), 7214–7224 DOI: 10.1021/ma00078a016.

(12) Lo Verso, F.; Egorov, S. A.; Milchev, A.; Binder, K. Spherical Polymer Brushes under Good Solvent Conditions: Molecular Dynamics Results Compared to Density Functional Theory. *J. Chem. Phys.* **2010**, *133* (18), 184901 DOI: 10.1063/1.3494902.

(13) Dong, J.; Zhou, J. Solvent-Responsive Behavior of Polymer-Brush-Modified Amphiphilic Gold Nanoparticles. *Macromol. Theory Simulations* **2013**, *22* (3), 174–186 DOI: 10.1002/mats.201200078.

(14) Ohno, K.; Morinaga, T.; Takeno, S.; Tsujii, Y.; Fukuda, T. Suspensions of Silica Particles Grafted with Concentrated Polymer Brush: Effects of Graft Chain Length on Brush Layer Thickness and Colloidal Crystallization. *Macromolecules* **2007**, *40* (25), 9143–9150 DOI:

10.1021/ma071770z.

(15) Lindberg, E.; Elvingson, C. Monte Carlo Simulation of Polymer Brushes Attached to a Spherical Surface. *J. Chem. Phys.* **2001**, *114* (14), 6343 DOI: 10.1063/1.1355236.

(16) Grünewald, T. A.; Lassenberger, A.; van Oostrum, P. D. J.; Rennhofer, H.; Zirbs, R.; Capone, B.; Vonderhaid, I.; Amenitsch, H.; Lichtenegger, H. C.; Reimhult, E. Core–Shell Structure of Monodisperse Poly(Ethylene Glycol)-Grafted Iron Oxide Nanoparticles Studied by Small-Angle X-Ray Scattering. *Chem. Mater.* **2015**, *27* (13), 4763–4771 DOI: 10.1021/acs.chemmater.5b01488.

(17) Dukes, D.; Li, Y.; Lewis, S.; Benicewicz, B.; Schadler, L.; Kumar, S. K. Conformational Transitions of Spherical Polymer Brushes: Synthesis, Characterization, and Theory. *Macromolecules* **2010**, *43* (3), 1564–1570 DOI: 10.1021/ma901228t.

(18) Doane, T. L.; Chuang, C. H.; Hill, R. J.; Burda, C. Nanoparticle ζ -Potentials. *Acc. Chem. Res.* **2012**, *45* (3), 317–326 DOI: 10.1021/ar200113c.

(19) Doane, T. L.; Cheng, Y.; Babar, A.; Hill, R. J.; Burda, C. Electrophoretic Mobilities of PEGylated Gold NPs. *J. Am. Chem. Soc.* **2010**, *132* (44), 15624–15631 DOI: 10.1021/ja1049093.

(20) Díaz, S. A.; Sen, S.; Boeneman Gemmill, K.; Brown, C. W.; Oh, E.; Susumu, K.; Stewart, M. H.; Breger, J. C.; Lasarte Aragonés, G.; Field, L. D.; Deschamps, J. R.; Král, P.; Medintz, I. L. Elucidating Surface Ligand-Dependent Kinetic Enhancement of Proteolytic Activity at Surface-Modified Quantum Dots. *ACS Nano* **2017**, *11* (6), 5884–5896 DOI: 10.1021/acsnano.7b01624.

(21) Boisselier, E.; Astruc, D. Gold Nanoparticles in Nanomedicine: Preparations, Imaging, Diagnostics, Therapies and Toxicity. *Chem. Soc. Rev.* **2009**, *38* (6), 1759 DOI: 10.1039/b806051g.

(22) Cabuzu, D.; Cirja, A.; Puiu, R.; Grumezescu, A. M. Biomedical Applications of Gold Nanoparticles. *Curr. Top. Med. Chem.* **2015**, *15* (16), 1605–1613 DOI: 10.2174/1568026615666150414144750.

(23) Pincus, P. Colloid Stabilization with Grafted Polyelectrolytes. *Macromolecules* **1991**, *24* (10), 2912–2919 DOI: 10.1021/ma00010a043.

(24) Toral, R.; Chakrabarti, A. Monte Carlo Study of Polymer Chains End-Grafted onto a Spherical Interface. *Phys. Rev. E* **1993**, *47* (6), 4240–4246 DOI: 10.1103/PhysRevE.47.4240.

(25) Heikkilä, E.; Martinez-Seara, H.; Gurtovenko, A. A.; Vattulainen, I.; Akola, J. Atomistic Simulations of Anionic Au144(SR)60 Nanoparticles Interacting with Asymmetric Model Lipid Membranes. *Biochim. Biophys. Acta - Biomembr.* **2014**, *1838* (11), 2852–2860 DOI: 10.1016/j.bbamem.2014.07.027.

(26) Dahal, U. R.; Wang, Z.; Dormidontova, E. E. Hydration and Mobility of Poly(Ethylene Oxide) Brushes. *Macromolecules* **2017**, *50* (17), 6722–6732 DOI: 10.1021/acs.macromol.7b01369.

(27) Marrink, S. J.; Tieleman, D. P. Perspective on the Martini Model. *Chem. Soc. Rev.* **2013**, *42* (16), 6801 DOI: 10.1039/c3cs60093a.

(28) Lin, J.; Zhang, H.; Chen, Z.; Zheng, Y. Penetration of Lipid Membranes by Gold Nanoparticles: Insights into Cellular Uptake, Cytotoxicity, and Their Relationship. *ACS Nano* **2010**, *4* (9), 5421–5429 DOI: 10.1021/nn1010792.

(29) Rossi, G.; Fuchs, P. F. J.; Barnoud, J.; Monticelli, L. A Coarse-Grained MARTINI Model of Polyethylene Glycol and of Polyoxyethylene Alkyl Ether Surfactants. *J. Phys. Chem. B* **2012**, *116* (49), 14353–14362 DOI: 10.1021/jp3095165.

(30) Wassenaar, T. A.; Pluhackova, K.; Böckmann, R. A.; Marrink, S. J.; Tieleman, D. P. Going Backward: A Flexible Geometric Approach to Reverse Transformation from Coarse Grained to Atomistic Models. *J. Chem. Theory Comput.* **2014**, *10* (2), 676–690 DOI: 10.1021/ct400617g.

(31) Tay, K. A.; Bresme, F. Wetting Properties of Passivated Metal Nanocrystals at Liquid−Vapor Interfaces: A Computer Simulation Study. *J. Am. Chem. Soc.* **2006**, *128* (43), 14166–14175 DOI: 10.1021/ja061901w.

(32) Dahal, U. R.; Dormidontova, E. E. Spontaneous Insertion, Helix Formation, and Hydration of Polyethylene Oxide in Carbon Nanotubes. *Phys. Rev. Lett.* **2016**, *117* (2), 027801 DOI: 10.1103/PhysRevLett.117.027801.

(33) Dahal, U. R.; Dormidontova, E. E. The Dynamics of Solvation Dictates the Conformation of Polyethylene Oxide in Aqueous, Isobutyric Acid and Binary Solutions. *Phys. Chem. Chem. Phys.* **2017**, *19* (15), 9823–9832 DOI: 10.1039/C7CP00526A.

(34) Stacchiola, D.; Park, J. B.; Liu, P.; Ma, S.; Yang, F.; Starr, D. E.; Muller, E.; Sutter, P.; Hrbek, J. Water Nucleation on Gold: Existence of a Unique Double Bilayer. *J. Phys. Chem. C* **2009**, *113* (34), 15102–15105 DOI: 10.1021/jp904875h.

(35) Velasco-Velez, J.-J.; Wu, C. H.; Pascal, T. A.; Wan, L. F.; Guo, J.; Prendergast, D.; Salmeron, M. The Structure of Interfacial Water on Gold Electrodes Studied by X-Ray Absorption Spectroscopy. *Science (80-.).* **2014**, *346* (6211), 831–834 DOI: 10.1126/science.1259437.

(36) Huang, Y.; Gupta, V. K. Effects of Physical Heterogeneity on the Adsorption of Poly (Ethylene Oxide) at a Solid - Liquid Interface. *Macromolecules* **2001**, *34* (11), 3757–3764.

(37) Won, Y.-Y.; Davis, H. T.; Bates, F. S.; Agamalian, M.; Wignall, G. D. Segment Distribution of the Micellar Brushes of Poly(Ethylene Oxide) via Small-Angle Neutron Scattering. *J. Phys. Chem. B* **2000**, *104* (30), 7134–7143 DOI: 10.1021/jp000457v.

(38) Maccarini, M.; Briganti, G.; Rucareanu, S.; Lui, X.; Sinibaldi, R.; Sztucki, M.; Lennox, R. B. Characterization of Poly(Ethylene Oxide)-Capped Gold Nanoparticles in Water by Means of Transmission Electron Microscopy, Thermogravimetric Analysis, Mass Density, and Small Angle Scattering. *J. Phys. Chem. C* **2010**, *114* (15), 6937–6943 DOI: 10.1021/jp9118088.

(39) Bekiranov, S.; Bruinsma, R.; Pincus, P. Solution Behavior of Polyethylene Oxide in Water as a Function of Temperature and Pressure. *Phys. Rev. E* **1997**, *55* (1), 577–585 DOI:

10.1103/PhysRevE.55.577.

(40) Milner, S. T.; Witten, T. A.; Cates, M. E. Theory of the Grafted Polymer Brush. *Macromolecules* **1988**, *21* (8), 2610–2619 DOI: 10.1021/ma00186a051.

(41) Murat, M.; Grest, G. S. Structure of a Grafted Polymer Brush: A Molecular Dynamics Simulation. *Macromolecules* **1989**, *22* (3), 4054–4059 DOI: 10.1021/ma00200a041.

(42) Shikata, T.; Okuzono, M.; Sugimoto, N. Temperature-Dependent Hydration/Dehydration Behavior of Poly(Ethylene Oxide)s in Aqueous Solution. *Macromolecules* **2013**, *46* (5), 1956–1961 DOI: 10.1021/ma3026282.

(43) Wada, R.; Fujimoto, K.; Kato, M. Why Is Poly(Oxyethylene) Soluble in Water? Evidence from the Thermodynamic Profile of the Conformational Equilibria of 1,2-Dimethoxyethane and Dimethoxymethane Revealed by Raman Spectroscopy. *J. Phys. Chem. B* **2014**, *118* (42), 12223–12231 DOI: 10.1021/jp5048997.

(44) Wu, J.; Chen, S. Investigation of the Hydration of Nonfouling Material Poly(Ethylene Glycol) by Low-Field Nuclear Magnetic Resonance. *Langmuir* **2012**, *28* (4), 2137–2144 DOI: 10.1021/la203827h.

(45) Dormidontova, E. E. Role of Competitive PEO−Water and Water−Water Hydrogen Bonding in Aqueous Solution PEO Behavior. *Macromolecules* **2002**, *35* (3), 987–1001 DOI: 10.1021/ma010804e.

(46) Dormidontova, E. E. Influence of End Groups on Phase Behavior and Properties of PEO in Aqueous Solutions. *Macromolecules* **2004**, *37* (20), 7747–7761 DOI: 10.1021/ma035609.

(47) Shikata, T.; Takahashi, R.; Sakamoto, A. Hydration of Poly(Ethylene Oxide)s in Aqueous Solution As Studied by Dielectric Relaxation Measurements. *J. Phys. Chem. B* **2006**, *110* (18), 8941–8945 DOI: 10.1021/jp060356i.

(48) Branca, C.; Magazù, S.; Maisano, G.; Migliardo, F.; Migliardo, P.; Romeo, G. Hydration Study of PEG/Water Mixtures by Quasi Elastic Light Scattering, Acoustic and Rheological Measurements. *J. Phys. Chem. B* **2002**, *106* (39), 10272–10276 DOI: 10.1021/jp014345v.

(49) Branca, C.; Faraone, A.; Magazú, S.; Maisano, G.; Migliardo, P.; Villari, V. PolyEthylene Oxide: A Review of Experimental Findings by Spectroscopic Techniques. *J. Mol. Liq.* **2000**, *87* (1), 21–68 DOI: 10.1016/S0167-7322(00)00129-X.

(50) Hey, M. J.; Ilett, S. M. Poly(Ethylene Oxide) Hydration Studied by Differential Scanning Calorimetry. *J. Chem. Soc. Faraday Trans.* **1991**, *87* (22), 3671–3675 DOI: 10.1039/ft9918703671.

(51) Sagawa, N.; Shikata, T. Hydration Behavior of Poly(Ethylene Oxide)s in Aqueous Solution as Studied by near-Infrared Spectroscopic Techniques. *J. Phys. Chem. B* **2013**, *117* (37), 10883–10888 DOI: 10.1021/jp405794t.

(52) Branca, C.; Magazù, S.; Maisano, G.; Migliardo, P.; Villari, V. Conformational Distribution of Poly(Ethylene Oxide) in Molten Phase and in Aqueous Solution by Quasi-

Elastic and Inelastic Light Scattering. *J. Phys. Condens. Matter* **1998**, *10* (45), 10141–10157 DOI: 10.1088/0953-8984/10/45/004.

(53) Hey, M. J.; Ilett, S. M.; Mortimer, M.; Oates, G. Water in Poly(Ethylene Oxide): Differential Scanning Calorimetry and Nuclear Magnetic Resonance Experiments. *J. Chem. Soc. Faraday Trans.* **1990**, *86* (14), 2673–2674 DOI: 10.1039/ft9908602673.

(54) Huang, L.; Nishinari, K. Interaction between Poly(Ethylene Glycol) and Water as Studied by Differential Scanning Calorimetry. *J. Polym. Sci. Part B Polym. Phys.* **2001**, *39* (5), 496–506 DOI: 10.1002/1099-0488(20010301)39:5<496::AID-POLB1023>3.0.CO;2-H.

(55) Hager, S. L.; Macrury, T. B. Investigation of Phase Behavior and Water Binding in Poly(Alkylene Oxide) Solutions. *J. Appl. Polym. Sci.* **1980**, *25* (8), 1559–1571 DOI: 10.1002/app.1980.070250805.

(56) Żwirbla, W.; Sikorska, A.; Linde, B. B. J. Ultrasonic Investigations of Water Mixtures with Polyethylene Glycols 200, 400 and Ethylene Glycol. *J. Mol. Struct.* **2005**, *743* (1–3), 49–52 DOI: 10.1016/j.molstruc.2005.02.019.

(57) Kaatze, U.; Gottmann, O.; Podbielski, R.; Pottel, R.; Terveer, U. Dielectric Relaxation in Aqueous Solutions of Some Oxygen-Containing Linear Hydrocarbon Polymers. *J. Phys. Chem.* **1978**, *82* (1), 112–120 DOI: 10.1021/j100490a025.

(58) Bieze, T. W. N.; Barnes, A. C.; Huige, C. J. M.; Enderby, J. E.; Leyte, J. C. Distribution of Water around Poly(Ethylene Oxide): A Neutron Diffraction Study. *J. Phys. Chem.* **1994**, *98* (26), 6568–6576 DOI: 10.1021/j100077a024.

(59) Unsworth, L. D.; Sheardown, H.; Brash, J. L. Protein Resistance of Surfaces Prepared by Sorption of End-Thiolated Poly(Ethylene Glycol) to Gold: Effect of Surface Chain Density. *Langmuir* **2005**, *21* (3), 1036–1041 DOI: 10.1021/la047672d.

7 Summary and Future Work

In this thesis, we presented the result of atomistic molecular dynamics simulation of polyethylene oxide chains under different conditions. So far, very little work had been done on hydration of water-soluble polymer under confinement and in polymer brushes. The results of our simulations provide a significant step forward in our understanding of water-soluble polymers in solutions, binary mixture of protic solvents, under nanoconfinement and in nanostructures. In chapter 3, we explored the fundamental properties of PEO in pure solutions as well as in binary mixtures and were able to modify the force field parameters to account for correct hydration behavior based on theoretical models. In chapter 4, we extended our understanding of PEO chains in solutions and explored the behavior of PEO under nanoconfinement. Classical theories by de Gennes[1] and Odijk[2] provide the scaling analysis for the flexible and rigid polymers under different confinements. Comparing the unique scaling behavior shown by PEO with classical theories paves a pathway in understanding highly flexible polymer under confinement and we believe that the result of this analysis will be helpful for researches studying biopolymers like protein and DNA in nanochannels and nanopores. In chapter 5 and chapter 6, we explored the polymer brushes and more specifically a very high grafting density PEO brushes on planar gold sheet and spherical gold nanoparticles. For planar brushes, the highest grafting densities used in the simulations are beyond the experimentally synthesized density in present time. This study of hydration and dynamics these planar brushes can be insightful for experimentalists who are striving to synthesize very high grafting density brushes for various industrial and biomedical applications. While it is hard to synthesize high grafting density brush for planar surface, there are reports of very high grafting density for spherical brushes including some reports[3] suggesting enormously high grafting density

$7\ nm^{-2}$. Much of the higher grafting density brushes, specially hydration of PEO brushes has not been explored in detail to our knowledge and we believe that understanding the effect of grafting density as well as curvature on conformation and hydration of PEO brushes would be useful for designing new materials.

In future, we hope to extend our research to biologically important macromolecules like protein and DNA and explore different aspects of hydration and conformational transitions. There are simulation reports that graphene nanopore can be used for DNA sequencing.[4] Further, the study of DNA and protein inside carbon nanotube and understanding the role water plays inside that confinement would be an exciting step to explore.

Hydration and conformation of PEO grafted to spherical gold nanoparticles can be directly compared to that in self-assembled copolymer micelles e.g. PB-PEO, PPO-PEO or PE-PEO micelles. The interfacial properties of these polymeric micelles play an important role in micelles' applications and hence the comparative study of polymeric micelles with spherical gold micelle will be insightful.

We believe that the outcomes of these studies are of fundamental importance and will make significant impact for designing, improving and modifying the nanomaterials in future.

References

(1) Gennes, P.-G. de. *Scaling Concepts in Polymer Physics*; Cornell University Press: Ithaca,NY, 1979.

(2) Odijk, T. On the Statistics and Dynamics of Confined or Entangled Stiff Polymers. *Macromolecules* **1983**, *16* (8), 1340–1344.

(3) Maccarini, M.; Briganti, G.; Rucareanu, S.; Lui, X.; Sinibaldi, R.; Sztucki, M.; Lennox, R. B. Characterization of Poly (Ethylene Oxide) -Capped Gold Nanoparticles in Water by Means of Transmission Electron Microscopy , Thermogravimetric Analysis , Mass Density , and Small Angle Scattering. **2010**, 6937–6943.

(4) Wells, D. B.; Belkin, M.; Comer, J.; Aksimentiev, A. Assessing Graphene Nanopores for Sequencing DNA. *Nano Lett.* **2012**, *12* (8), 4117–4123.